

MODELING TEMPORAL VARIATION OF SCOURING AT DUAL BRIDGE PIERS

A THESIS SUBMITTED TO  
THE GRADUATE SCHOOL OF NATURAL AND APPLIED SCIENCES  
OF  
MIDDLE EAST TECHNICAL UNIVERSITY

BY

MERİÇ SELAMOĞLU

IN PARTIAL FULFILLMENT OF THE REQUIREMENTS  
FOR  
THE DEGREE OF DOCTOR OF PHILOSOPHY  
IN  
CIVIL ENGINEERING

JUNE 2015



Approval of the thesis:

**MODELING TEMPORAL VARIATION OF SCOURING AT DUAL  
BRIDGE PIERS**

submitted by **MERİÇ SELAMOĞLU** in partial fulfillment of the requirements  
for the degree of **Doctor of Philosophy in Civil Engineering Department,**  
**Middle East Technical University** by,

Prof. Dr. Gülbin Dural Ünver  
Dean, Graduate School of **Natural and Applied Sciences** \_\_\_\_\_

Prof. Dr. Ahmet Cevdet Yalçiner  
Head of Department, **Civil Engineering** \_\_\_\_\_

Prof. Dr. A. Melih Yanmaz  
Supervisor, **Civil Engineering Department, METU** \_\_\_\_\_

Assoc. Prof. Dr. Mete Köken  
Co-supervisor, **Civil Engineering Department, METU** \_\_\_\_\_

**Examining Committee Members:**

Prof. Dr. Zafer Bozkuş  
Civil Engineering Dept., METU \_\_\_\_\_

Prof. Dr. A. Melih Yanmaz  
Civil Engineering Dept., METU \_\_\_\_\_

Prof. Dr. Ayşe Burcu Altan Sakarya  
Civil Engineering Dept., METU \_\_\_\_\_

Assoc. Prof. Dr. Şahnaz Tiğrek  
Civil Engineering Dept., Batman University \_\_\_\_\_

Asst. Prof. Dr. Müsteyde Baduna Koçyiğit  
Civil Engineering Dept., Gazi University \_\_\_\_\_

**Date:** June 08, 2015

**I hereby declare that all information in this document has been obtained and presented in accordance with academic rules and ethical conduct. I also declare that, as required by these rules and conduct, I have fully cited and referenced all material and results that are not original to this work.**

Name, Last name: Meriç Selamođlu

Signature :

## **ABSTRACT**

### **MODELING TEMPORAL VARIATION OF SCOURING AT DUAL BRIDGE PIERS**

Selamođlu, Meriç

Ph.D., Department of Civil Engineering

Supervisor : Prof. Dr. A. Melih Yanmaz

Co-Supervisor: Assoc. Prof. Dr. Mete Koken

June 2015, 130 pages

Computation of temporal evolution of scour depth around bridge piers is essential for the efficient design of bridge pier footings. In this thesis, empirical scour-prediction equations and a semi-empirical model are developed to predict the temporal variation of maximum clear-water scour depth at dual cylindrical uniform piers with identical size in tandem arrangement. Experiments are conducted using different pier size, pier spacing, and flow intensities. The semi-empirical model is based on sediment continuity approach and volumetric sediment transport rate from the scour hole using a sediment pickup function. The results of the semi-empirical model are presented as design charts giving the dimensionless scour depth versus time relation, for practical use. Results of the proposed model are found to be in relatively good agreement with the experimental results, in the test range.

Keywords: Bridge, Pier, Dual Piers, Clear-Water Scour, Sediment Pickup

## ÖZ

### İKİLİ KÖPRÜ AYAKLARINDAKİ OYULMANIN ZAMANSAL DEĞİŞİMİNİN MODELLENMESİ

Selamoğlu, Meriç

Doktora, İnşaat Mühendisliği Bölümü

Tez Yöneticisi : Prof. Dr. A. Melih Yanmaz

Ortak Tez Yöneticisi : Doç. Dr. Mete Köken

Haziran 2015, 130 sayfa

Köprü ayaklarının uygun tasarımı için, ayaklar etrafındaki oyulmanın zamansal gelişiminin araştırılması önemlidir. Bu tezde, arka arkaya konumlanmış, aynı çapa sahip silindirik ikili köprü ayaklarındaki maksimum oyulmanın zamansal değişimini tespit etmek amacıyla, görgül denklemler türetilmiş ve yarı-görgül bir model geliştirilmiştir. Farklı ayak çapı, ayaklar arası mesafe ve akım koşullarında deneyler gerçekleştirilmiştir. Yarı-görgül model, sürüntü maddesi sürekliliği ve sürüntü maddesi sıçrama fonksiyonu kullanılarak oyulma çukurundan taşınan sürüntü maddesinin hacimsel ifadesine dayanmaktadır. Yarı-görgül modelin sonuçları, pratikte kullanım kolaylığı sağlamak amacıyla boyutsuz oyulma derinliğinin boyutsuz zamana oranını belirten tasarım eğrileri ile sunulmuştur. Deneysel koşullar altında, önerilen model sonuçlarının deneysel sonuçlarla uyumlu olduğu görülmüştür.

Anahtar Kelimeler: Köprü, Orta Ayak, İkili Orta Ayak, Temiz Su Oyulması, Sürüntü Maddesi Sıçraması

To my dear family

## ACKNOWLEDGEMENTS

First of all, I would like to express my deepest gratitude to my supervisor Prof. Dr. A. Melih Yanmaz for his never ending support, guidance, encouragement, and patience throughout this study. Being his student is an invaluable experience for me and I feel myself fortunate to work with him since the very beginning of my graduate study. I appreciate him for sharing his academic knowledge and experience with me. Also, I would like to thank him for teaching me life lessons whenever I need.

I would like to express my sincere appreciation to my co-supervisor Assoc. Prof. Dr. Mete Kken for his invaluable guidance. His contributions have vital role in this study. I learned so much from his experience and I will learn much more in the future studies that we will work on together.

I would also like to thank the members of my thesis monitoring committee, Assoc. Prof. Dr. Őahnaz Tięrek and Assist. Prof. Dr. Msteyde Baduna Koęyięit for their contributions, comments, and suggestions throughout this study.

I would like to thank my dear friends and colleagues Assist. Prof. Dr. M. Tuęrul Ylmaz and Dr. Melih alamak for their supports every time I needed. I am very pleased to work with them and I would also like to thank them for all those tasteful coffee breaks.

I would like to express my appreciation to the faculty members, research assistants, and administrative staff of Water Resources Laboratory. I am very lucky to work with them in such a peaceful environment. Special thanks to Prof. Dr. Zuhal Akyrek and Tlin Ecevit for their lovely attitude. I would also like to thank the assistants and technical staff of Hydromechanics Laboratory for

their invaluable helps throughout my experimental studies. I would like to thank Prof. Dr. Zafer Bozkuş for his efforts to improve the experimental setup.

I would like to express my sincere gratitude to my dear friends and colleagues Alper Önen, Ezgi Köker, Tuğçe Yıldırım, and Ürün Bakar for bringing joy to my life and supporting me whenever I needed. I would like to thank to my dear friends Cem Sonat, Gizem Okyay, Gözde Göksu Gürsoy, N. Aslıcan Yılmaz, and Yaprak Onat who live far away but always there for me. I would like to thank my best friend Bilge Ufuk Güler Aksom for her love and support.

I would like to express my sincere gratitude to my dear grandfather Reha Selamoğlu, grandmother Güler Açıkgöz, aunt Nihal Necipoğlu and Necipoğlu family for their love and faith in me. I would like to thank my brother Arda Selamoğlu for his love, support and making me the luckiest sister ever. My deepest gratitude goes to my dear parents Celal and Hacer Selamoğlu. I would like to thank them for their never ending love and faith in me. I am proud of being their daughter.

Finally, I would like to thank my angels up above, Naşide Selamoğlu and İbrahim Açıkgöz for watching over me.

## TABLE OF CONTENTS

ABSTRACT .....	v
ÖZ.....	vi
ACKNOWLEDGEMENTS .....	viii
TABLE OF CONTENTS .....	x
LIST OF TABLES .....	xiii
LIST OF FIGURES .....	xiv
LIST OF SYMBOLS AND ABBREVIATIONS.....	xix
CHAPTERS	
1. INTRODUCTION.....	1
1.1 Statement of the Problem .....	1
1.2 Objectives of this Study.....	2
1.3 Description of the Thesis.....	3
2. LOCAL SCOUR AT BRIDGE PIERS .....	5
2.1 Introductory Remarks.....	5
2.2 Dimensional Analysis of Scouring Parameters .....	7
2.2.1 Effect of Scaling and Froude Number.....	8
2.2.2 Effect of Approach Flow Depth .....	10
2.2.3 Effect of Flow Intensity.....	11
2.2.4 Effect of Sediment Grading.....	11
2.2.5 Effect of Pier and Sediment Size.....	12

2.2.6	Effect of Time .....	12
2.2.7	Effect of Pier Groups.....	16
2.3	Clear-Water Scour Prediction Methods for Bridge Piers.....	21
2.3.1	Melville and Coleman (2000) Method .....	22
2.3.2	Richardson and Davis (2001) Method.....	22
2.3.3	Oliveto and Hager (2002) Method .....	23
3.	EXPERIMENTAL STUDY .....	25
3.1	Experimental Study .....	25
3.1.1	Experimental Setup and Equipment.....	25
3.1.2	Scope of the Experiments.....	28
3.1.3	Experiments Part I.....	32
3.1.4	Experiments Part II.....	44
4.	EVALUATION OF THE EXPERIMENTAL RESULTS .....	47
4.1	Evaluation of the Experimental Results .....	47
4.1.1	Reinforcing and Sheltering Effect of Dual Piers.....	47
4.1.2	Shear Stress Variation in the Scour Hole around Upstream Pier .....	48
4.1.3	Shape of the Scour Hole.....	49
4.1.4	Maximum Scour Depth Location between Piers.....	51
4.2	Scour Prediction Equations .....	60
5.	DEVELOPMENT OF THE SEMI-EMPIRICAL MODEL.....	61
5.1	The Semi-Empirical Model.....	61
5.1.1	Selection of $\beta$ Combination and Solution Method .....	68
5.1.2	Selection of $\psi$ values .....	69
5.2	Comparison of Scour Prediction Models .....	71

5.3	Design Charts .....	84
6.	CONCLUSIONS .....	89
6.1	Summary and Conclusions .....	89
6.2	Novelty of the Study.....	92
6.3	Recommendations for Future Research.....	93
	REFERENCES .....	95
	APPENDICES	
A.	Bed Topography Maps of the Scour Hole .....	101
B.	Experimental Scour Depth .....	125
	CURRICULUM VITAE .....	129

## LIST OF TABLES

### TABLES

Table 3.1 Characteristic particle sizes of the bed material.....	28
Table 3.2 Scope of the experiments .....	31
Table 4.1 Radial and angular coordinates for runs E2-E3.....	52
Table 4.2 Radial and angular coordinates for runs E4-E7 .....	53
Table 5.1 Decision table for solution method and $\beta$ combination.....	69
Table 5.2 Decision table for $\psi$ value .....	70
Table 5.3 Coefficient and exponents of the functional form of $\beta_I$ .....	71
Table 5.4 Comparison of semi-empirical model with empirical equation .....	83
Table B.1 Experimental $d_s - t$ values .....	126

## LIST OF FIGURES

### FIGURES

Figure 2.1 Vortex systems around a bridge pier (Yanmaz, 2002).....	6
Figure 2.2 Variation of relative scour depth against pier Froude number (Yanmaz, 2002).....	9
Figure 2.3 Variation of relative scour depth against relative approach flow depth (Yanmaz, 2002) .....	10
Figure 2.4 Variation of scour depth with flow intensity (Yanmaz, 2002) .....	11
Figure 2.5 Variation of scour depth with time (Yanmaz, 2002) .....	13
Figure 2.6 Variation of $S$ with respect to $T_s$ in Yanmaz's semi-empirical model (Yanmaz, 2006).....	15
Figure 2.7 Schematic representation of the reinforcing effect (Redrawn from Nazariha (1996)).....	18
Figure 3.1 Plan view of the test flume (not to scale).....	27
Figure 3.2 SeaTek transducer arrays and electronics package (SeaTek, 2015) .....	28
Figure 3.3 Discharge versus head over the sharp-crested weir .....	29
Figure 3.4 Bed topography maps of (a) Run E2 and (b) Run E3 at $t = 360$ min....	34
Figure 3.5 Three-dimensional view of the scour holes of (a) Run E2 and (b) Run E3 at $t=360$ min .....	35
Figure 3.6 Photograph of the final scour hole of Run E3 .....	36
Figure 3.7 Scour hole cross-section of Run E2 at the front pier ( $x=50.75$ cm).....	37
Figure 3.8 Scour hole cross-section of Run E2 at the dune ( $x=65$ cm).....	37
Figure 3.9 Scour hole cross-section of Run E2 at the rear pier ( $x=73.25$ cm) .....	38
Figure 3.10 Scour hole cross-section of Run E3 at the front pier ( $x=50.75$ cm)....	38
Figure 3.11 Scour hole cross-section of Run E3 at the dune ( $x=69.5$ cm).....	39

Figure 3.12 Scour hole cross-section of Run E3 at the rear pier (x=80.75 cm) .....	39
Figure 3.13 Bed profile of Run E2 (y=0) .....	41
Figure 3.14 Bed profile of Run E3 (y=0) .....	42
Figure 3.15 Experimental results for $d_s - t$ relation .....	45
Figure 3.16 Comparison of scour depth at different axes for Run E11-12 .....	46
Figure 4.1 Variation of bed shear stress at the pier nose.....	49
Figure 4.2 Definition sketch for the characteristic dimensions of the scour hole ..	50
Figure 4.3 Correlation between $X/X_{max} - Z/Z_{max}$ .....	50
Figure 4.4 Correlation between $Y/Y_{max} - Z/Z_{max}$ .....	51
Figure 4.5 Correlation between $Y'/Y'_{max} - Z/Z_{max}$ .....	51
Figure 4.6 Location of the maximum scour depth between piers for Run E2 .....	54
Figure 4.7 Location of the maximum scour depth between piers for Run E3 .....	55
Figure 4.8 Location of the maximum scour depth between piers for Run E4 .....	56
Figure 4.9 Location of the maximum scour depth between piers for Run E5 .....	57
Figure 4.10 Location of the maximum scour depth between piers for Run E6 .....	58
Figure 4.11 Location of the maximum scour depth between piers for Run E7 .....	59
Figure 5.1 Variation of $\beta$ with time for Runs E11.....	64
Figure 5.2 Variation of $\beta$ with time for Runs E12 .....	65
Figure 5.3 Variation of $\beta$ with time for Runs E13 .....	65
Figure 5.4 Variation of $\beta$ with time for Runs E14 .....	66
Figure 5.5 Variation of $\beta$ with time for Runs E15 .....	66
Figure 5.6 Variation of $\beta$ with time for Runs E16 .....	67
Figure 5.7 Variation of $\beta$ with time for Runs E17 .....	67
Figure 5.8 Comparison for Run E11-8.....	72
Figure 5.9 Comparison for Run E11-10.....	73
Figure 5.10 Comparison for Run E11-12.....	73
Figure 5.11 Comparison for Run E12-8.....	74
Figure 5.12 Comparison for Run E12-10.....	74
Figure 5.13 Comparison for Run E12-12.....	75
Figure 5.14 Comparison for Run E13-8.....	75

Figure 5.15 Comparison for Run E13-10 .....	76
Figure 5.16 Comparison for Run E13-12 .....	76
Figure 5.17 Comparison for Run E14-8 .....	77
Figure 5.18 Comparison for Run E14-10 .....	77
Figure 5.19 Comparison for Run E14-12 .....	78
Figure 5.20 Comparison for Run E15-8 .....	78
Figure 5.21 Comparison for Run E15-10 .....	79
Figure 5.22 Comparison for Run E15-12 .....	79
Figure 5.23 Comparison for Run E16-8 .....	80
Figure 5.24 Comparison for Run E16-10 .....	80
Figure 5.25 Comparison for Run E16-12 .....	81
Figure 5.26 Comparison for Run E17-8 .....	81
Figure 5.27 Comparison for Run E17-10 .....	82
Figure 5.28 Comparison for Run E17-12 .....	82
Figure 5.29 Design chart for $\lambda = 0.5$ and $k = 85.23$ .....	85
Figure 5.30 Design chart for $\lambda = 0.33$ and $k = 85.23$ .....	85
Figure 5.31 Design chart for $\lambda = 0.25$ and $k = 85.23$ .....	86
Figure 5.32 Design chart for $\lambda = 0.33$ and $k = 71.59$ .....	86
Figure 5.33 Design chart for $\lambda = 0.25$ and $k = 71.59$ .....	87
Figure 5.34 Design chart for $\lambda = 0.33$ and $k = 45.45$ .....	87
Figure 5.35 Design chart for $\lambda = 0.25$ and $k = 45.45$ .....	88
Figure A.1 Bed topography map of run E2 at $t = 5$ min.....	102
Figure A.2 Bed topography map of run E2 at $t = 10$ min.....	102
Figure A.3 Bed topography map of run E2 at $t = 15$ min.....	103
Figure A.4 Bed topography map of run E2 at $t = 20$ min.....	103
Figure A.5 Bed topography map of run E2 at $t = 30$ min.....	104
Figure A.6 Bed topography map of run E2 at $t = 45$ min.....	104
Figure A.7 Bed topography map of run E2 at $t = 60$ min.....	105
Figure A.8 Bed topography map of run E2 at $t = 80$ min.....	105
Figure A.9 Bed topography map of run E2 at $t = 100$ min.....	106

Figure A.10 Bed topography map of run E2 at t = 150 min.....	106
Figure A.11 Bed topography map of run E2 at t = 360 min.....	107
Figure A.12 Bed topography map of run E3 at t = 5 min.....	107
Figure A.13 Bed topography map of run E3 at t = 10 min.....	108
Figure A.14 Bed topography map of run E3 at t = 15 min.....	108
Figure A.15 Bed topography map of run E3 at t = 20 min.....	109
Figure A.16 Bed topography map of run E3 at t = 30 min.....	109
Figure A.17 Bed topography map of run E3 at t = 45 min.....	110
Figure A.18 Bed topography map of run E3 at t = 60 min.....	110
Figure A.19 Bed topography map of run E3 at t = 80 min.....	111
Figure A.20 Bed topography map of run E3 at t = 100 min.....	111
Figure A.21 Bed topography map of run E3 at t = 150 min.....	112
Figure A.22 Bed topography map of run E3 at t = 360 min.....	112
Figure A.23 Bed topography map of run E4 at t = 5 min.....	113
Figure A.24 Bed topography map of run E4 at t = 20 min.....	113
Figure A.25 Bed topography map of run E4 at t = 60 min.....	114
Figure A.26 Bed topography map of run E4 at t = 100 min.....	114
Figure A.27 Bed topography map of run E4 at t = 150 min.....	115
Figure A.28 Bed topography map of run E4 at t = 360 min.....	115
Figure A.29 Bed topography map of run E5 at t = 5 min.....	116
Figure A.30 Bed topography map of run E5 at t = 20 min.....	116
Figure A.31 Bed topography map of run E5 at t = 60 min.....	117
Figure A.32 Bed topography map of run E5 at t = 100 min.....	117
Figure A.33 Bed topography map of run E5 at t = 150 min.....	118
Figure A.34 Bed topography map of run E5 at t = 360 min.....	118
Figure A.35 Bed topography map of run E6 at t = 5 min.....	119
Figure A.36 Bed topography map of run E6 at t = 20 min.....	119
Figure A.37 Bed topography map of run E6 at t = 60 min.....	120
Figure A.38 Bed topography map of run E6 at t = 100 min.....	120
Figure A.39 Bed topography map of run E6 at t = 150 min.....	121

Figure A.40 Bed topography map of run E6 at $t = 360$ min.....	121
Figure A.41 Bed topography map of run E7 at $t = 5$ min.....	122
Figure A.42 Bed topography map of run E7 at $t = 20$ min.....	122
Figure A.43 Bed topography map of run E7 at $t = 60$ min.....	123
Figure A.44 Bed topography map of run E7 at $t = 100$ min.....	123
Figure A.45 Bed topography map of run E7 at $t = 150$ min.....	124
Figure A.46 Bed topography map of run E7 at $t = 360$ min.....	124

## LIST OF SYMBOLS AND ABBREVIATIONS

$A$	surface area of the scour hole
$A_0$	initial cross-sectional area of the primary vortex
$A_p$	unit area for sediment pickup
$A_s$	cross-sectional area of the primary vortex at any scour depth
$A_t$	cross-sectional area of the primary vortex at any time
$A^*$	dimensionless surface area of the scour hole
$a$	coefficient
$b$	pier diameter
$c_1, c_2$	coefficient
$D_{50}$	median sediment size
$D_v$	thickness of the separated boundary layer
$D_*$	dimensionless particle diameter
$d$	pier spacing
$d_0$	approach flow depth
$d_s$	scour depth
$d_{se}$	equilibrium scour depth
$E$	sediment pickup rate
$F$	square root of Shields' parameter
$F_d$	densimetric particle Froude number
$F_r$	flow Froude number
$F_{rp}$	pier Froude number
$g$	gravitational acceleration
$H$	head over the sharp-crested weir
$i$	number of piers normal to the flow
$j$	number of piers in-line with the flow
$K_b$	factor for bed condition

$K_d$	factor for effect of relative pier size
$K_I$	flow intensity factor
$K_{ij}$	factor for group effect of piers
$K_j$	factor for group effect of piers
$K_s$	factor for effect of pier shape
$K_{yb}$	factor for the combined effects of flow depth and pier size
$K_z$	factor for armoring effect
$K_\alpha$	factor for effect of angle of approach flow
$K_\sigma$	adjustment coefficient for sediment grading
$k$	ratio of pier diameter to median sediment size
$L_p$	pier length
$L_R$	reference length
$m$	coefficient
$p$	coefficient
$Q$	discharge
$Q_{si}$	sediment transport rate into the scour hole
$Q_{so}$	sediment transport rate from the scour hole
$R$	hydraulic radius
$R^2$	correlation coefficient
$Re$	flow Reynolds number
$R_p$	particle Reynolds number
$r$	radial coordinate
RMSE	root mean square error of the estimate
$S$	dimensionless scour depth
$S_0$	bed slope
$T$	transport-stage parameter due to scouring
$T_d$	dimensionless time of scour
$T_s$	dimensionless time
$t$	time
$t_e$	time to develop equilibrium scour depth
$t_R$	reference time
$u$	mean approach flow velocity

$u_c$	mean threshold velocity of approach flow
$u_*$	shear velocity in the approach flow
$u_{*c}$	critical shear velocity of the sediment
$V$	volume of the scour hole
$V^*$	dimensionless volume of the scour hole
$X$	longitudinal scour hole width at any time
$X_{\max}$	maximum longitudinal scour hole width
$x_1, x_2, x_3$	exponent
$Y$	transversal scour hole width at any time
$Y_{\max}$	maximum longitudinal scour hole width
$Y'$	transversal scour hole width at rear pier at any time
$Y'_{\max}$	maximum transversal scour hole width at rear pier
$Z$	bed level at any time
$Z_{\max}$	maximum bed level
$\alpha$	angle of approach flow with the pier axis
$\beta$	coefficient of proportionality
$\Delta$	relative density
$\gamma$	specific weight of water
$\theta$	angular coordinate
$\lambda$	pier diameter to pier spacing ratio
$\nu$	kinematic viscosity of water
$\phi$	angle of repose of the sediment
$\rho$	water density
$\rho_s$	sediment density
$\sigma_g$	geometric standard deviation of sediment size distribution
$\tau_0$	bed shear stress of the approach flow
$\tau_b$	bed shear stress on flat region of the scour hole
$\tau_{bc}$	critical bed shear stress on flat region of the scour hole
$\tau_{cr}$	critical bed shear stress on flat bed
$\psi$	factor depending on turbulent fluctuations and oscillation of primary vortex



## CHAPTER 1

### INTRODUCTION

#### 1.1 Statement of the Problem

The most common reason for failure of bridges on alluvial beds is the excessive local scouring at bridge infrastructural elements, i.e. piers and abutments. To avoid or decrease the failure risk of bridges due to excessive scouring, foundations of these elements and necessary scour countermeasures need to be properly designed via detailed investigation of local scour mechanism (Yanmaz and Apaydın, 2012). Therefore, determination of local scour depth in close vicinity of bridge foundations has received significant attention since the mid of the 20<sup>th</sup> century (Köse and Yanmaz, 2010). Concentrating on the local scour at bridge piers, most of the previous studies have been devoted to the determination of equilibrium scour depth at single piers. Complex nature of scouring process with three-dimensional flow-pier-sediment interaction raised the difficulties in analytical formulation of the local scour phenomenon (Yanmaz and Altınbilek, 1991; Nazariha, 1996). Therefore, numerous empirical equations have been derived for the prediction of the equilibrium depth of scour for particular range of experimental conditions, such as flow characteristics, bridge pier characteristics and sediment properties. Despite the availability of many scour-prediction equations, there is no single equation, which is valid for wide ranges of the aforementioned parameters. This is mainly because of the complexity of modeling

the phenomenon concerning the combined effects of three-dimensional separation at bridge piers with highly turbulent characteristics, non-uniformity of sediment, development and interaction of vortex systems around piers, and time-dependent flow pattern and sediment transport mechanism in the scour hole. Although every equation is valid for its derivation condition, when these are applied to a common problem, the results may differ widely from each other, as a consequence of model calibration absence. Due to observational difficulties during floods, very limited field data are available, which results in model calibration problems. Therefore, none of the available empirical equations is applicable to universal conditions.

## **1.2 Objectives of this Study**

Bridge foundations are mostly designed in pier groups in the field, rather than a single pier. In case of group of piers, the scouring process becomes further complex due to the interaction of local scour mechanisms of piers in close vicinity. When groups of piers are in a range that their individual scour holes overlap, flow-pier-sediment interaction is exposed to additional scour mechanisms, compared to a single pier case. Therefore, prediction of local scour at pier groups via empirical equations derived for single pier cases will ignore these additional pier group scour mechanism. In contrast to the single pier case, there are few studies on the pier groups. Those available studies on pier groups emphasize the group effect on the maximum local scour depth by developing empirical correction factors to available scour prediction equations for single pier cases.

The aim of this study is to obtain empirical equations and to develop a semi-empirical model to predict the temporal variation of the maximum clear-water scour depth at dual cylindrical uniform piers in tandem arrangement. The semi-empirical model development is based on the application of sediment continuity equation and volumetric sediment transport rate from the scour hole. Temporal evolution of the scour hole volume around the dual piers is obtained by the experimental data and the sediment transport rate from scour hole is formulated

using a sediment pickup function. The findings are integrated in the sediment continuity equation of the scour hole and the temporal variation of the maximum scour depth, which occurs at the upstream pier, is obtained. The results of the semi-empirical model are presented in the design charts for the dimensionless form of scour depth and duration, for the practical use in the prediction of maximum scour depth variation at tandem piers. This study aims to meet the lack of explicit prediction of time-dependent maximum scour depth at dual bridge piers.

In the scope of the thesis, series of experiments are conducted in a laboratory medium. Pier models with different sizes are tested. The tests are run under different flow intensities in clear-water scour range. Therefore, the model includes the effect of pier size and flow intensity on the scour depth. Moreover, experiments are conducted with different spacing in between in a range that scour holes around front and rear piers are overlapping. This model enables a designer to perform proper foundation design, considering flow-sediment interaction. With a known design flow rate and its time to peak value, the expected depth of scour is obtained corresponding to this time level.

### **1.3 Description of the Thesis**

This thesis is composed of five chapters with the following contents:

In Chapter 1, an introduction to the thesis is presented by giving the problem statement and objectives of the study.

The mechanism of local scour at bridge piers is explained by highlighting the effects of parameters in Chapter 2. A detailed explanation for the time effect and pier group effect is given, while the previous studies in the literature are reviewed.

The experimental studies of this thesis are introduced in Chapter 3, giving the details of the test setup and scope of the experiments.

In Chapter 4, the results of the experiments are presented and discussed. Empirical scour prediction equations are also proposed in this chapter.

In Chapter 5, development of the semi-empirical model to predict the time-dependent maximum scour depth at dual piers is explained. Comparison of the experimental and computed variation of scour depth relative to time is given with reference to both empirical and semi-empirical approaches. Design charts for the prediction of time-dependent dimensionless scour depth are presented.

A summary and conclusions of the thesis are given in Chapter 6. The novelty of the study is explained and some recommendations for the future works are given.

In Appendix A, the bed topography maps obtained in the Experiments Part I are presented.

The variation of maximum scour depth with time obtained in the Experiments Part II is shown in tabular form in Appendix B.

## CHAPTER 2

### LOCAL SCOUR AT BRIDGE PIERS

#### 2.1 Introductory Remarks

A brief information about the development of the scour process at single piers is given first. Similar trends also develop around group of piers. However, additional effects concerning interaction of vortex systems are more pronounced in this case, which is explained later in this chapter.

The presence of a bridge pier in a flow field reduces the net flow area, thus accelerates the local flow field. Water surface elevation at the upstream face of the pier increases due to a sudden decrease of velocity and formation of a stagnation pressure plane. Increase in the water surface elevation depends on the mean velocity of the approach flow,  $u$ , and the geometric characteristics of the bridge pier. The three-dimensional turbulent boundary layer separates due to increase in pressure at the upstream face of the pier. Since  $u$  decreases from the free surface downwards, the stagnation pressures,  $\rho u^2/2$ , also decrease from the surface downwards. Here,  $\rho$  is the density of water. Decrease in the stagnation pressure results in a downward pressure gradient, so a downward velocity component. So-called horse-shoe vortices at the bed level are created by the interference of the downward velocity component with the approach flow as shown in Figure 2.1. The downflow acts like a vertical jet grooving the bed in front of the pier and the eroded material is carried around the pier by the combined action of accelerating

flow and the spiral motion of the horse-shoe vortex. The horse-shoe vortex extends downstream through the sides of the pier for a distance of few pier diameters, then loses its identity and becomes part of the general turbulence. The strength of these vortices depends on the flow Reynolds number,  $R_e$  and the geometric characteristics of the bridge pier.

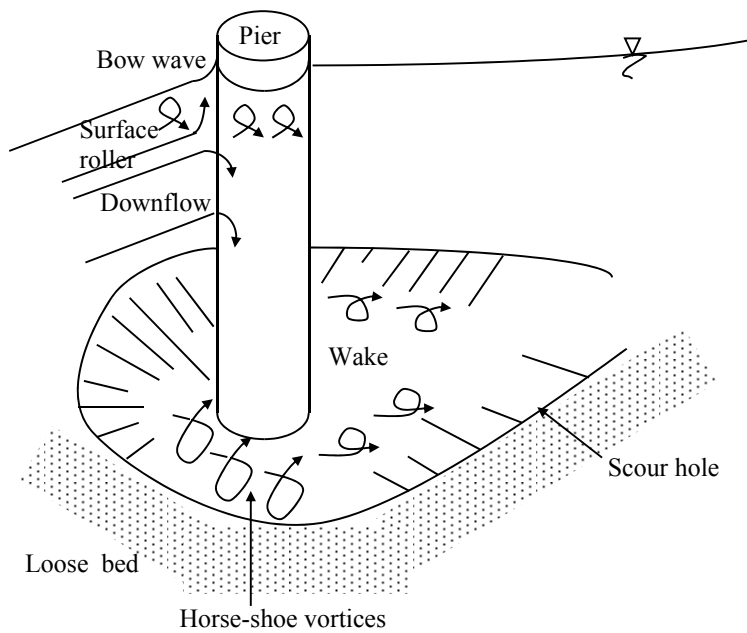


Figure 2.1 Vortex systems around a bridge pier (Yanmaz, 2002)

Wake vortices, which occur at the sides and back of the pier, develop as a result of shear stress gradients in the separated negative-pressure zone around the bridge pier, as shown in Figure 2.1. Transportation of the eroded material from the bed to the downstream by the wake vortices are related to the flow intensity and the geometric characteristics of the pier. The eroded particles are carried in the downstream direction until the effect of wake vortices diminish. The horse-shoe vortices are stronger than wake vortices. Thus, the maximum scour depths are observed at the upstream side of the pier. To identify relevant variables involved in the scouring phenomenon, a dimensional analysis is presented below for a single pier. The effects of governing variables are discussed in the following sections.

Further information is given in detail for the group effect of piers on scour development process.

## 2.2 Dimensional Analysis of Scouring Parameters

Estimation of the maximum scour depth at a bridge pier is required for the safe design of a bridge on alluvial river. Several researchers have studied the problem extensively. However, no single analytically derived equation is available due to the complexity of the scouring process, such as combined effects of complex turbulent boundary layer, time-dependent flow pattern, and sediment transport mechanism in the scour hole (Yanmaz and Altınbilek, 1991). To examine the interrelationship of the dimensionless terms, which are effective on the development of the scour hole around bridge piers, a dimensional analysis is performed. The following functional relationship can be proposed for a vertically mounted single uniform pier on a wide river with cohesionless bed material.

$$f(d_s, \rho, \nu, g, d_0, u, \alpha, u_c, S_0, \rho_s, D_{50}, \sigma_g, b, K_s, t) = 0 \quad (2.1)$$

where  $d_s$  is the depth of scour,  $\nu$  is the kinematic viscosity of water,  $g$  is the gravitational acceleration,  $d_0$  is the depth of approach flow,  $\alpha$  is the angle of approach flow with the pier axis,  $u_c$  is the mean threshold velocity of approach flow,  $S_0$  is the bed slope,  $\rho_s$  is the sediment density,  $D_{50}$  is the median sediment size,  $\sigma_g$  is the geometric standard deviation of sediment size distribution,  $b$  is the characteristic size of pier perpendicular to flow direction,  $K_s$  is the factor indicating the effect of pier shape, and  $t$  is time. For the sake of simplicity in describing the scouring mechanism, prismatic channel is considered with bed material of quartz sand. Pier shape is selected to be uniformly cylindrical and angle of attack of flow is  $0^\circ$ . Therefore, both  $S_0$  and relative density,  $\Delta$  values are constant, where  $\Delta = (\rho_s - \rho) / \rho$ ,  $K_s = 1$ , and the correction factor for  $\alpha$ , i.e.  $K_\alpha = 1$ . Further information is available on the effect of pier shape and alignment on the scour depth (Yanmaz, 2002). By using Buckingham's  $\pi$  theorem, the

dimensionless terms are determined (Shames, 1992). By taking  $\rho$ ,  $u$ , and  $b$  as repeating variables and arranging the dimensionless terms, the following expression is obtained:

$$\frac{d_s}{b} = f_1 \left( \frac{u}{\sqrt{gd_0}}, \frac{uD_{50}}{\nu}, \frac{d_0}{b}, \frac{u}{u_c}, \frac{ut}{b}, \frac{b}{D_{50}}, \sigma_g \right) \quad (2.2)$$

where  $d_s/b$  is the relative scour depth,  $u/\sqrt{gd_0}$  is the flow Froude number ( $F_r$ ),  $uD_{50}/\nu$  is the particle Reynolds number ( $R_p$ ),  $d_0/b$  is the relative approach flow depth,  $u/u_c$  is said to be flow intensity, which reflects the type of bed regime, and  $b/D_{50}$  is the relative pier size. For fully-developed turbulent flow with live bed characteristics, effect of Reynolds number may be ignored. Therefore,

$$\frac{d_s}{b} = f_2 \left( F_r, \frac{d_0}{b}, \frac{u}{u_c}, \frac{ut}{b}, \frac{b}{D_{50}}, \sigma_g \right) \quad (2.3)$$

Effects of the governing parameters given in Eq. (2.3) on the scouring phenomenon are discussed in following sections.

### 2.2.1 Effect of Scaling and Froude Number

The scale effect for experiments on piers has been discussed by Ettema et al. (1998). The Froude number may be re-defined to specifically account for the effect of local energy gradients for flow around piers. By dividing the stagnation pressure head at the upstream face of a pier, by the pier size the dimensionless term in the form of the square of the pier Froude number,  $F_{rp} = u^2/gb$  can be obtained. Ettema et al. (1998) indicated that the scour depth at piers do not scale linearly with pier size unless there is complete geometric similitude of pier, flow, and bed material. Similitude of experimental scour depth data to the field data requires the constancy of  $F_r$ ,  $u/u_c$ , and  $d_0/b$ . However, in flume experiments, bed materials which have comparable sizes as the prototype are normally used since very fine particles in a laboratory medium would be subject to suspension. Therefore, to maintain similar modes of sediment transportation, the dimensionless

term accounting for the sediment coarseness,  $b/D_{50}$ , cannot satisfy the length scale selected according to the other geometric characteristics, such as pier width, flow depth, etc. So, the constancy of  $b/D_{50}$  cannot be maintained.

To attain a desired particle mobility level, the value of  $u/u_c$  should be the same in the laboratory and the field. This implies that greater values of  $u$  are needed in a laboratory medium than required in Froude number simulation. Hence,  $F_r$  used in experiments may be greater than that of the corresponding field conditions. On the other hand, as can be seen in Figure 2.2, relative scour depth,  $d_s/b$ , increases with increasing  $F_r$  in the range of the available data. However, to formulate the effect of  $F_r$ , a wider range of data is needed. Therefore, greater scour depths relative to the pier width can be obtained under clear-water conditions in a laboratory medium, than any likely to occur in field. As a concluding remark, empirical scour prediction equations using laboratory data overestimate the scour depths, and hence can be assumed to give conservative values for the design.

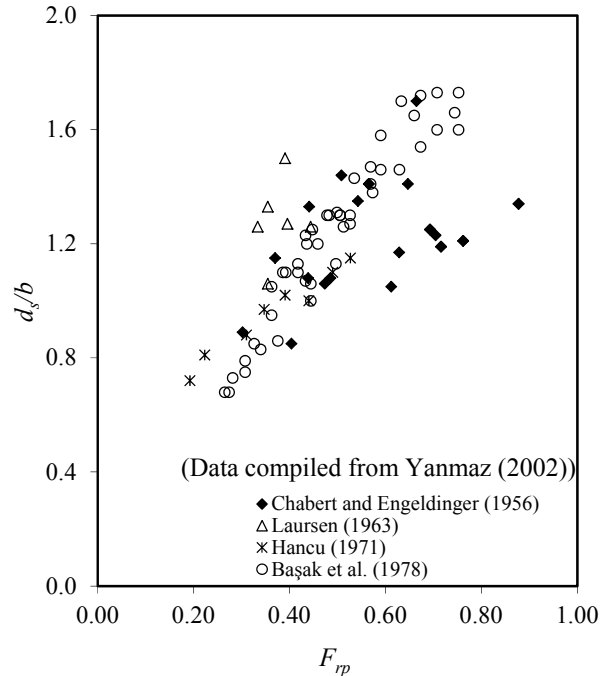


Figure 2.2 Variation of relative scour depth against pier Froude number (Yanmaz, 2002)

## 2.2.2 Effect of Approach Flow Depth

Existence of a pier in a flow section would lead to the development of a surface roller, which rotates in counter-clockwise direction, i.e. in the opposite direction of the horse-shoe vortex at the bed level. For shallow flows, the surface roller tends to retard the downflow. Therefore, it leads to reduction of scour depth. Melville and Coleman (2000) classify piers as narrow, intermediate width, and wide with respect to  $d_0/b$  ratio using the following limiting values: For deep flows with narrow piers ( $d_0/b > 1.43$ ), the scour depth is independent of flow depth but depends on  $b$ . Conversely, for shallow flows with wider piers ( $d_0/b \leq 0.2$ ), the scour depth is independent of  $b$  but varies linearly with  $d_0$ . For intermediate width piers, i.e.  $0.2 < d_0/b \leq 1.43$ , the scour depth is proportional to the square root of the product of  $d_0$  and  $b$ . When the available clear-water data in the literature are plotted as  $d_s/b$  versus  $d_0/b$ , it is observed that the design curves suggested by Melville and Coleman (2000) bound the available clear-water scour data (See Figure 2.3). Furthermore, the studies of Melville and Coleman (2000) show that the live bed data are also bounded by these limiting curves.

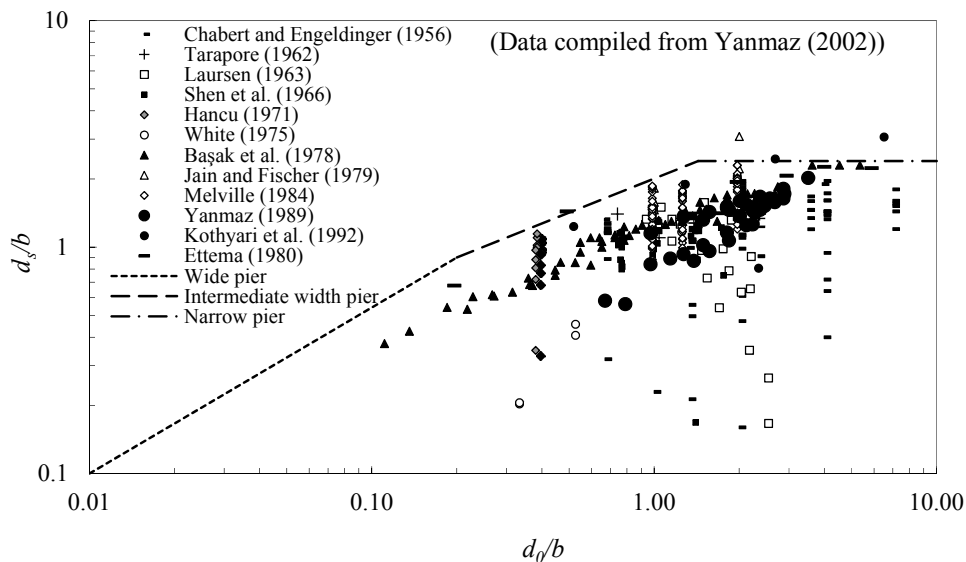


Figure 2.3 Variation of relative scour depth against relative approach flow depth (Yanmaz, 2002)

### 2.2.3 Effect of Flow Intensity

For clear-water conditions, the scour depth increases considerably with increasing approach flow velocity up to a threshold peak at which a maximum value is attained, as can be seen from Figure 2.4. Provided that the sediment is uniform, the scour depth increases almost linearly with flow intensity to its maximum value at the threshold velocity,  $u/u_c = 1$  (Melville and Chiew, 1999). According to previous studies in the literature, the scour depth decreases from its threshold peak to a minimum at about  $u/u_c = 1.5-2.0$ . At this value of flow intensity, the bed generally has steepest features. Depth of scour increases again with further increase in the flow intensity up to a new peak value at the transition flat bed condition. Over the transition flat bed, the form drag component of energy loss is absent and a great amount of flow energy is used for sediment transport and scouring. At still higher relative velocities under upper flow regime, bed forms develop again and dissipate some of the flow energy. Then, the scour depth decreases slightly. However, there are limited data for this range.

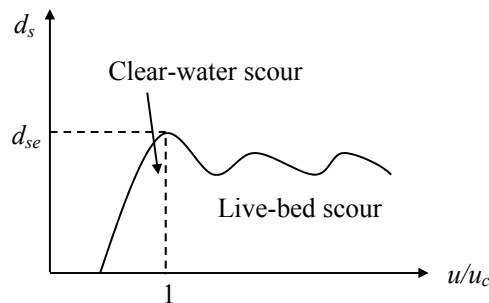


Figure 2.4 Variation of scour depth with flow intensity (Yanmaz, 2002)

### 2.2.4 Effect of Sediment Grading

Based on their laboratory experiments, Raudkivi and Ettema (1983) stated that sediment grading has a strong effect on the equilibrium depth of clear-water scour. As the geometric standard deviation of the grain size distribution increases, larger grains apply an armoring effect to the underlying sediment, and hence the depth of scour decreases. An adjustment coefficient,  $K_\sigma$ , relative to uniform sediment is

introduced by Raudkivi (1986). Yanmaz (2002) proposed a best-fit equation to the graphical representation of Raudkivi (1986) for  $1.0 \leq \sigma_g \leq 5.0$  as follows:

$$K_\sigma = 0.013\sigma_g^5 - 0.22\sigma_g^4 + 1.41\sigma_g^3 - 4.09\sigma_g^2 + 5.01\sigma_g - 1.12 \quad (2.4)$$

For a typical gravel-river with  $\sigma_g = 3.5$ , the expected scour depth is only 20% of the scour depth that is likely to occur for uniformly graded sediment case. The effect of sediment grading on the depth of live-bed scour is further complex. However, there is very limited information on this topic.

### 2.2.5 Effect of Pier and Sediment Size

Effect of relative pier size,  $b/D_{50}$ , on the development of scour has been investigated by Ettema (1980). The results indicated that the particles are coarse compared to the groove excavated by the downflow for the range of  $b/D_{50} < 25$ , and the erosion process is hindered. A significant fraction of the downflow penetrates the coarse bed material and dissipates its energy (Breusers and Raudkivi, 1991). The relative scour depth is observed to be independent of the relative pier size for  $b/D_{50} \geq 25$ . An adjustment coefficient,  $K_d$ , is introduced by Melville and Coleman (2000) for  $b/D_{50} < 25$ :

$$K_d = 0.57 \log \left( 2.24 \frac{b}{D_{50}} \right) \quad (2.5)$$

### 2.2.6 Effect of Time

Previous studies are mostly concentrated on determination of equilibrium scour depth at single piers using steady flow conditions. Limited studies based on determination of scour depth in unsteady flow conditions are conducted e.g. Kothyari et al. (1992), Hager and Unger (2010), Schillinger (2011), and Kalantari (2014). The equilibrium scour depth under clear-water conditions is attained when combined effects of the temporal mean shear stress, the weight component, and the turbulent agitation are in equilibrium in the scour hole. The equilibrium condition

is reached asymptotically with time, as can be seen in Figure 2.5 and in a laboratory medium it takes several days (Breusers et al., 1977; Raudkivi, 1986; Melville and Chiew, 1999; Melville and Coleman, 2000). For the time to develop the equilibrium scour depth,  $t_e$ , several criteria were proposed by researchers (Cardoso and Bettess, 1999; Melville and Chiew, 1999; Simarro-Grande and Martin-Vide, 2004). Generally, in a 24-hour experimental duration, the equilibrium scour depth is accepted to be reached, when the increase in the depth of scour is below a threshold value. Melville and Chiew (1999) and Grimaldi et al. (2006) proposed this increase to be less than 5% and 1.7% of the pier diameter, respectively, and Fael et al. (2006) suggested it to be less than  $2D_{50}$ . Setia (2008) stated that in laboratory medium, equilibrium scour condition cannot be reached even in 100 hours of experimental duration. However, peak value of the design hydrograph in the field may not last long as the time to reach the equilibrium condition (Melville and Chiew, 1999; Mia and Nago, 2003). Therefore, design of pier foundations on the basis of equilibrium scour depths under clear-water conditions may overestimate the design depth of footings, resulting in uneconomical design. For a known time to peak value of the design flood hydrograph, smaller scour depths are obtained relative to the case of equilibrium condition, which reduce the total cost of construction (Yanmaz and Altunbilek, 1991; Yanmaz, 2006). Therefore, a realistic mean for hydraulic design is provided by investigation of temporal evolution of scour depth.

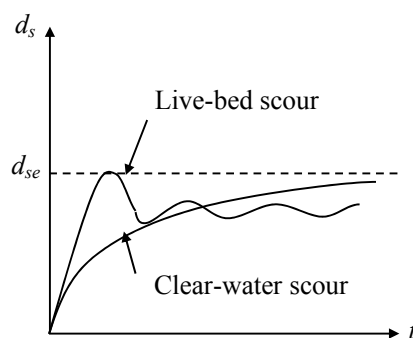


Figure 2.5 Variation of scour depth with time (Yanmaz, 2002)

The studies on the temporal variation of scour depth at single bridge piers have been pioneered by Chabert and Engeldinger (1956) and Ettema (1980). While mainly focusing on the determination of equilibrium time,  $t_e$ , Melville and Chiew (1999) proposed a method for the temporal development of pier scour on the basis of experimental data of Ettema (1980) and new experiments. They proposed the following equation for the temporal evolution of scour depth:

$$\frac{d_s}{d_{se}} = \exp \left\{ -0.03 \left| \frac{u_c}{u} \ln \left( \frac{t}{t_e} \right) \right|^{1.6} \right\} \quad (2.6)$$

where,  $d_{se}$  is the equilibrium scour depth. In Section 2.3, some of the empirical equations to predict  $d_{se}$  will be presented. For the implementation of Eq. (2.6),  $t_e$  can be determined by (Melville and Chiew, 1999):

$$t_e (\text{days}) = 48.26 \frac{b}{u} \left( \frac{u}{u_c} - 0.4 \right) \quad \frac{d_0}{b} > 6 \quad (2.7a)$$

$$t_e (\text{days}) = 30.89 \frac{b}{u} \left( \frac{u}{u_c} - 0.4 \right) \left( \frac{d_0}{b} \right)^{0.25} \quad \frac{d_0}{b} \leq 6 \quad (2.7b)$$

The time-dependent clear-water scour depth has been studied by Kothyari et al. (1992) and Kothyari and Kumar (2012) at circular uniform and circular compound piers, respectively. With the use of the concept of primary vortex introduced in Kothyari et al. (1992), they also developed a relation for the time variation of shear stresses inside the scour hole. A semi-empirical model was developed by Yanmaz and Altınbilek (1991) to predict the clear-water scour depth at single cylindrical and square piers. Their model was updated by Yanmaz (2006) for cylindrical piers. This model is based on the application of the sediment continuity equation to the scour hole around a single cylindrical pier under clear-water conditions. In his model, variation of depth of scour with time is calculated by the first order nonlinear equation (Eq. (2.8)). For practical use,  $d_s$  versus  $t$  relation is converted to dimensionless scour depth,  $S$  versus dimensionless time,  $T_s$  as can be seen in

Eq. (2.9). Furthermore, the dimensionless relation is presented as design charts in Figure 2.6.

$$\frac{d(d_s)}{dt} = \frac{1.2 \left( \frac{u_* t}{b} \right)^{-0.95} \left( \frac{d_s}{b \tan \phi} \right)^{0.37} TD_*^{0.24} \sigma_g^{1.9} D_{50} \sqrt{\Delta g D_{50}} \left( \frac{2d_s}{\tan \phi} + b \right)}{\frac{\pi \Delta}{\tan \phi} \left( \frac{d_s^2}{\tan \phi} + b d_s \right)} \quad (2.8)$$

$$\frac{dS}{dT_s} = \frac{aS^{0.37} (2S \cot \phi + 1)}{T_s^{0.95} (S^2 \cot \phi + S)} \quad (2.9)$$

where,

$$a = 0.231 (\tan \phi)^{0.63} \left( \frac{u_* b}{D_{50} \sqrt{\Delta g D_{50}}} \right)^{-0.95} TD_*^{0.24} \sigma_g^{1.9} \quad (2.10)$$

Details of the model development and the terms appearing in the Eqs. (2.8-2.10) will be discussed in Chapter 5.

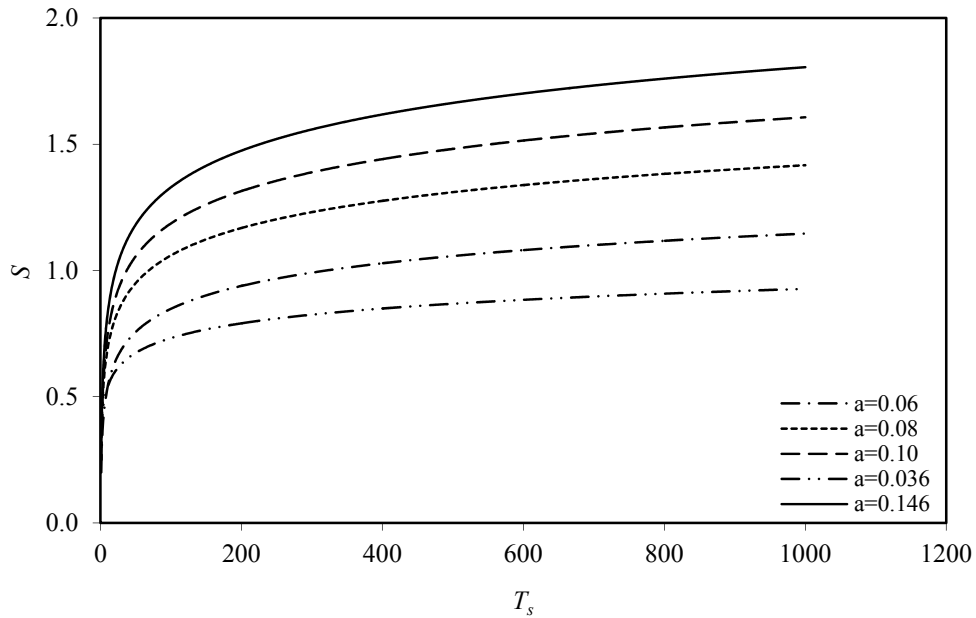


Figure 2.6 Variation of  $S$  with respect to  $T_s$  in Yanmaz's semi-empirical model (Yanmaz, 2006)

Mia and Nago (2003) proposed further semi-empirical model to determine the time development of scour depth at circular uniform piers and Lu et al. (2011) modified the model for circular compound piers. They both utilized the concept of primary vortex by Kothyari et al. (1992). Guo (2014) proposed a semi-empirical model to determine the temporal variation of clear water scour at piers in prototype conditions. Hong et al. (2012) introduced a model for time-dependent variation of clear water scour at cylindrical piers using support vector regression approach.

The scour hole volume in the semi-empirical studies mentioned above was approximated by the volume of an inverted frustum of a cone. The time-dependent evolution of pier scour has been further studied by Kothyari and Ranga Raju (2001), Oliveto and Hager (2002), Chang et al. (2004), Sheppard et al. (2004), and Oliveto and Hager (2005).

### **2.2.7 Effect of Pier Groups**

A bridge foundation may be designed including group of piers, instead of a single pier, according to geotechnical and structural requirements. In case of pier groups, the piers may be placed in many different arrangements. Pier groups may be arranged as tandem, where two piers are located at the centerline aligned with the flow; as side-by-side, where two piers are located normal to the flow; or as  $(i \times j)$ , where  $i$  is the number of piers normal to the flow and  $j$  is the number of piers in-line with the flow. Piers may also be staggered or triangular, where the piers are placed with an angle between each other relative to the flow axis. Due to sediment-laden flow interaction between piers, the scour mechanism is further complex and prediction of the local scour depth is relatively difficult compared to a single pier case (Ataie-Ashtiani and Beheshti, 2006). For this reason, there is comparatively limited information in the literature on the effect of pier groups on scouring.

Previous experimental studies on pier groups are mostly on the basis of effect of spacing between piers on the equilibrium scour depth. Bařak et al. (1978) studied the maximum scour depth at groups of three cylindrical piers with reference to the effect of pier spacing and angle of attack of flow with respect to pier axis. They proposed empirical design charts for the effect of spacing. Elliott and Baker (1985) studied the scour depth at a single row of multiple piers normal to the flow. To estimate the scour depth at pier groups, they proposed a correction factor for the equation proposed by Breusers et al. (1977), which predicts the equilibrium scour depth at single piers. The proposed correction factor includes the effect of pier spacing on the scour depth. Melville and Coleman (2000) proposed an equation for the estimation of equilibrium scour depth at single piers. In case of pier groups, they recommended the use of correction factors for single row of piers ( $i \times 1$ ) and double row of piers ( $i \times j$ ). For staggered arrangement of equal sized and tandem arrangement of unequal size of piers, Beg (2014) and Beg and Beg (2015) studied the effect of pier spacing. Çeřme (2005) and Bozkuř and Çeřme (2010) conducted experiments with inclined dual piers in tandem arrangement and they investigated the effect of inclination of piers on the scour depth. Similarly, Özalp (2013) studied the effect of inclination of piers in case of three and four piers in-line with the flow. In all studies, it is concluded that as the inclination of the front pier increases in downstream direction, the strength of downflow and horse-shoe vortex decreases, therefore the maximum scour depth decreases.

As the main objective of this study covers the maximum scour depth at piers in tandem arrangement, it is worth to focus on the scour mechanisms involved in this arrangement and the previous studies on the topic. In addition to downflow, horse-shoe vortex, and wake vortex, which are the major driving agents in single pier scour, there are other mechanisms when pier groups exist. In tandem arrangement of piers, these additional mechanisms are namely reinforcing, sheltering, and vortex shedding (Hannah, 1978).

The mechanism affecting the scour depth at the front pier is reinforcing. In this mechanism, the scour depth at the front pier increases by overlapping of the scour holes around front and rear piers. In case of a single pier, bed material is picked up from the scour hole by horse-shoe vortices and carried downstream for a distance and then dropped in the scour hole again due to insufficient energy to be carried far from the scour hole itself. However, in the case of existence of a pier at the downstream, overlapping of the holes results in reduction of both the bed level and bed slope of the exit path of front pier as can be seen in Figure 2.7. Reduced bed level and slope result in the decrease of energy required to carry the eroded material from the scour hole. Thus, sediment is easily transported from the scour hole of front pier and the scour depth at its upstream face increases. The intensity of reinforcing decreases with increasing pier spacing and angle of attack of flow (Hosseini and Amini, 2015). Yet, the effect of angle of attack of flow is out of consideration in the present study.

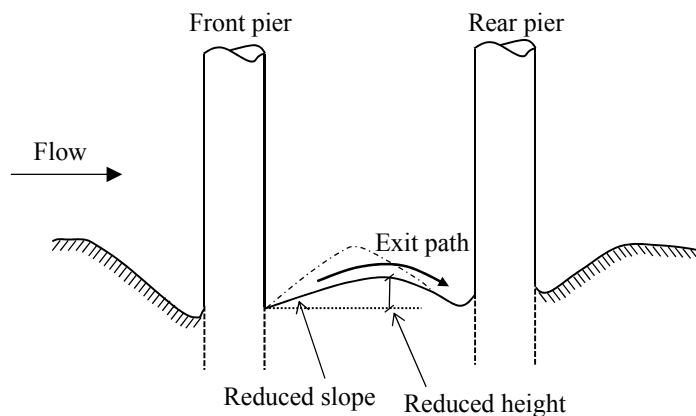


Figure 2.7 Schematic representation of the reinforcing effect (Redrawn from Nazariha (1996))

In sheltering mechanism, existence of a front pier decreases the approach velocity for the rear pier, since approach flow first hits the front pier. Also, the eroded material from the front pier deposits at the upstream of the rear pier, causing a

flow deflection upwards from the bed and around the rear pier (Nazariha, 1996). The deflected flow results in reduced horse-shoe vortex strength at the rear pier. In combination with the decreased approach velocity of flow, reduced horse-shoe vortex strength leads to reduced scour depth at the upstream face of the rear pier. The effectiveness of sheltering mechanism decreases and then ceases with increasing pier spacing.

Vortex shedding helps lifting of the bed material from rear pier. When vortices shed from the front pier, they move downstream following paths at the sides of the pier. The distance between the path of shed vortex and its convection speed directly affect its strength of scouring at rear pier. However, in tandem arrangement of piers, the rear pier does not interfere with the path of shed vortices. Therefore, this mechanism is not as effective as piers with staggered arrangement.

Tandem arrangement of piers and the effect of pier spacing have received the attention of several researchers. The scour depth at dual piers in tandem and side-by-side arrangement has been studied by Hannah (1978) with different spacings between piers. Breusers and Raudkivi (1991) interpreted the experimental results of Hannah (1978) who performed experiments under clear-water conditions with uniform sediment of  $D_{50} = 0.75$  mm and  $\sigma_g = 1.32$ . For piers in tandem arrangement, the scour depth at the upstream of the front pier was the same as for a single pier  $d_s$  under  $\lambda = 1$ , where  $\lambda$  is the ratio of pier diameter ( $b$ ) to center-to-center spacing between piers ( $d$ ). With increasing pier spacing ( $\lambda < 1$ ), a maximum value of  $d_s$  was experienced at  $\lambda \approx 0.33$  due to the reinforcing effect. From its maximum value,  $d_s$  was decreased with decreasing  $\lambda$ . The reinforcing effect was maintained until about  $\lambda < 0.09$  for the aforementioned experimental conditions. For larger spacing, the interference of scour holes diminished and the scour depth was the same as for a single pier and separate scour holes formed around bridge piers.

Nazariha (1996) conducted experiments on different arrangement of pier groups. In tandem arrangement case with  $\lambda \geq 0.2$ , it was observed that pier spacing,

reinforcing, and sheltering are dominant in the scour mechanism. For higher values of  $\lambda$ , greater depths of scour were obtained.

Another study on different arrangement of pier groups was conducted by Salim and Jones (1998). They modified a correction factor introduced by Gao et al. (1993) to predict the maximum scour depth at group of piers in-line with the flow. They proposed the correction factor to the HEC-18 (Hydrologic Engineering Center) scour depth equation for single piers proposed by Richardson and Davis (2001) as follows:

$$K_j = 1 + 0.85 \left[ \frac{(j-1)}{\left(1 + \frac{1}{\lambda}\right)^2} \right] \quad (2.11)$$

where,  $K_j$  is the factor for the effect of pier groups (in-line with the flow). The factor implies that the effect of a rear pier on the scour depth at the upstream of front pier will decrease with decreasing  $\lambda$  value.

In the studies on tandem arrangement of piers, Beg (2004) and Ataie-Ashtiani and Beheshti (2006) stated that the scour depth at the upstream of front pier reaches its maximum value when  $\lambda \approx 0.33$  while the scour depths were obtained slightly lower than the maximum value when  $\lambda = 0.5$ . Ataie-Ashtiani and Beheshti (2006) also proposed two correction factors to HEC-18 equation (Richardson and Davis, 2001) and equation by Melville and Coleman (2000) as presented in Eq. (2.12) and (2.13), respectively.

$$K_{ij} = 1.11 \frac{(j)^{0.0396}}{\left[ (i)^{0.5225} \left( \frac{1}{\lambda} - 1 \right)^{0.1153} \right]} \quad (2.12)$$

$$K_{ij} = 1.118 \frac{(j)^{0.0895}}{\left[ (i)^{0.8949} \left( \frac{1}{\lambda} - 1 \right)^{0.1195} \right]} \quad (2.13)$$

Gao et al. (2013) also studied the effect of pier spacing in case of pier groups. They concluded that in tandem arrangement case, the maximum scour depth at the upstream of front pier occurs when  $\lambda = 0.33$ . They obtained a similar trend with the findings of Hannah (1978). The concept of effect of pier spacing in case of tandem arrangement has also been studied by Heidarpour et al. (2010) and Diweddar (2013).

Furthermore, a numerical investigation was conducted by Kim et al. (2014) for the local scour at group of piers. They have investigated the temporal variation of the scour depth in addition to the effect of pier spacing on it. They concluded that the maximum value of equilibrium scour depth is obtained when  $\lambda \approx 0.4$ .

All the aforementioned researchers concluded that the maximum scour depth at a group of piers placed in-line with the flow occurs at the upstream face of the frontmost pier and spacing between the piers affects the maximum scour depth.

### **2.3 Clear-Water Scour Prediction Methods for Bridge Piers**

Many scour prediction equations have been reported in the literature, which can be found in Yanmaz (2002). However, the results of the proposed methods, which were mainly derived from experimental studies in laboratory medium, differ widely from each other. Each method is normally assumed to be valid for the range of its experimental conditions. Very limited field data of scour are available due to the observational difficulties during floods, which leads to the problem of model calibration. That is why there is no single method for pier scour, which is applicable to universal design conditions. The following methods will only be given because of their practical importance. Corresponding equations can be multiplied with  $K_j$  and  $K_{ij}$  to estimate the scour depth of pier groups, for the range of experimental conditions similar to those where the factors were derived.

### 2.3.1 Melville and Coleman (2000) Method

Melville and Coleman (2000) propose the following equation composed of several multiplicative adjustment factors for general scour at single bridge piers

$$d_{se} = K_{yb} K_I K_d K_s K_\alpha \quad (2.14)$$

where  $K_{yb}$  is a factor accounting for the combined effects of flow depth and pier size,  $K_I$  is the flow intensity factor, which is unity for live bed conditions and is  $u/u_c$  for clear water scour in uniform bed,  $K_d$  can be determined from Eq. (2.5) for  $b/D_{50} < 25$ ,  $K_s$  is 1.0 for cylindrical piers and rectangular piers with rounded noses, and 1.1 for square piers, and  $K_\alpha$  is a factor to account for the effect of angle of approach flow which can be determined by  $(\cos\alpha + (L_p/b)\sin\alpha)^{0.65}$  for non-cylindrical piers, where  $L_p$  is the length of pier. The adjustment factors  $K_{yb}$  can be determined from  $2.4b$ ,  $2(d_0b)^{0.5}$  and  $4.5d_0$  for  $d_0/b > 1.43$ ,  $0.2 \leq d_0/b \leq 1.43$ , and  $d_0/b < 0.2$ , respectively.

### 2.3.2 Richardson and Davis (2001) Method

This method is widely used in the USA and is also referred to as the Colorado State University (CSU) equation or HEC-18 procedure. The equilibrium depth of scour,  $d_{se}$ , around a single pier is given by Richardson and Davis (2001):

$$\frac{d_{se}}{b} = 2.0 K_s K_\alpha K_b K_z \left( \frac{d_0}{b} \right)^{0.35} F_r^{0.43} \quad (2.15)$$

where  $K_b$  is a factor to account for bed condition, which can be taken as 1.1 for clear-water scour, plane bed and small dunes, and 1.2 and 1.3 for medium and large dunes, respectively. The adjustment factor  $K_z$  accounts for the armoring effect of the bed material. For  $D_{50} < 2$  mm or  $D_{95} < 20$  mm, the value of  $K_z$  can be taken as unity. For coarser materials, i.e.  $D_{50} \geq 2$  mm and  $D_{95} \geq 20$  mm, the value of  $K_z$  attain smaller values than unity with its minimum value of 0.4.

### 2.3.3 Oliveto and Hager (2002) Method

Oliveto and Hager (2002) proposed the following equation for clear water scour at cylindrical bridge piers.

$$\frac{d_s}{L_R} = 0.068\sigma_g^{-0.5} F_d^{1.5} \log T_d \quad (2.16)$$

where  $L_R$  is the reference length ( $b^{2/3} d_0^{1/3}$ ),  $F_d$  is the densimetric particle Froude number ( $u/(\Delta g D_{50})^{0.5}$ ),  $T_d$  is the dimensionless time of scour ( $t/t_R$ ), and  $t_R$  is the reference time ( $L_R/(\Delta g D_{50})^{0.5}$ ). This equation is independent of equilibrium scouring parameters. Therefore, it is of practical importance, over Eq. (2.6).



## CHAPTER 3

### EXPERIMENTAL STUDY

#### 3.1 Experimental Study

The experimental study presented here is conducted in the Hydromechanics Laboratory of Civil Engineering Department, Middle East Technical University, Ankara. The main objectives of the experimental study are to obtain the temporal variation of characteristics of scour hole at dual piers, such as volume and surface area of the scour hole, and the time-variation of the maximum scour depth at dual piers.

##### 3.1.1 Experimental Setup and Equipment

The experiments are conducted in a rectangular flume 15.2-m-long, 0.72-m-wide, and 1.0-m-deep. As can be seen from Figure 3.1, this main channel is composed of different sections. Water is supplied from an overhead tank to the main channel by an inflow pipe, and an ultrasonic flow meter is installed on the pipe to adjust the inflow rate. Steel meshes are placed in the first 1.6-m-long pool part of the channel, to reduce the turbulence of the inflow. This part is followed by a 4.0-m-long varnished concrete section, with a bed slope of 0.001. To provide a gradual transition from concrete bed to sediment section, pebbles are placed at the upstream of the 4.5-m-long working section (Özalp, 2013). A 0.3-m thick layer of

bed material is used to fill the working section with the same slope, 0.001, such that a constant bed slope is maintained along the flume.

The working section is followed by another concrete section with similar characteristics of those of the upstream of the flume. The flow is then discharged to a downstream pool where the sediment is trapped. With an outflow pipe installed at the downstream pool of the test flume, the sediment-free flow is discharged to a settling pool and then to a secondary channel. With a point gage, the head on the sharp crested weir in the secondary channel is read to check the inflow rate. Finally, the outflow is spilled into the underground tank of the laboratory.

Dual piers in this study are modeled with cylindrical PVC pipes. Piers are screwed on a plexiglass board with desired spacing between them, to maintain their relative locations throughout the experiments. The piers are then buried in the sediment section at a reasonable depth and the bed level is adjusted with a trowel. The front pier is located approximately 7.85 m downstream of the flume inlet.

Throughout the experimental study, bed level measurements around the piers are carried out with SeaTek 5 MHz Ultrasonic Ranging System. This equipment consists of 32 transducers operating submerged to measure the bed elevation. It is composed of 3 fixed stainless steel arrays of 8 transducers having 2 cm spacing between them, 8 individual transducers, and an electronics package (SeaTek, 2015). The system works simultaneously with a communication program CrossTalk, to generate output. A photograph of the transducer arrays and electronics package is presented in Figure 3.2.

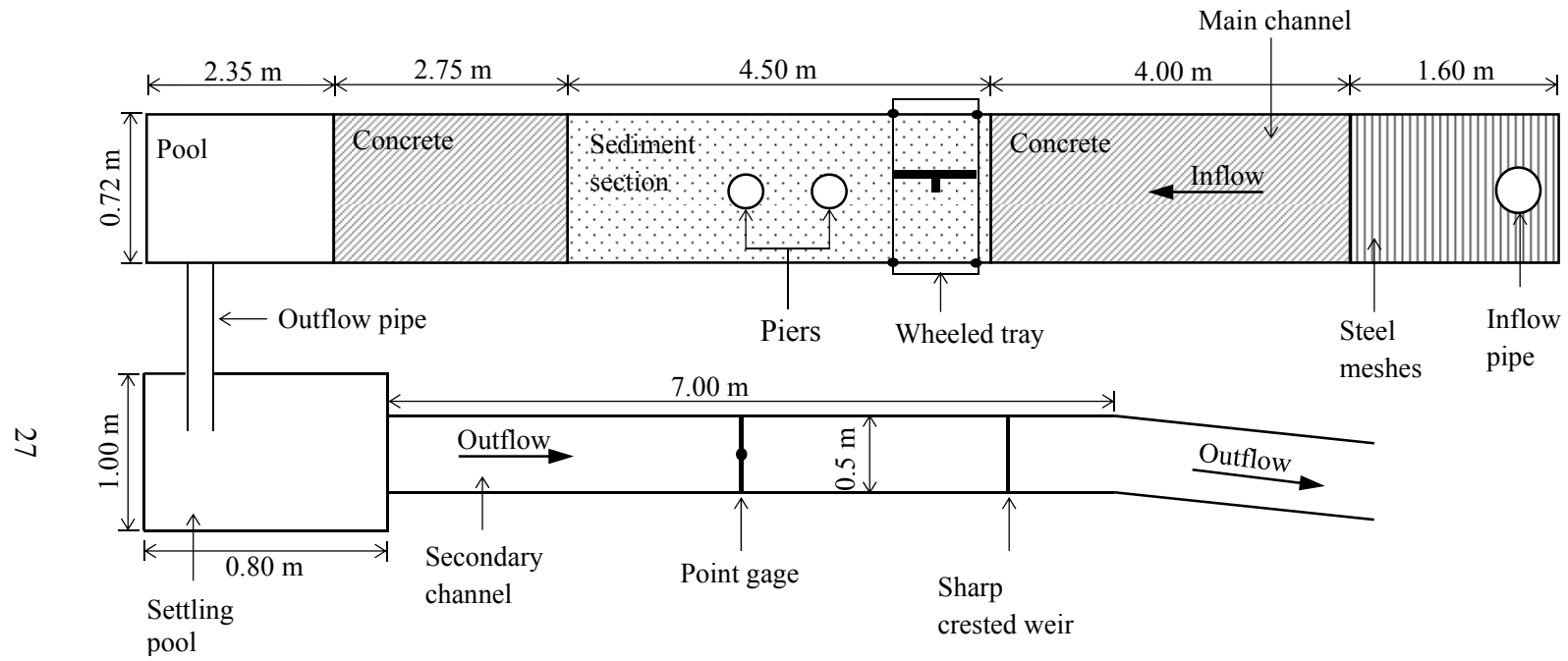


Figure 3.1 Plan view of the test flume (not to scale)



Figure 3.2 SeaTek transducer arrays and electronics package (SeaTek, 2015)

### 3.1.2 Scope of the Experiments

In the working section of the experimental setup, quartz sand is used with sieve analysis results obtained by Özalp (2013) as presented in Table 3.1. The subscripts in the table refer to percent fineness of the corresponding particle sizes. Accordingly, the median size of the bed material is 0.88 mm and its geometric standard deviation,  $\sigma_g = D_{84.1}/D_{50} = 1.284$  is calculated from Yanmaz (2002) and the material is accepted to be uniform (Dey et al., 1995; Melville and Coleman, 2000).

Table 3.1 Characteristic particle sizes of the bed material

$D_{10}$ (mm)	0.63
$D_{15.9}$ (mm)	0.68
$D_{50}$ (mm)	0.88
$D_{60}$ (mm)	0.92
$D_{84.1}$ (mm)	1.13

In the experiments, dual pier models with identical size are placed in tandem arrangement. The cylindrical pier models have three different diameters,  $b = 7.5$  cm, 6.3 cm, and 4.0 cm. The maximum pier size is specified as 7.5 cm in order to avoid contraction scour in the experiments. According to Yanmaz (1989), contraction scour effect is negligible for less than 10% of contraction ratio which is defined as pier size to channel width. Three different center-to-center pier

spacing ( $d$ ), are tested, such as  $d = 2b$ ,  $3b$ , and  $4b$ . Therefore, the pier diameter to spacing ratio,  $\lambda = 0.25$ ,  $0.33$ , and  $0.50$  are used.

Before specifying the test range of flow intensity, preliminary experiments are conducted to calibrate the discharge measurement. As mentioned in the previous section, the inflow discharge,  $Q$  is adjusted by checking the flow meter measurement and the head over the sharp-crested weir ( $H$ ) in the secondary channel. In the preliminary experiments, the discharge is slightly increased and decreased with the valve on the inflow pipe, and the measured discharge versus the head over the weir is recorded. This calibration part of the experiments is performed for several times. The average values of  $H$  with respect to corresponding  $Q$  values are plotted and presented in Figure 3.3. Using the equation presented in Figure 3.3, the discharge measurements by the flowmeter is continuously checked throughout the experiments.

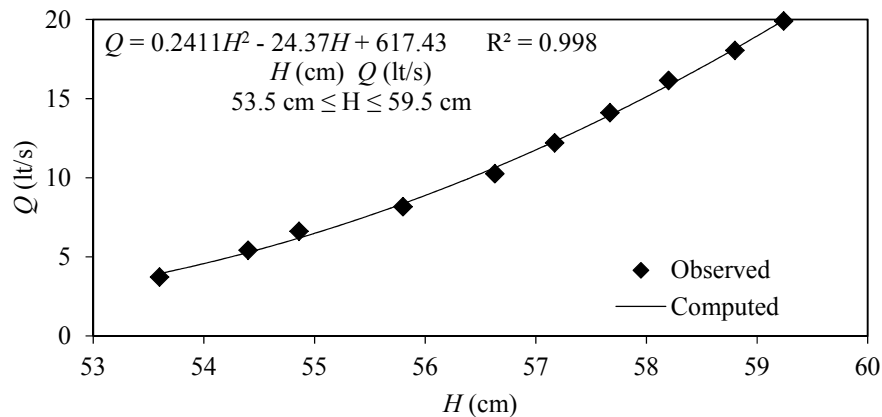


Figure 3.3 Discharge versus head over the sharp-crested weir

Once the discharge is set to a desired value, the approach flow depth is measured by transparent rulers attached to the glass wall of the flume. Almost uniform flow is attained in the flume according to flow depth measurement at several locations along the test section. The experiments are run under three different flow intensities,  $u/u_c = 0.917$ ,  $0.936$ , and  $0.946$ , and their corresponding flow Froude numbers are  $0.443$ ,  $0.428$ , and  $0.413$ , respectively. In this study, flow intensity is

defined by  $u/u_c$ . Since the maximum clear-water scour depth occurs when  $u = u_c$ , this ratio gives information about the degree of proximity of flow to the critical condition to initiate sediment motion at the bed. Flow intensities smaller than 0.917 are not tested, since the corresponding flow depths are small enough not to permit scour measurements accurately. For the flow intensities higher than 0.946, movement of some bed material is observed at the upstream of the piers. Therefore to restrict the flow in clear-water condition, higher values of flow intensity is not tested. In the experimental study, clear-water scour conditions are maintained, i.e. the shear velocity of the approach flow ( $u_*$ ) is less than the critical shear velocity of the sediment ( $u_{*c}$ ) according to Shields' criterion (Garde and Ranga Raju, 2006). The critical shear velocity,  $u_{*c}$  and the mean threshold velocity,  $u_c$  can be determined from Melville and Coleman (2000) as follows:

$$u_{*c} = 0.0115 + 0.0125D_{50}^{1.4} \quad (3.1)$$

$$\frac{u_c}{u_{*c}} = 5.75 \log \left( 5.53 \frac{d_0}{D_{50}} \right) \quad (3.2)$$

From Eq. (3.1)  $u_{*c}$  is calculated as 0.022 m/s and from Eq. (3.2)  $u_c = 0.303, 0.312, 0.32$  m/s for  $Q = 8, 10, 12$  lt/s, respectively. In the course of the experiments,  $u$  is always smaller than  $u_c$  and  $u_*$  is always smaller than  $u_{*c}$ . Therefore, clear-water scour conditions are maintained throughout the study. The scope of the experiments is presented in Table 3.2. As can be seen from Table 3.2, two parts of experiments are conducted in the course of this thesis. In Experiments Part I (E2-E7), the temporal variation of the scour hole topography is obtained around dual piers. The common scour hole volume and its surface area are determined explicitly as a function of dimensionless time,  $T_s$  and  $\lambda$ . Experiments Part II (E11-E17) is conducted to obtain the evolution of the maximum scour depth at the upstream of the front pier and sides of both piers. The findings of this part and volume expression determined in the first part are used to develop the semi-empirical model explained in Chapter 5.

Table 3.2 Scope of the experiments

<i>Part I</i>							
Run	$b$ (cm)	$\lambda$	$d_0$ (cm)	$Q$ (lt/s)	$u/u_c$	$u_*/u_{*c}$	$F_d$
E2 (11 runs)	7.5	0.33	5.50	12	0.946	0.986	2.54
E3 (11 runs)	7.5	0.25	5.50	12	0.946	0.986	2.54
E4 (6 runs)	6.3	0.33	5.50	12	0.946	0.986	2.54
E5 (6 runs)	6.3	0.25	5.50	12	0.946	0.986	2.54
E6 (6 runs)	4.0	0.33	5.50	12	0.946	0.986	2.54
E7 (6 runs)	4.0	0.25	5.50	12	0.946	0.986	2.54
<i>Part II</i>							
Run	$b$ (cm)	$\lambda$	$d_0$ (cm)	$Q$ (lt/s)	$u/u_c$	$u_*/u_{*c}$	$F_d$
E11-8	7.5	0.50	4.00	8	0.917	0.856	2.33
E11-10	7.5	0.50	4.75	10	0.936	0.924	2.45
E11-12	7.5	0.50	5.50	12	0.946	0.986	2.54
E12-8	7.5	0.33	4.00	8	0.917	0.856	2.33
E12-10	7.5	0.33	4.75	10	0.936	0.924	2.45
E12-12	7.5	0.33	5.50	12	0.946	0.986	2.54
E13-8	7.5	0.25	4.00	8	0.917	0.856	2.33
E13-10	7.5	0.25	4.75	10	0.936	0.924	2.45
E13-12	7.5	0.25	5.50	12	0.946	0.986	2.54
E14-8	6.3	0.33	4.00	8	0.917	0.856	2.33
E14-10	6.3	0.33	4.75	10	0.936	0.924	2.45
E14-12	6.3	0.33	5.50	12	0.946	0.986	2.54
E15-8	6.3	0.25	4.00	8	0.917	0.856	2.33
E15-10	6.3	0.25	4.75	10	0.936	0.924	2.45
E15-12	6.3	0.25	5.50	12	0.946	0.986	2.54
E16-8	4.0	0.33	4.00	8	0.917	0.856	2.33
E16-10	4.0	0.33	4.75	10	0.936	0.924	2.45
E16-12	4.0	0.33	5.50	12	0.946	0.986	2.54
E17-8	4.0	0.25	4.00	8	0.917	0.856	2.33
E17-10	4.0	0.25	4.75	10	0.936	0.924	2.45
E17-12	4.0	0.25	5.50	12	0.946	0.986	2.54

As mentioned in Chapter 2, equilibrium clear-water scour depth is reached after very long test duration. However, the literature lacks an explicit equation for the equilibrium time determination in case of group of piers in tandem arrangement. Therefore, to have an idea, it may be rational to calculate the equilibrium time of clear-water scour at a single pier. Using the equilibrium time equation proposed by Melville and Chiew (1999) in Eq. (2.7b),  $t_e$  is calculated to be in the range of 58 to 93 hours for the experimental conditions of this study. Considering the main objective to investigate the temporal variation of scour hole characteristics, it is planned to study the initial and development phases of scouring. Among four phases of scouring, namely initial, development, stabilization, and equilibrium phases, 85-95% of the equilibrium scour depth is reached at the end of these first two rapid evolution phases (Hoffmans and Verheij, 1997; Link, 2006; Zanke, 1978). Also, Melville and Chiew (1999) state that, the scour depth at single cylindrical pier is about 50-80% of the equilibrium scour depth after 10% of the equilibrium time, depending on the approach flow velocity. In consideration of these studies on the scour depth evolution, the maximum test duration in Experiments Part I and Part II is specified as 6 hours. This test duration corresponds to relatively long durations in the prototype. For instance, 6 hours of test duration corresponds to  $6*(50)^{0.5}=42$  hours in prototype conditions, for a 1:50 scaled Froude modeling. This is a reasonable time to peak value for most simple storms with single peaks. Moreover, as mentioned before, peak value of the design hydrograph is normally not last long as the time to reach the equilibrium condition.

### **3.1.3 Experiments Part I**

In this part, the aim is to obtain three-dimensional bed topography maps of the scour hole at tandem piers and to determine the time wise variation of the scour hole characteristics. The experiments in this part are carried out with a constant flow intensity of  $u/u_c = 0.946$ , regarding the similarity of the clear-water scour hole characteristics under varying flow intensities. Experiments are started with a flat bed. The outlet valve is closed at the beginning, while the flume is filled with

water very slowly not to disturb the bed material, until the desired approach flow depth is reached. By adjusting the inflow valve, the discharge is set to the desired value and then outlet valve is fully opened. Each run is stopped at specified durations for the scour depth measurements in the erosion and accretion zones in order to obtain three-dimensional bed topography maps. In the E4-E7 runs, the mapping times are 5, 20, 60, 100, 150, and 360 minutes. However, in the E2-E3 runs, larger pier size is used and so larger scour hole is expected. Therefore, mapping times are specified more frequently, such as 5, 10, 15, 20, 30, 45, 60, 80, 100, 150, and 360 minutes. At each mapping time, the experiment is paused gently for not disturbing the bed topography. After making the measurements, the experiment is resumed until the next mapping time. Finally, the scour hole topography is mapped at the end of the experiments and then the flume is drained. For the next experiment, the pier size and/or spacing is modified, placed in the test section, and the bed is then flattened to repeat the test and mapping procedure.

For bed topography mapping, the ultrasonic transducers are fixed to a plexiglass T-shaped frame. The frame is attached to the wheeled tray on the flume, enabling movement in transversal and longitudinal directions along the test section. The measurements are taken around and between the piers for mapping the erosion and accretion zones of scouring. Considering the total number of mapping times of the Experiments Part I as seen in Table 3.2, 46 time-dependent bed topography maps are created, which are presented in Appendix A. Bed topography maps of runs E2 and E3, and corresponding three-dimensional views of the scour hole at  $t = 360$  min can be seen in Figure 3.4 and Figure 3.5, respectively. In the bed topography maps and the three dimensional view of the scour hole, grey circular cylinders represent the pier models, respectively. A photograph of the final scour hole of Run E3 can be seen in Figure 3.6. The direction of flow is indicated with a blue arrow in Figures 3.4 – 3.6 and Figures A.1. – A.46. Similar to the scour hole at single piers, the plan view of the scour hole boundary around dual piers is also horse-shoe shaped, as can be seen in Figure 3.4. Although in the early stages of scouring the horse-shoe shape is not fully developed, the shape is more

pronounced after  $t = 60$  min, and is definitely observed at the end of the experiments.

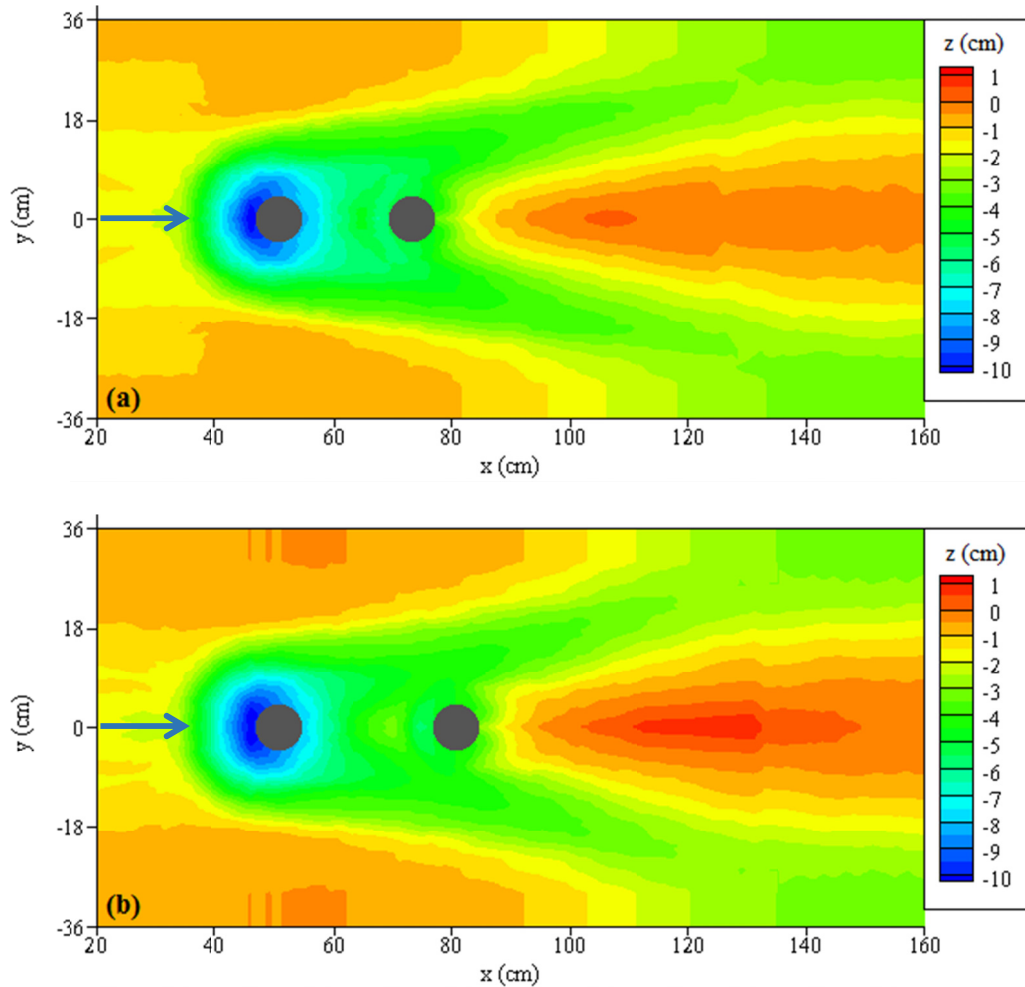


Figure 3.4 Bed topography maps of (a) Run E2 and (b) Run E3 at  $t = 360$  min

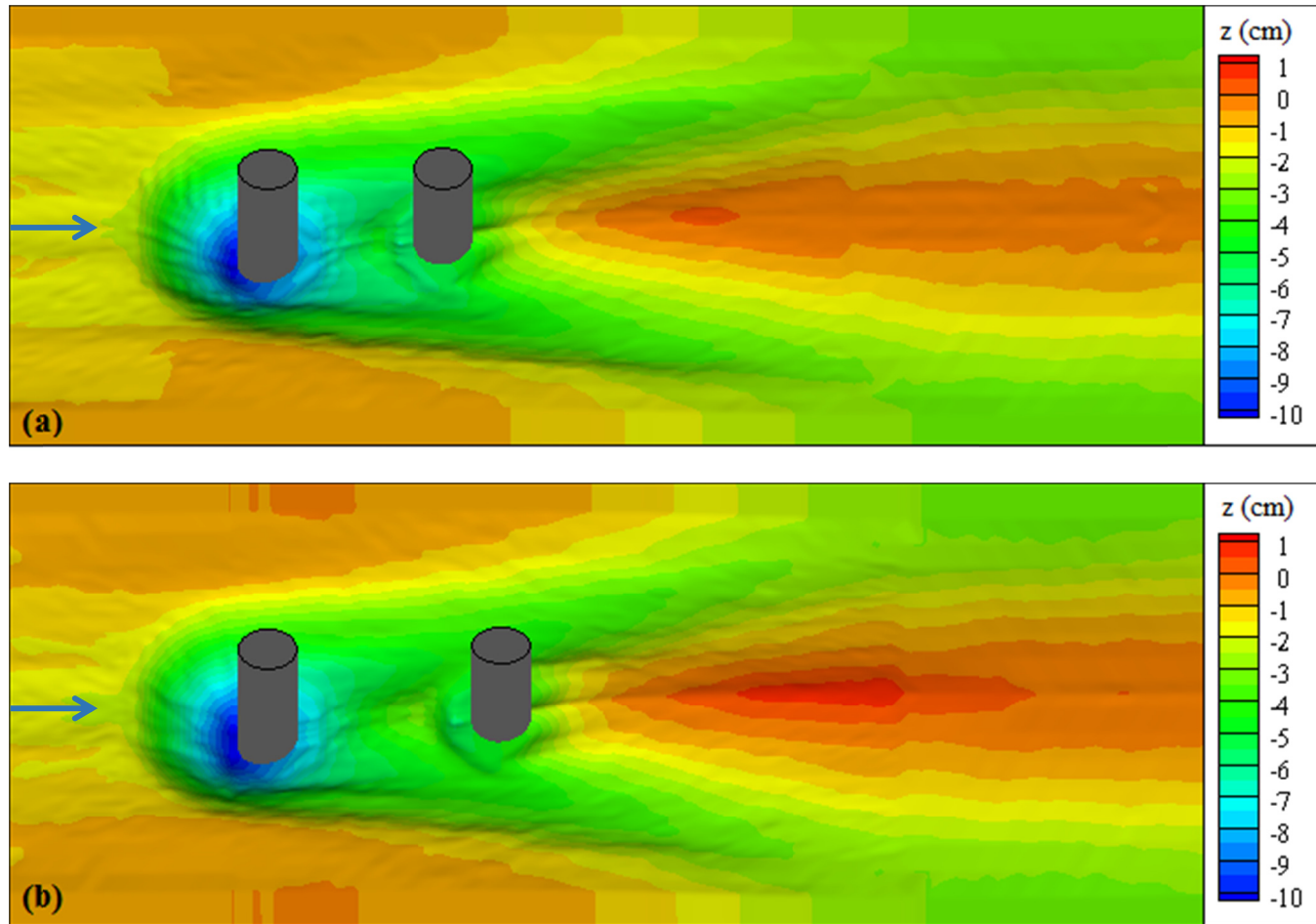


Figure 3.5 Three-dimensional view of the scour holes of (a) Run E2 and (b) Run E3 at  $t=360$  min



Figure 3.6 Photograph of the final scour hole of Run E3

The profile of the scour holes at the centerline along the flow direction are extracted from the maps. In addition, the cross-section of the scour holes normal to the flow direction are extracted at the centerline of the front pier, the rear pier, and the accretion zone peak between piers, which is called dune. For the runs E2 and E3, these profiles and cross-sections at three different times throughout the experiments are presented in Figures 3.7 – 3.14, while similar cross-sections and profiles are obtained for other runs. The time-dependent variation of cross-sections and profiles can be observed in these figures. As can be seen from the cross-sections in Figures 3.7 – 3.12, the scour holes are widening and deepening in time. Side slopes of the scour hole at front pier cross-sections remain constant throughout the experiments (See Figures 3.7 and 3.10). Location of the maximum scour depth at the sides of the front piers along y-direction also remains constant in time. However, the maximum scour depth at the dune cross-section and rear pier cross-section moves towards the centerline of flow direction in time. Therefore, shape of the scour hole at these cross-sections show variation in time.

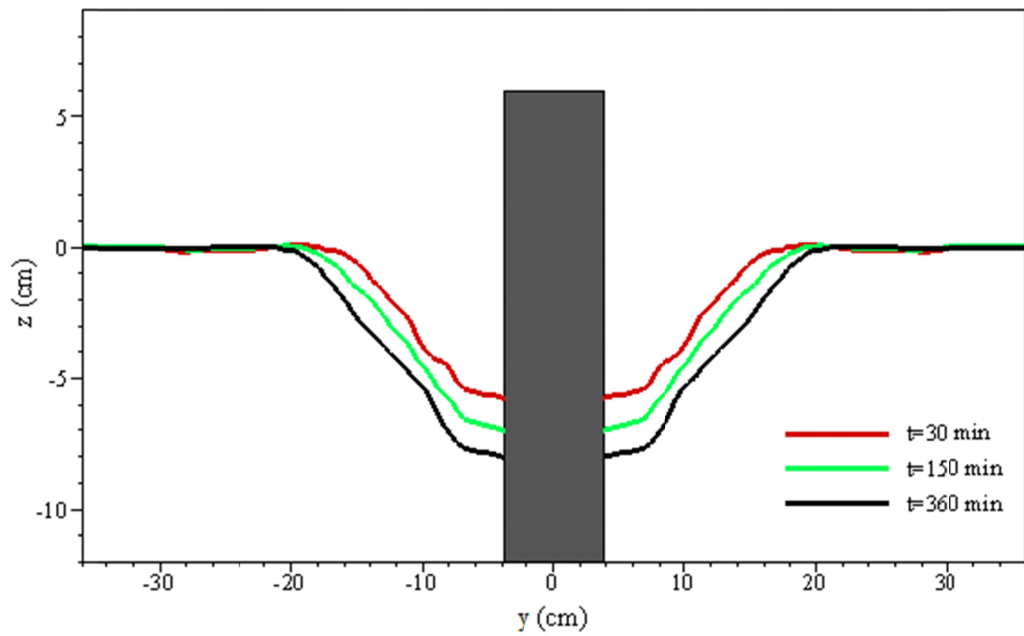


Figure 3.7 Scour hole cross-section of Run E2 at the front pier ( $x=50.75$  cm)

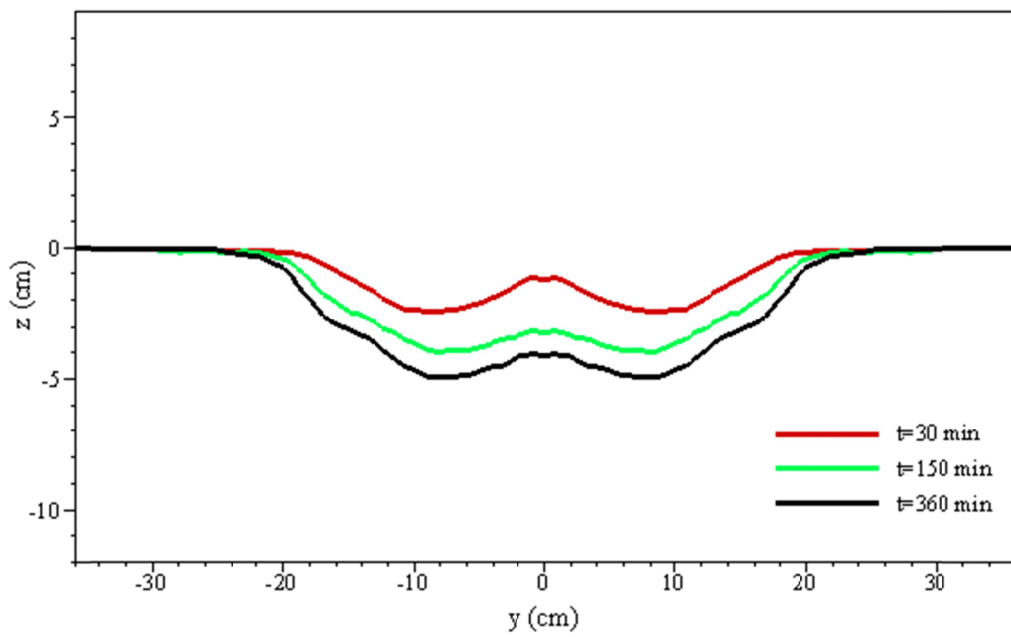


Figure 3.8 Scour hole cross-section of Run E2 at the dune ( $x=65$  cm)

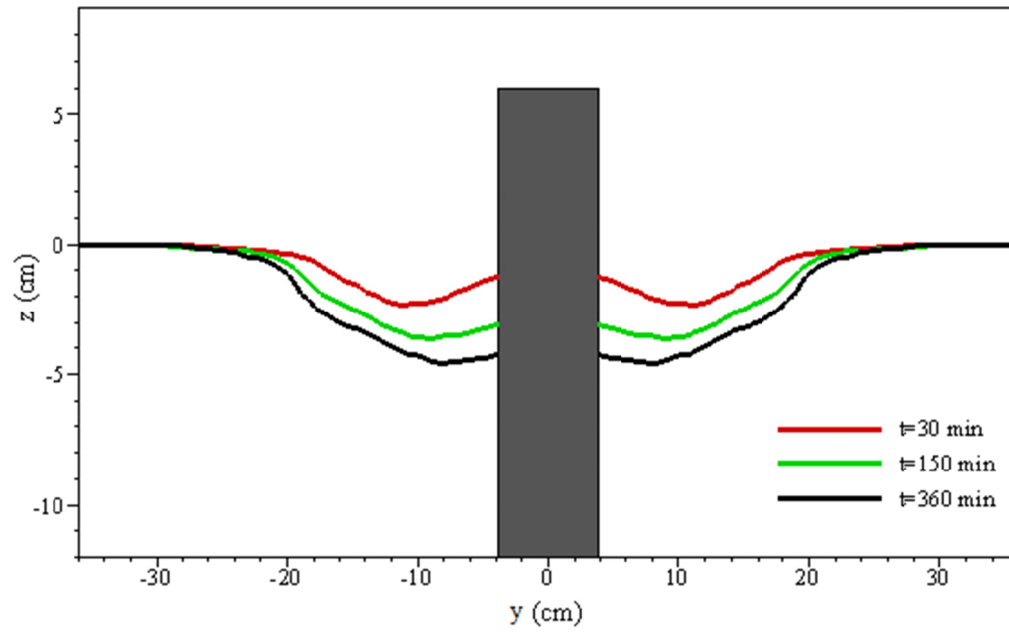


Figure 3.9 Scour hole cross-section of Run E2 at the rear pier ( $x=73.25$  cm)

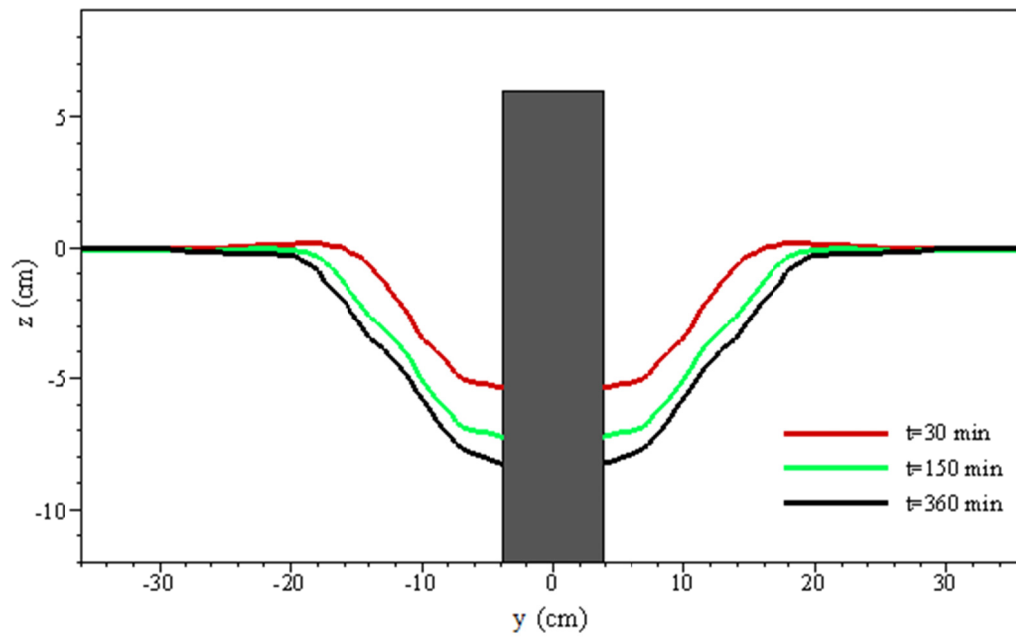


Figure 3.10 Scour hole cross-section of Run E3 at the front pier ( $x=50.75$  cm)

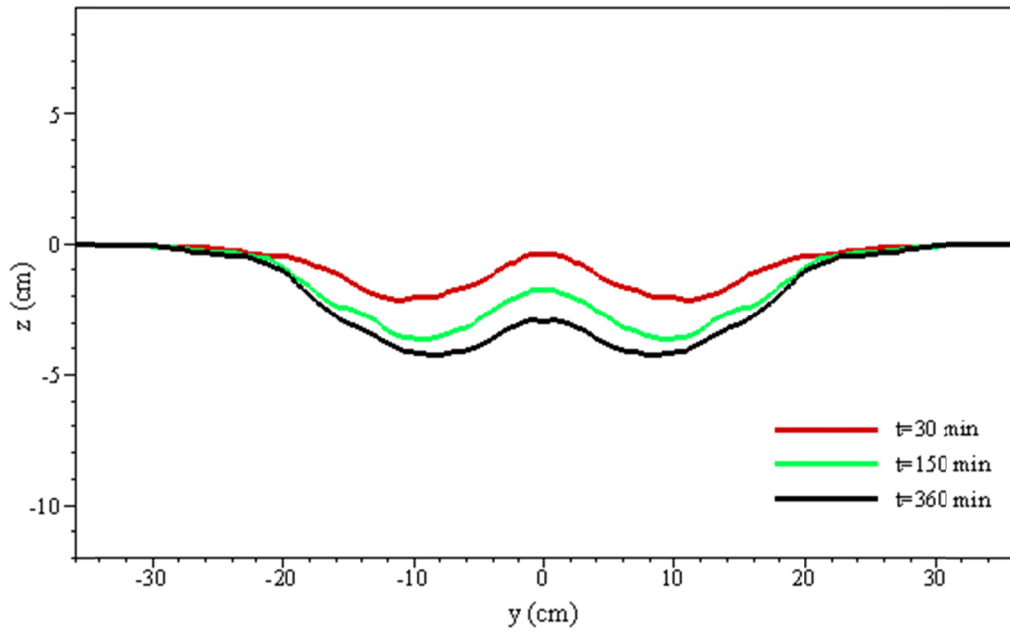


Figure 3.11 Scour hole cross-section of Run E3 at the dune ( $x=69.5$  cm)

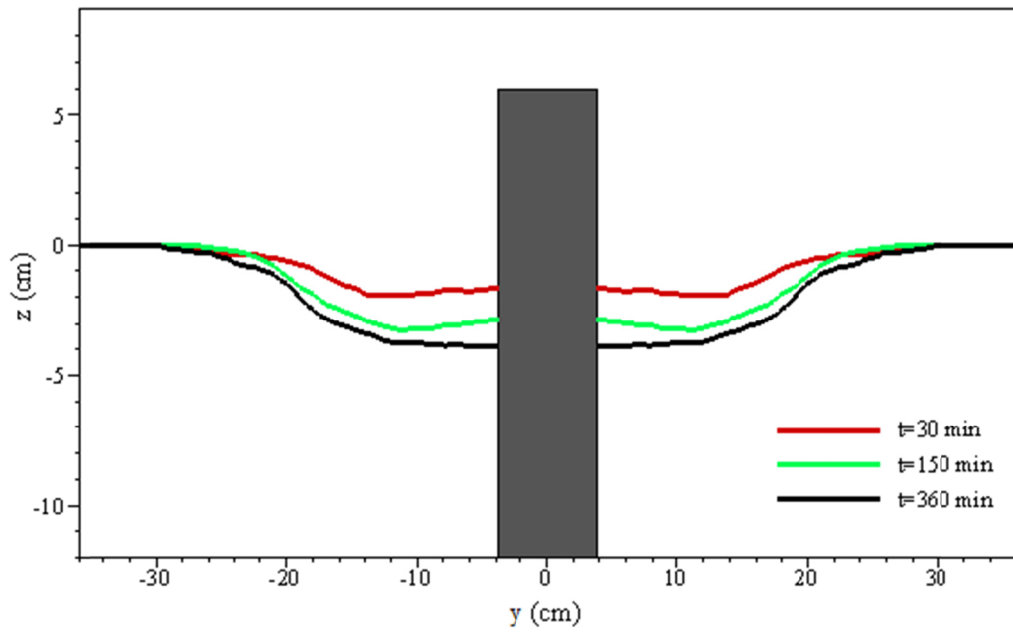


Figure 3.12 Scour hole cross-section of Run E3 at the rear pier ( $x=80.75$  cm)

When the profiles of runs E2 and E3 are examined from Figures 3.13 and 3.14, it is observed that the maximum scour depth occurs at the upstream of the front pier. Similar to the side slopes (See Figures 3.7 and 3.10), the longitudinal slopes of the front pier does not change in time. Therefore, the shape of the scour hole at the front pier remains constant throughout the experiments. Considering the longitudinal slopes observed in Figures 3.13 and 3.14, slopes at the downstream of the front pier (from front pier face to dune), upstream of the rear pier (from dune to rear pier face), and downstream of the rear pier (from rear pier face to downstream accretion zone) also remain constant in time. Slopes at the upstream of the front pier and rear pier are almost identical and approximately equal to the angle of repose of the sediment. Furthermore, slopes at the downstream of both piers are equal too.

The maximum scour depth between piers is observed at the downstream face of the front pier, along the centerline of the flow direction, i.e.  $y=0$ . However, when the bed topography maps are examined, it is observed that the location of maximum scour depth between piers has an eccentricity in both positive and negative  $y$ -direction, which will be discussed in detail in Chapter 4.

Dune location along the flow direction remains constant in time for both runs. The distance of the dune from the center of rear pier is obtained as a percentage of pier spacing,  $d$ . For runs E2 and E3, where the pier size is the same but the pier spacing or in other words  $\lambda$  is different, the distance of dune to the center of the rear pier is equal to 37% and 38% of  $d$ , respectively. Therefore, it can be presumed that, pier size to spacing ratio does not have considerable effect on the location of the dune.

Since the rate of scouring is higher in the beginning of the experiments, the accretion zone at the downstream of the rear pier is relatively steep. However, the accretion propagates downstream in time and its profile becomes flatter, as can be seen in Figures 3.13 and 3.14. At a further distance from the rear pier, close to the end of the sediment section, the profile attains the initial condition of bed profile.

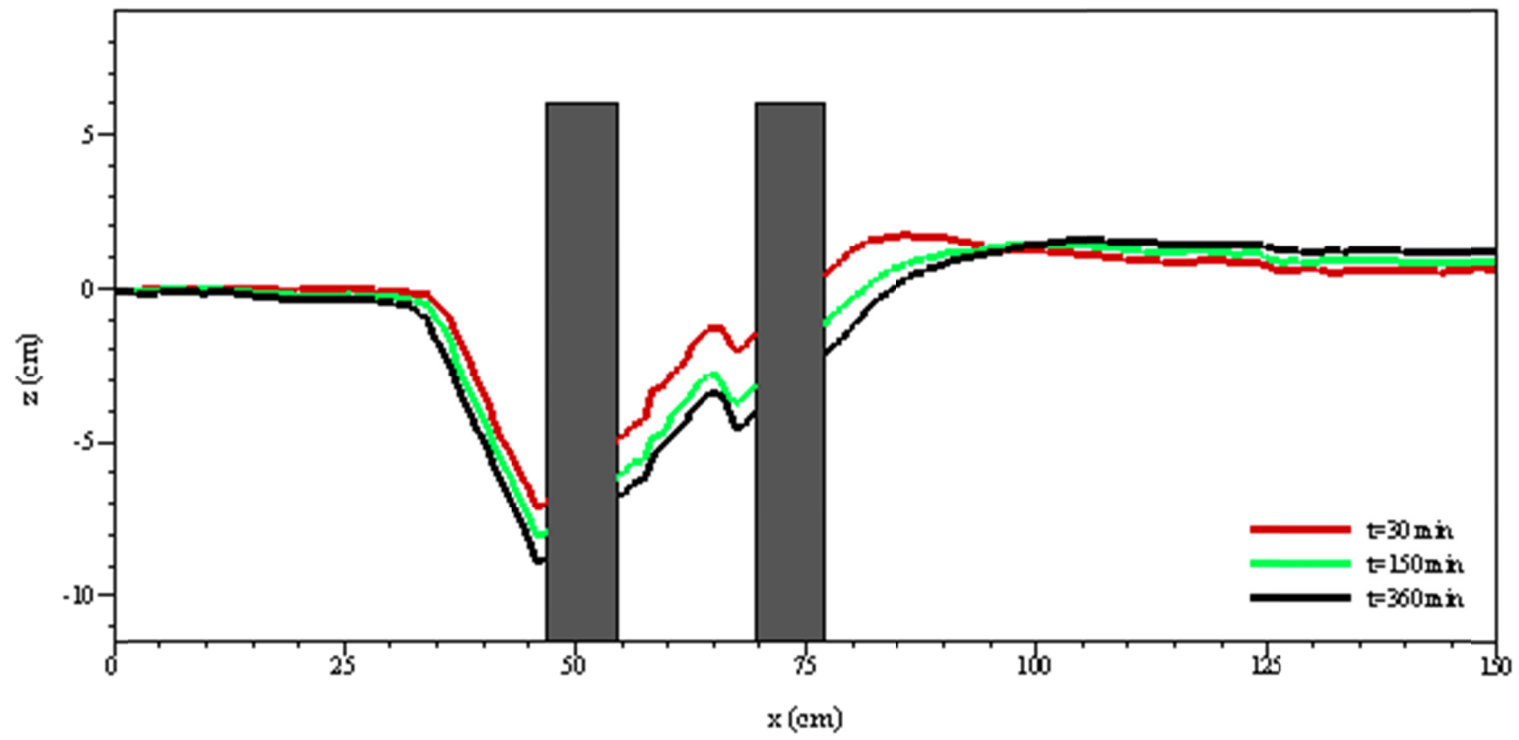


Figure 3.13 Bed profile of Run E2 ( $y=0$ )

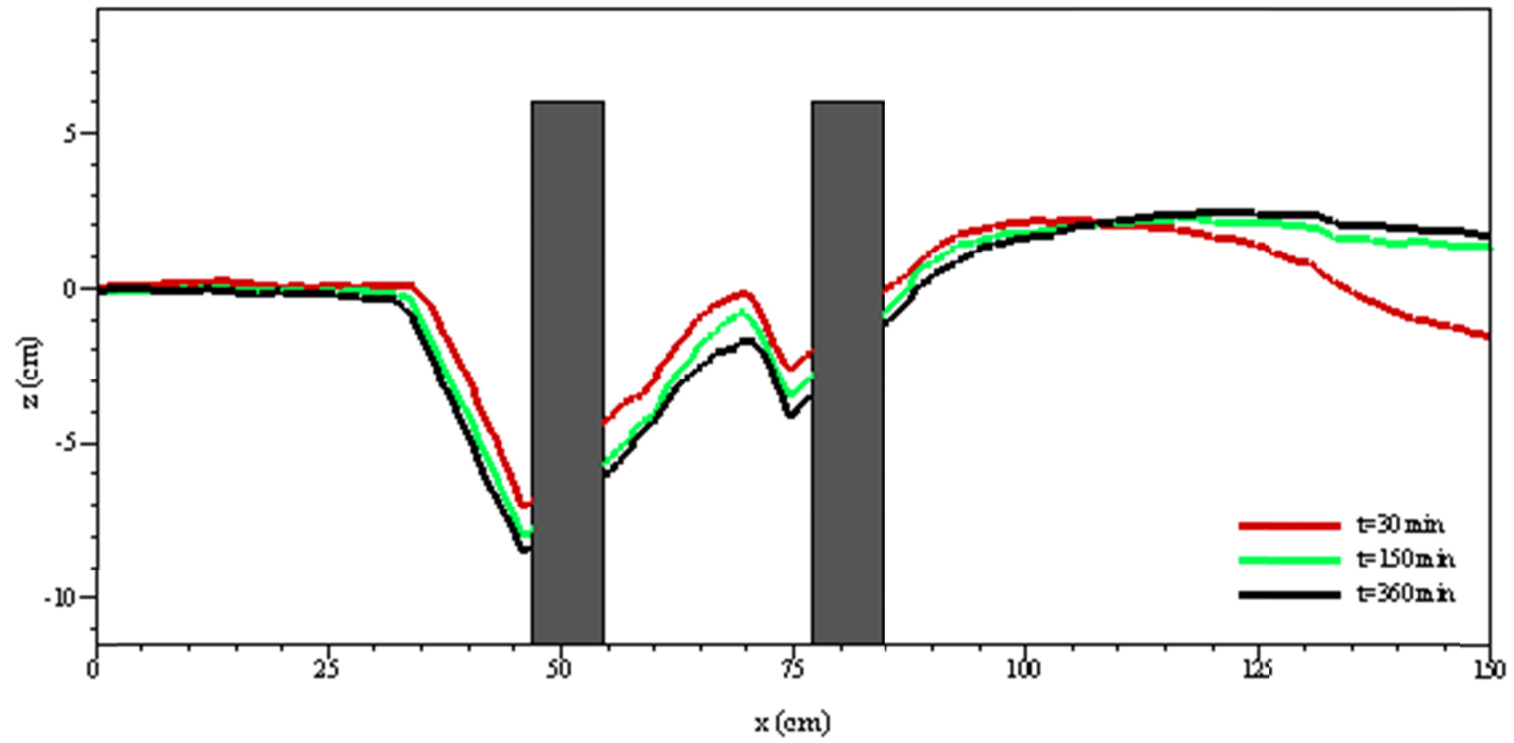


Figure 3.14 Bed profile of Run E3 ( $y=0$ )

A software, which is based on triangularisation method is used to calculate the volume ( $V$ ) and surface area ( $A$ ) of the scour hole around dual piers composed of irregular contours. Therefore, variation of  $V$  and  $A$  with time is obtained from the 46 experiments in this part. For practical purposes,  $V$ ,  $A$  and  $t$  are transformed to dimensionless volume ( $V^*$ ) and surface area of the scour hole ( $A^*$ ) and dimensionless time ( $T_s$ ), respectively. Here,  $V^*$  is defined as the ratio of  $V$  to the cross-sectional area of the piers times the maximum scour depth ( $d_s$ ) which is measured at the upstream of the front pier, i.e.  $(2V/(\pi b^2 d_s))$  and  $A^*$  is defined as the ratio of  $A$  to the cross-sectional area of the piers  $(2A/\pi b^2)$ . Dimensionless  $T_s$  is determined from  $tD_{50}(AgD_{50})^{0.5}/b^2$ , which is previously used by Yanmaz and Altınbilek (1991), Dey (1996), and Yanmaz (2006) for pier scour modeling. Considering 46 experiments, representative regression equations are determined for  $V^*$  and  $A^*$ . As mentioned before,  $V^*$  and  $A^*$  are determined as a function of  $T_s$  and  $\lambda$ , which includes the effect of pier spacing on the volume and surface area of the scour hole around tandem piers. The regression equations of  $V^*$  and  $A^*$  are obtained with correlation coefficients ( $R^2$ ) of 0.92 and 0.82, respectively:

$$V^* = 1.469\lambda^{-0.387}T_s^{0.327} \quad (3.3)$$

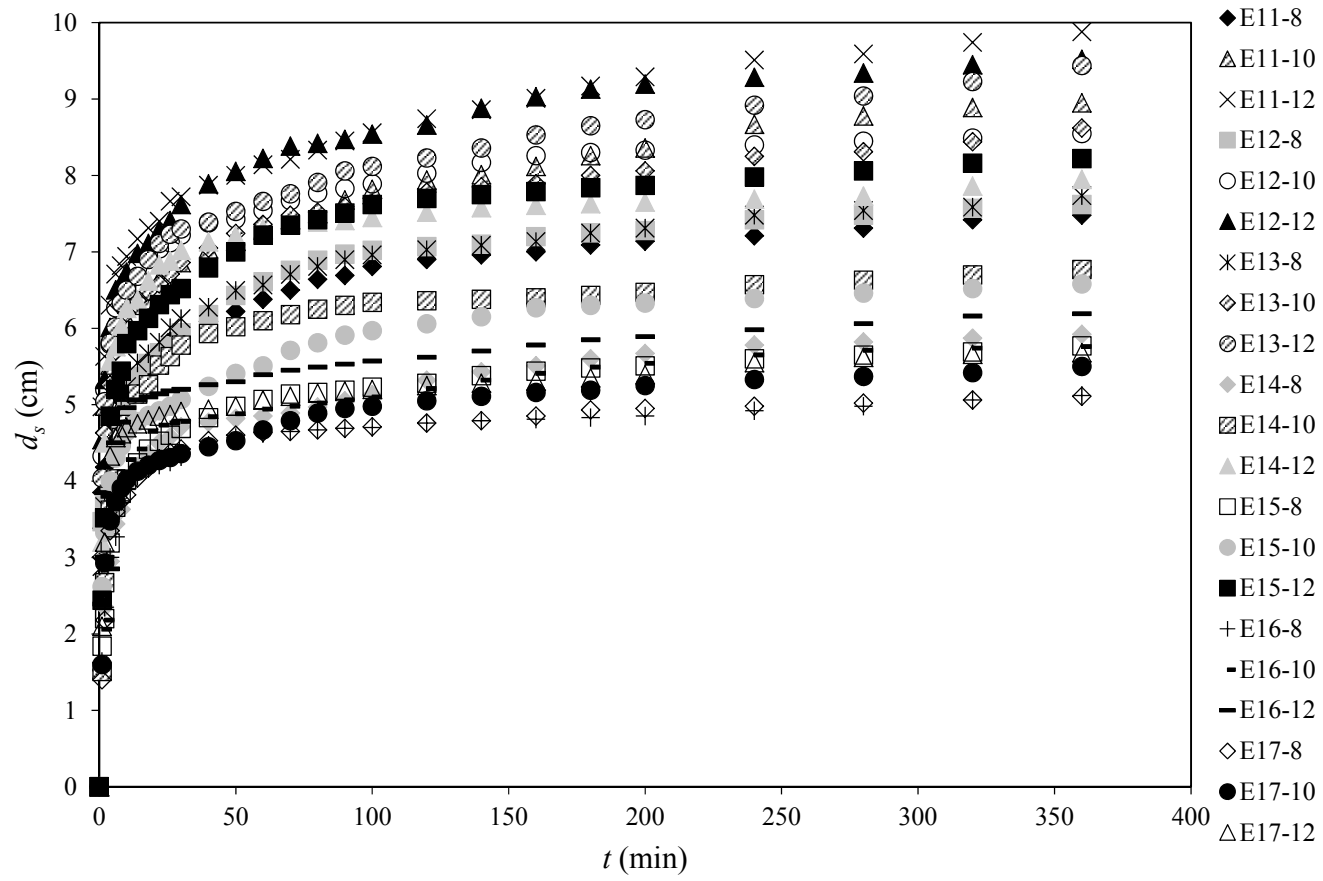
$$A^* = 4.291\lambda^{-0.286}T_s^{0.355} \quad (3.4)$$

In the development of the semi-empirical model to determine the temporal variation of maximum scour depth at tandem piers, Eq. (3.3) is used. Here, in this part of the experimental study, two values of  $\lambda$  are tested, such as 0.33 and 0.25. Smaller pier spacing or in another saying, larger value of  $\lambda$  value is not used due to the limitation by the size of the frame holding the transducers, which inhibits measurement between the piers. However, by means of the similarity of the scour conditions, it is presumed that  $V^*$  can represent the overall conditions tested in this study. This assumption is also supported by the comparison of computed scour depths with the experimental values for the case when  $\lambda=0.5$ . The  $A^*$  relation can

be used as a tool to calculate the scour protection area. However, detailed study can be conducted using longer flow durations to end up with more concrete results.

### 3.1.4 Experiments Part II

In this part of the experimental study, it is aimed to determine the evolution of maximum scour depth at specified axes around the piers with more frequent intervals. Different than the Experiments Part I, the transducers are attached to the piers, allowing the continuous measurement of scour depths throughout the experiments. Four separate frames, each with eight transducers, are attached to the piers. Two of them are placed at the longitudinal centerline of upstream and transversal centerline of side of the front pier. The other two are placed at transversal centerline of side of the rear pier and mid distance between the piers. Similar to the results of Part I, the maximum scour depths are expected and also observed at the upstream face of the front pier at the centerline axis. In the scope of the thesis, the concentration is focused on the evolution of the maximum depth in the semi-empirical model development, for design purposes. Therefore, in this study, only the maximum scour depth measurements are utilized in the model development. With this consideration, it is aimed to propose a combined footing for both piers whose depth is decided according to the maximum possible depth of scour in close vicinity to piers. Under the given experimental conditions in Table 3.2, 21 experiments are conducted and frequent measurements of the maximum scour depth is obtained and presented in Figure 3.15 and Appendix B. As stated in the literature and also observed in the experiments, evolution of maximum clear-water scour depth is very rapid in the beginning of the scouring process, while it slows down and then asymptotically tends to equilibrium condition, which can be clearly observed in Figure 3.15. Also it is obviously deducted that, for a particular flow intensity ( $u/u_c$ ) and  $\lambda$  value, the maximum scour depth increases with increasing pier size. In addition, for a particular  $b$  and  $\lambda$ , the maximum scour depth increases with increasing flow intensity. Furthermore, for a particular  $b$  and  $u/u_c$ , the maximum scour depth increases with increasing  $\lambda$  value (reinforcing effect).

Figure 3.15 Experimental results for  $d_s - t$  relation

As mentioned before, the scour depth measurements are obtained at different sections. To provide information about the tendency of the scour depth variation in time at the sides of both piers and a comparison with the maximum scour depth at the upstream face of the front pier, Figure 3.16 is presented for Run E11-12. It is observed that the scour depths at the side of the front pier are always less than that at its upstream face since vortices at the sides are swept by the flow. So their erosive capacities decrease. Also, the scour depths at the side of the rear pier are always smaller than that at the side of the front pier. Similar trends are also observed in other runs.

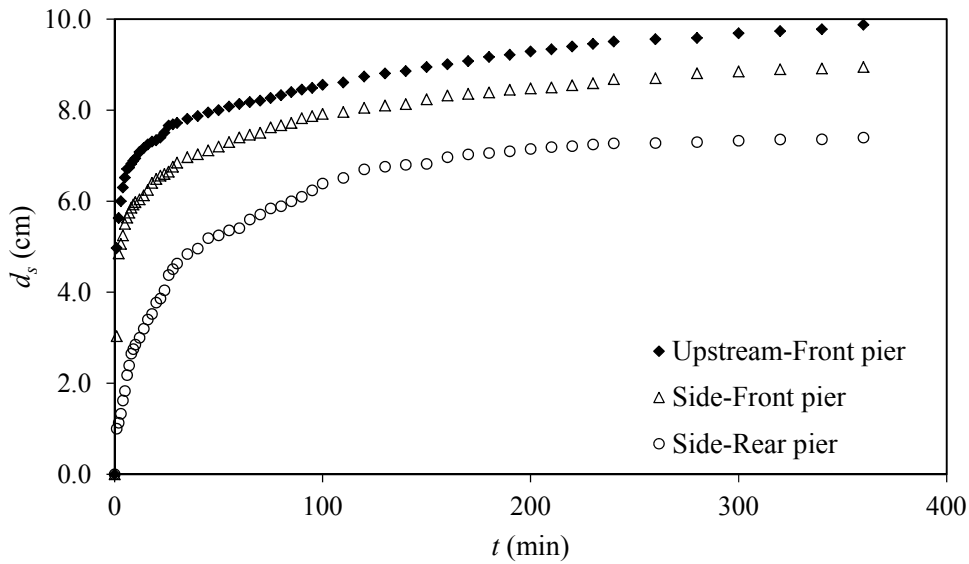


Figure 3.16 Comparison of scour depth at different axes for Run E11-12

## CHAPTER 4

### EVALUATION OF THE EXPERIMENTAL RESULTS

#### 4.1 Evaluation of the Experimental Results

##### 4.1.1 Reinforcing and Sheltering Effect of Dual Piers

In tandem arrangement of piers, the strength of the reinforcing effect depends on the  $\lambda$  value. In the Experiments Part I, the effect of  $\lambda$  on the reinforcing effect is observed and as expected regarding previous studies in the literature, higher values of maximum scour depth are obtained when  $\lambda = 0.33$  and  $d_s$  is slightly decreased for the case of  $\lambda = 0.25$  for all pier sizes. The results of the Experiments Part II agree with Part I, such as, the maximum scour depths for  $\lambda = 0.33$  are higher compared to  $\lambda = 0.25$ , for  $b = 6.3$  cm and 4.0 cm. For the largest pier, similar trend for  $\lambda = 0.33$  and 0.25 are observed, where the highest maximum scour depth is observed for  $\lambda = 0.5$ . To sum up, maximum scour depth reaches its highest value when  $\lambda = 0.5$  and it decreases with decreasing value of  $\lambda$ .

Due to existence of front pier, sheltering mechanism occurs in the scour process. The sheltering effect is clearly observed in the Experiments Part I, where the scour depth at the upstream of the rear pier is always less than the scour depth at the downstream of the front pier (See Figures 3.13 and 3.14).

#### 4.1.2 Shear Stress Variation in the Scour Hole around Upstream Pier

The time-variation of the bed shear stress on the flat region of the scour hole,  $\tau_b$  is determined using the bed shear stress model proposed by Kothyari et al. (1992). Although the model is valid for single piers, it is applied for the dual pier case in this study, to have an idea on the variation of bed shear stress at the upstream pier nose. According to their model, before the scour begins, the bed shear stress at the pier nose is approximately  $4\tau_0$ , where  $\tau_0 = \gamma RS_0$  is the bed shear stress of the approach flow,  $\gamma$  is the specific weight of water, and  $R$  is the hydraulic radius. The primary vortex area increases during scouring. Thus, the bed shear stress decreases and equilibrium scour condition is attained when  $\tau_b < \tau_{cr}$ , where  $\tau_{cr}$  is the critical bed shear stress on flat bed. The temporal variation of the shear stress at the pier nose is obtained by Eq. (4.1):

$$\tau_b = 4\tau_0 \left( \frac{A_0}{A_t} \right)^{0.57} \quad (4.1)$$

where,  $A_0 = (\pi/4)D_v^2$  is the initial cross-sectional area of the primary vortex at  $t = 0$ ,  $D_v = 0.28d_0(b/d_0)^{0.85}$  is the thickness of the separated boundary layer,  $A_t = A_0 + A_s$  is the cross-sectional area of the primary vortex at any time  $t$ ,  $A_s = (d_s^2/2)\cot\phi$  is the cross-sectional area of the scour hole when the scour depth is  $d_s$ , and  $\phi$  is the angle of repose of the sediment. Time-dependent bed shear stress at the pier nose is then calculated by Eq. (4.1) using experimental  $d_s - t$  relation to obtain the variation of  $A_s$  values. The variation of bed shear stress for the particular combination of  $\lambda = 0.33$  and  $u/u_c = 0.936$  is presented in Figure 4.1 by comparing two different pier sizes of  $b = 6.3$  cm and 4.0 cm. The bed shear stress at the approach flow,  $\tau_0$ , is also plotted for comparison purpose. As expected, the bed shear stress at the pier nose decreases in time. Also, bed shear stress decreases with decreasing pier size for a particular flow intensity and  $\lambda$ . Based on the study for equilibrium bed shear stress by Melville and Raudkivi (1977), Dey (1996) stated that  $\tau_b$  tends to  $0.3\tau_{cr}$  for clear-water scour at circular cylinders. The bed

shear stress is below  $\tau_{cr}$  at the end of the experiments, and they tend to different multiples of  $\tau_{cr}$  in the range of 0.51 – 0.71 for the ranges covered in all experiments.

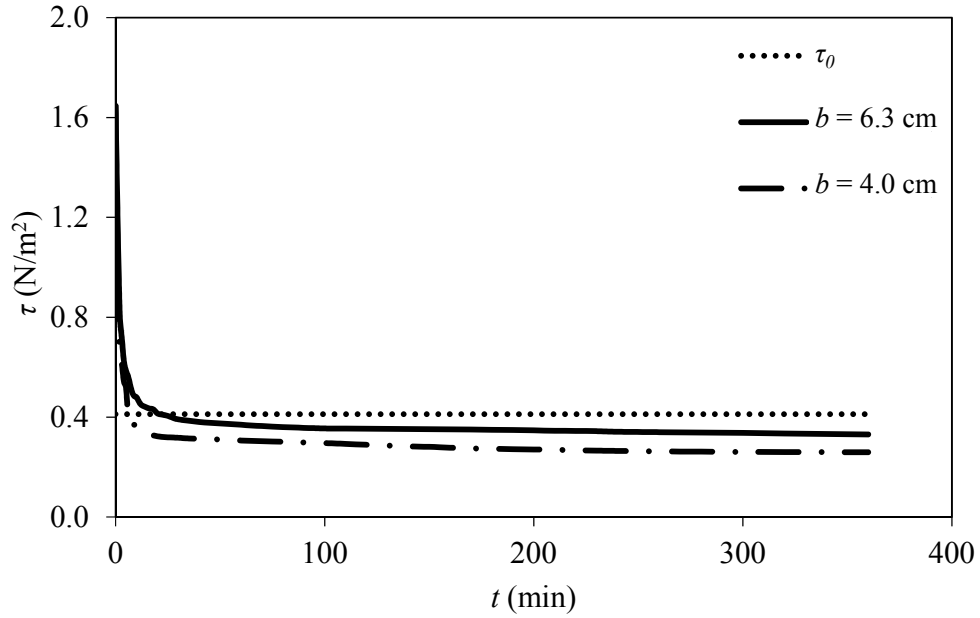


Figure 4.1 Variation of bed shear stress at the pier nose

#### 4.1.3 Shape of the Scour Hole

Using the bed topography maps presented in Appendix A, the change of the side inclination of the scour hole is determined. For this purpose, longitudinal scour width ( $X$ ), transversal scour width ( $Y$ ), and bed level ( $Z$ ) as shown in Figure 4.2 at each test duration of Experiments Part I are obtained by reading the coordinates of the scour hole boundaries in front of (longitudinal) and at the side of (transversal) the front pier. Similarly, at each test duration, transversal scour width ( $Y'$ ) and bed level ( $Z$ ) are obtained at the side of the rear pier. At the end of the experiments when  $t = 360$  min, these characteristic widths and levels are also obtained, namely  $X_{max}$ ,  $Y_{max}$ ,  $Y'_{max}$  and  $Z_{max}$ . To investigate the rate of change of side inclination of the scour hole at the front pier at longitudinal and transversal centerline axes and at the rear pier at transversal direction, the correlations between  $X/X_{max}$  -  $Z/Z_{max}$ ,

$Y/Y_{max} - Z/Z_{max}$ , and  $Y'/Y'_{max} - Z/Z_{max}$  are determined and presented in Figures 4.3 – 4.5, respectively. It is observed that the scour hole shape at the front pier remains nearly unchanged throughout the test duration and the side inclination of the scour hole is almost equal to the angle of repose of sediment except its rear face (See also Figures 3.7, 3.10, 3.13, and 3.14). However, at the side of the rear pier, cross-section of the scour hole varies in time, due to interchanging erosion of bed material according to scouring and accretion of bed material transported from the upstream scour hole (See Figure 4.5 and also Figures 3.9 and 3.12).

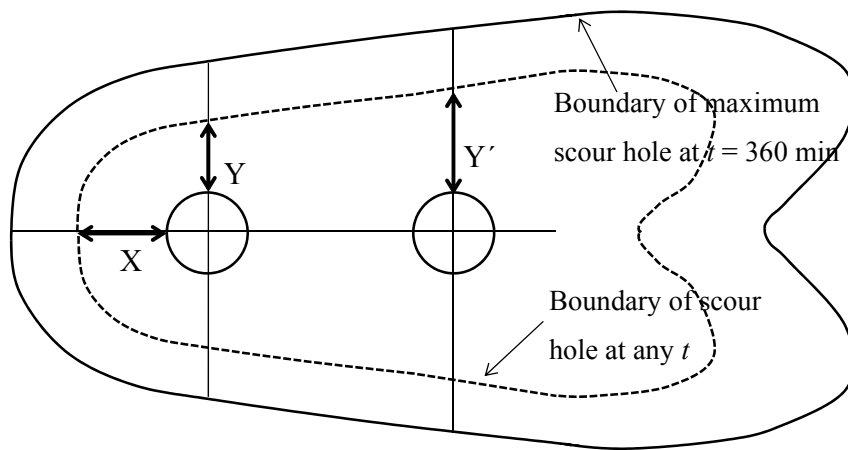


Figure 4.2 Definition sketch for the characteristic dimensions of the scour hole

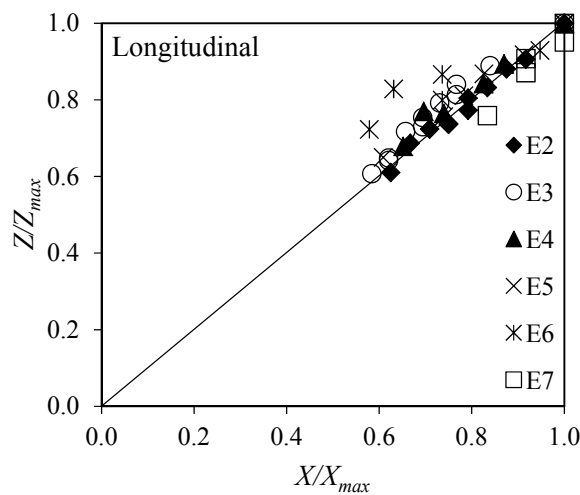


Figure 4.3 Correlation between  $X/X_{max} - Z/Z_{max}$

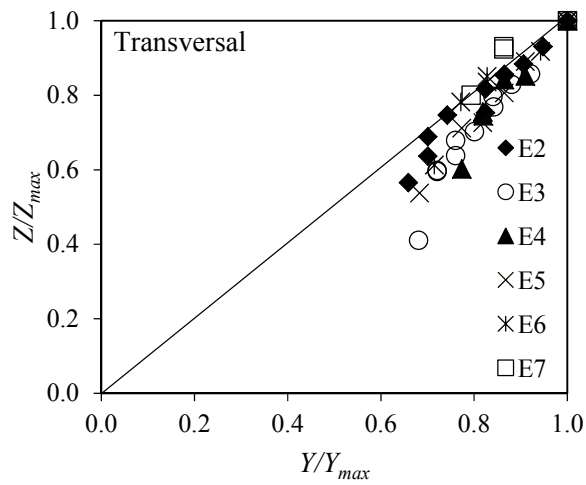


Figure 4.4 Correlation between  $Y/Y_{max} - Z/Z_{max}$

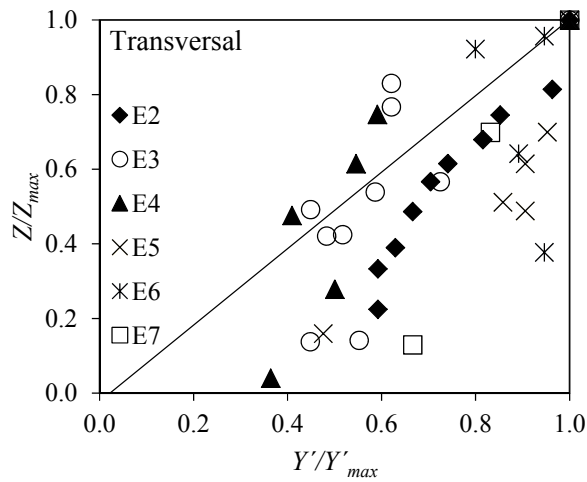


Figure 4.5 Correlation between  $Y'/Y'_{max} - Z/Z_{max}$

#### 4.1.4 Maximum Scour Depth Location between Piers

For any combination of pier size and spacing and flow intensity, the maximum scour depth in the combined scour hole of tandem piers is always observed at the upstream of the front pier, at any time (See Figures 3.13 and 3.14). Yet, the

maximum scour depth between the piers and its location is also investigated from the bed topography maps obtained in Experiments Part I. Since the downstream nose of the front pier (point A in Figures 4.6 – 4.11) is sheltered by the pier itself along the centerline in the wake region, this zone is under the effect of wake vortices. However, the zone where the maximum scour depth between piers occurs is under the combined effect of both horse-shoe and wake vortices. Therefore, the maximum scour depth occurs eccentrically with respect to pier axis as shown in Figures 4.6 – 4.11. The black arrows in these figures indicate the flow direction. The maximum scour depth generally occurs at ~2.5 cm downstream of the front piers' downstream face and its eccentricity from the centerline on both sides is 0.3-3.6 cm along the flow direction. In Table 4.1 and Table 4.2, locations of the maximum scour depth between piers for runs E2-E3 and E4-E7 are presented, respectively. In this table,  $r$  is the radial coordinate of the maximum scour depth location with respect to the center of the front pier and  $\theta$  is the angular coordinate with respect to the centerline along the flow direction. In the experiments, it is clearly observed that the time-dependent maximum scour depth between piers occur symmetrically with respect to axes of piers, as shown in Figures 4.6 – 4.11.

Table 4.1 Radial and angular coordinates for runs E2-E3

t (min)	E2		E3	
	r (cm)	$\theta$ (°)	r (cm)	$\theta$ (°)
5	5.90	12.74	8.19	58.74
10	6.19	21.80	5.78	5.96
15	6.19	21.80	5.78	5.96
20	5.90	12.74	6.19	21.80
30	6.19	21.80	6.31	24.33
45	6.31	24.33	6.19	21.80
60	6.31	24.33	5.78	5.96
80	6.78	32.05	5.76	2.99
100	6.78	32.05	6.31	24.33
150	6.78	32.05	5.78	5.96
360	6.78	32.05	6.06	18.29

Table 4.2 Radial and angular coordinates for runs E4-E7

t (min)	E4		E5		E6		E7	
	r (cm)	$\theta$ (°)	r (cm)	$\theta$ (°)	r (cm)	$\theta$ (°)	r (cm)	$\theta$ (°)
5	5.95	25.92	5.68	19.55	4.54	7.59	4.51	3.81
20	5.95	25.92	5.58	16.65	4.54	7.59	4.51	3.81
60	5.51	13.66	5.68	19.55	4.54	7.59	4.51	3.81
100	5.36	3.21	5.58	16.65	4.54	7.59	4.51	3.81
150	5.36	3.21	5.51	13.66	4.54	7.59	4.54	7.59
360	5.36	3.21	5.36	3.21	4.51	3.81	4.51	3.81

Reinforcing effect is also observed in the maximum scour depth between piers. For instance, for  $b = 7.5$  cm, approximately 7.5% increase in the maximum scour depth is observed for  $\lambda = 0.33$  relative to the case when  $\lambda = 0.25$ . Reinforcing effect is stronger, and the reduction in the exit slope and height (see Figure 2.7) is higher when  $\lambda = 0.33$ . In the smaller piers, the duration of the experiments is not sufficient to observe this effect.

Variation of the location of the maximum scour depth between piers can be seen on the sketches given in Figures 4.6 – 4.11. Radial and angular coordinates of the maximum scour depth locations with respect to the center of the front pier at an arbitrary time are also shown on the figures. Although more frequent measurements are taken for runs E2 and E3, the locations corresponding to the test times similar to runs E3-E7 are presented for one-to-one comparison.

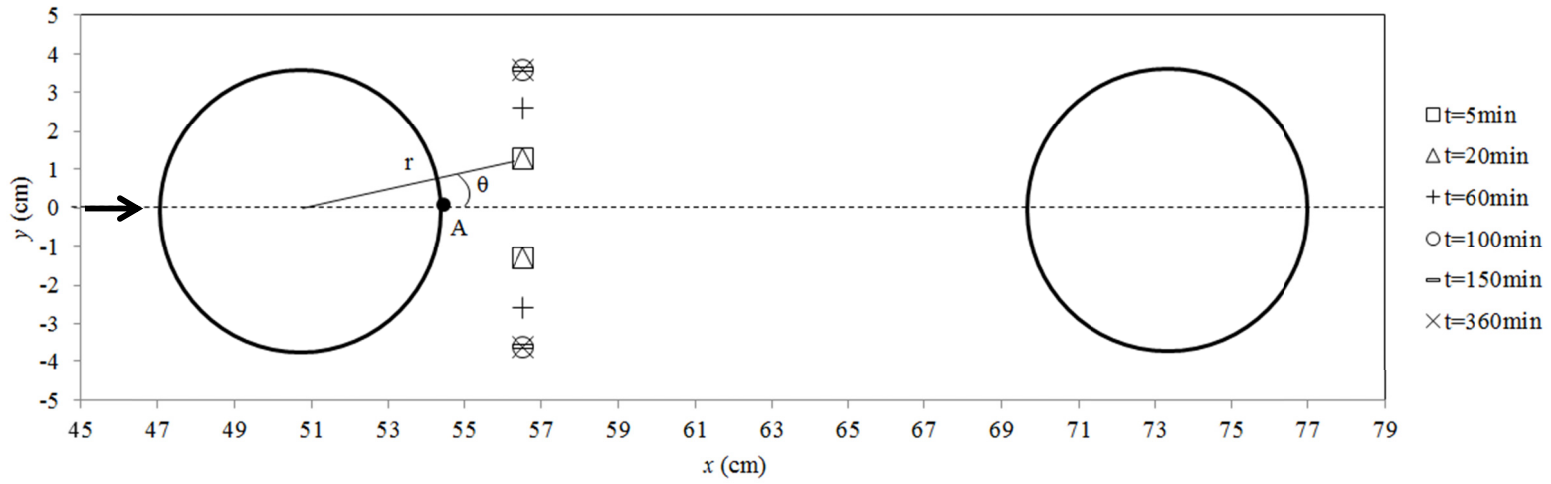


Figure 4.6 Location of the maximum scour depth between piers for Run E2

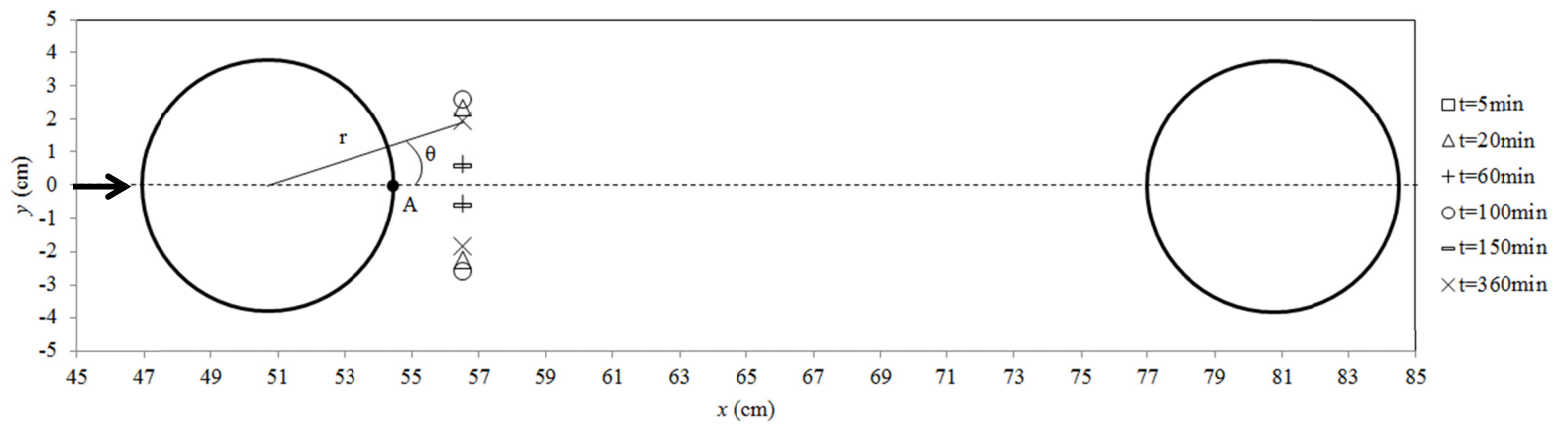


Figure 4.7 Location of the maximum scour depth between piers for Run E3

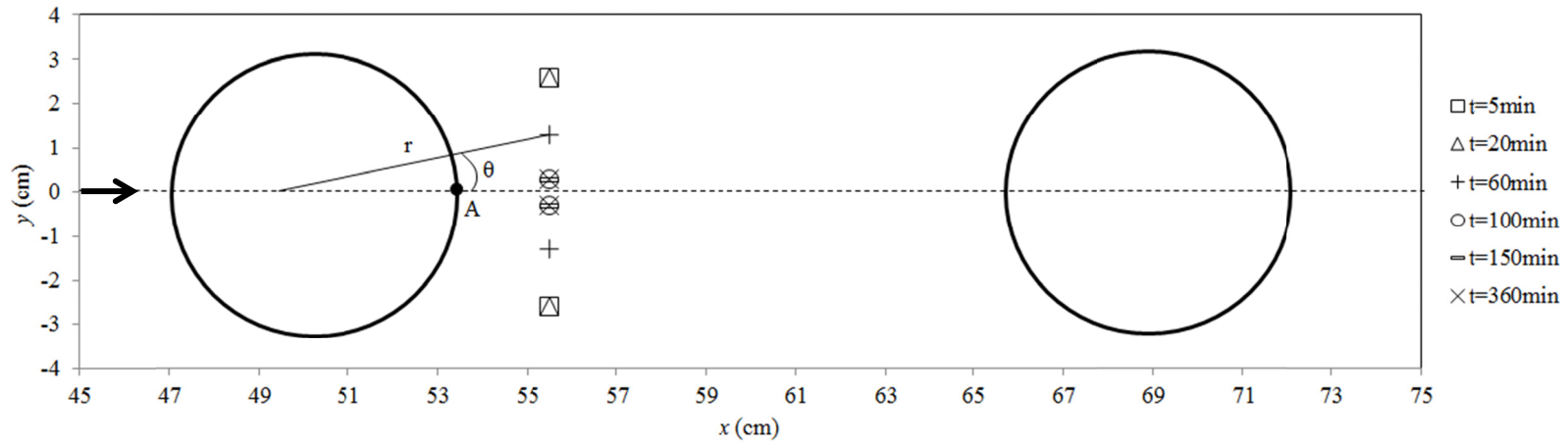


Figure 4.8 Location of the maximum scour depth between piers for Run E4

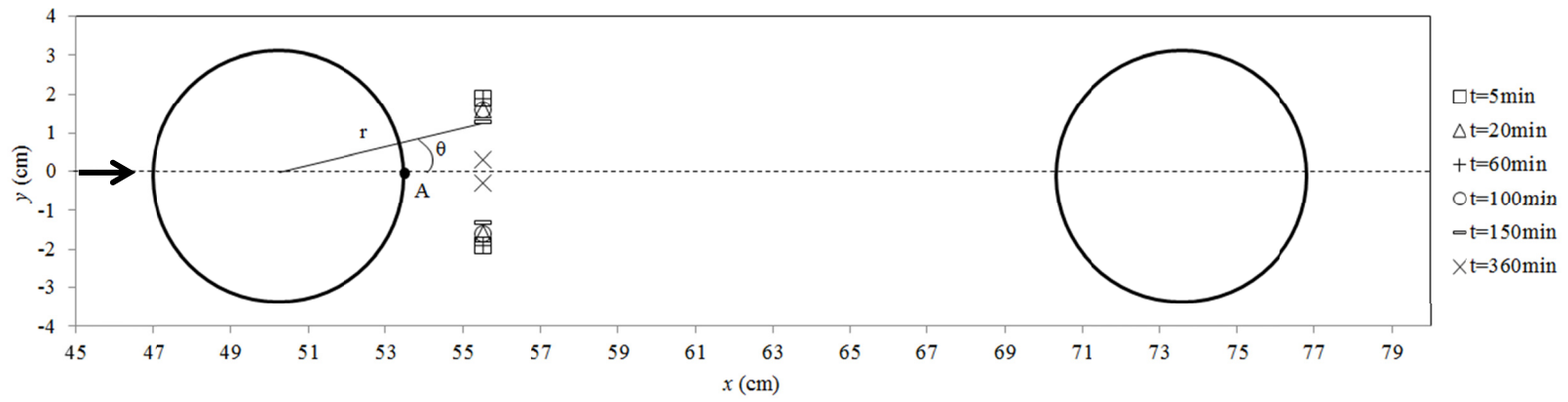


Figure 4.9 Location of the maximum scour depth between piers for Run E5

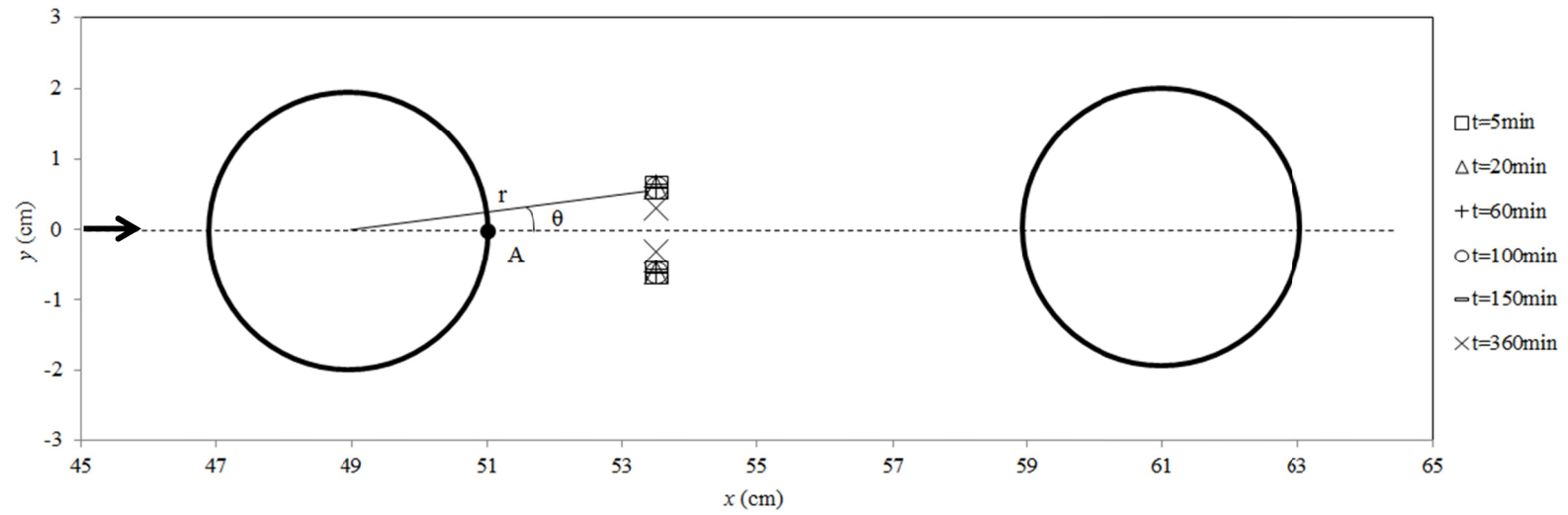


Figure 4.10 Location of the maximum scour depth between piers for Run E6

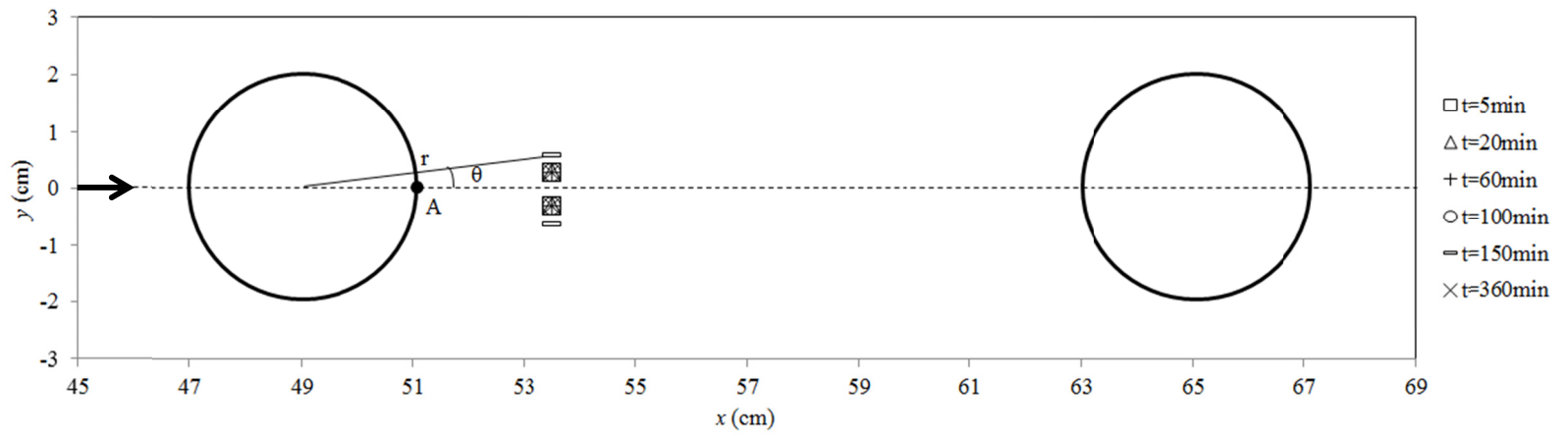


Figure 4.11 Location of the maximum scour depth between piers for Run E7

## 4.2 Scour Prediction Equations

Results of the Experiments Part I are grouped into three according to their  $\lambda$  values and multiple linear regression equations are obtained for the maximum scour depth at the upstream of front pier. Using the governing parameters included in scouring process as independent variables, the following regression equations are obtained with  $R^2 = 0.98, 0.83,$  and  $0.83,$  respectively:

$$\frac{d_s}{b} = 0.135 \left( \frac{d_0}{b} \right)^{0.337} (F_d)^{1.856} (T_s)^{0.112} \quad (\lambda = 0.5) \quad (4.2a)$$

$$\frac{d_s}{b} = 0.053 \left( \frac{d_0}{b} \right)^{0.152} (F_d)^{2.687} (T_s)^{0.126} \quad (\lambda = 0.33) \quad (4.2b)$$

$$\frac{d_s}{b} = 0.098 \left( \frac{d_0}{b} \right)^{0.154} (F_d)^{1.984} (T_s)^{0.123} \quad (\lambda = 0.25) \quad (4.2c)$$

These empirical equations will be compared with the experimental data in Chapter 5 together with the results of the semi-empirical model that will be discussed in the same chapter.

## CHAPTER 5

### DEVELOPMENT OF THE SEMI-EMPIRICAL MODEL

#### 5.1 The Semi-Empirical Model

In this chapter, the development of the semi-empirical model to determine the time-wise variation of clear-water scour depth at dual piers in tandem arrangement is explained. The model development is based on the sediment continuity equation as follows:

$$\frac{dV}{dt} = Q_{so} - Q_{si} \quad (5.1)$$

where,  $Q_{so}$  is the volumetric rate of sediment transport carried out from the scour hole and  $Q_{si}$  is the volumetric rate of sediment transport carried into the scour hole. In case of clear-water scour condition, there is no sediment flux into the scour hole from the upstream, therefore  $Q_{si} = 0$ . A sediment pickup rate is used to formulate  $Q_{so}$  (Yanmaz, 2006):

$$Q_{so} = \beta \frac{EA_p}{\Delta\rho_s} \quad (5.2)$$

where,  $\beta$  is the coefficient of proportionality which accounts for the scour hole geometry and properties of sediment and flow,  $E$  is the sediment pickup rate in mass per unit time and area, and  $A_p$  is the unit area from which the sediment is picked up. Yanmaz (1994) have discussed the use of numerous sediment pickup

functions reported in the literature. Considering the experimental condition of the current study, a proper pickup function proposed by Dey and Debnath (2001) is selected. This function, given in Eq. (5.3) is valid for horizontal, mild, steep, and adverse slopes, sediment size range of 0.24 – 1.55 mm, and both uniform and non-uniform sediments. Eq. (5.3) has been applied satisfactorily by Yanmaz (2006) and Yanmaz and Köse (2009) to single cylindrical piers and to abutments of different shapes, respectively.

$$E = 0.0006TD_*^{0.24}\sigma_g^{1.9}\rho_s\sqrt{\Delta gD_{50}} \quad (5.3)$$

where  $T = (\tau_b - \tau_{bc}) / \tau_{bc}$  is the transport-stage parameter due to scouring,  $\tau_b$  is the bed shear stress on the flat region of the scour hole,  $\tau_{bc} = \psi\tau_{cr}$  is the critical bed shear stress on the flat region of the scour hole,  $\psi$  is a factor depending on turbulent fluctuations and oscillation of primary vortex,  $\tau_{cr}$  is the critical bed shear stress on flat bed,  $D_* = D_s(\Delta g/\nu^2)^{1/3}$  is the dimensionless particle diameter. Parameter  $T$  represents the mobility of sediment particles during pickup in the scour hole (Dey and Debnath, 2001).

In the current study, the time-averaged value of  $\tau_b$ , which is calculated by Eq. (4.1) is assumed to be equal to  $\tau_0$  throughout the experiments, similar to the assumptions made by Yanmaz (2006) and Yanmaz and Köse (2009) in their previous studies. Additional force is exerted by the turbulent fluctuations and oscillation of primary vortex, toward the motion of sediment in the three-dimensional vortex mechanism of scouring. During scouring, the corresponding  $\psi$  term is not necessarily constant; however use of an average value of  $\psi$  brings practical solution. Moreover, as mentioned previously, equilibrium scour condition is attained when  $\tau_b$  tends to  $\psi\tau_{cr}$  (Dey and Barbhuiya, 2005). Therefore,  $\psi$  is a significant factor in scouring process and the representative  $\psi$  value in the computations needs to be determined carefully. For clear-water scour at abutments, Barbhuiya (2003) proposed the average value of  $\psi = 0.5$  and it is used by Dey and Barbhuiya (2005) and Yanmaz and Köse (2009) in their studies. Yanmaz (2006) also used  $\psi = 0.5$  for clear-water

scour at single cylindrical bridge piers, considering the fundamental similarity of the clear-water scour hole characteristics.

A sensitivity analysis is carried out in this study for  $\psi$  term and the most proper values of  $\psi$  are selected for different experimental conditions to have good agreement between experimental and computed scour depths.

Another important term in the sediment pickup theory, the coefficient of proportionality ( $\beta$ ) is determined by using the experimental results of the maximum scour depth variation in time. To begin with, volume of the scour hole is determined from Eq. (3.3) by inserting the values of  $V^*$  and  $T_s$ . The scour hole volume is then:

$$V = c_1 t^{0.327} d_s \quad (5.4)$$

Here,  $c_1 = 0.7345\pi\lambda^{-0.387}D_{50}^{0.327}(\Delta g D_{50})^{0.1635}b^{1.346}$ . Eq. (5.1) is solved together with Eqs. (5.2), (5.3), and (5.4). The  $\beta$  term is determined as follows:

$$\beta = \frac{\Delta\rho_s}{EA_p} \frac{dV}{dt} \quad (5.5)$$

For single cylindrical pier scour,  $A_p$  is defined as the projected width of scour hole normal to the flow at the upstream of the pier multiplied by the particle size (Yanmaz and Altınbilek, 1991; Yanmaz, 2006). For dual piers, representative pickup area can also be defined at the upstream of the front pier. Knowing that the side inclination of the scour hole at front pier remains unchanged with respect to time and almost equal to angle of repose of the sediment,  $A_p$  is calculated from  $(2d_s \cot\phi + b)D_{50}$ . To solve Eq. (5.5), time derivative of  $V$  is obtained as:

$$\frac{dV}{dt} = c_1 t^{0.327} \frac{d(d_s)}{dt} + 0.327 c_1 d_s t^{-0.673} \quad (5.6)$$

Finally, relevant parameters are inserted into Eq. (5.5), and  $\beta$  is obtained as:

$$\beta = \frac{\int c_1 c_2 t^{0.327} d(d_s) + \int 0.327 c_1 c_2 d_s t^{-0.673} dt}{\int (2d_s \cot \phi + b) dt} \quad (5.7)$$

where  $c_2 = \Delta\rho_s/ED_{50}$ . For the limits of the integration in Eq. (5.7), the experimental data of  $d_s$  versus  $t$  at the upstream face of the front pier as presented in Table B.1 are used and successive values of  $\beta$  are then computed. Variation of  $\beta$  in time can be found in Figures 5.1 – 5.7. As can be seen from the figures, sediment transport rate from the scour hole is high at the beginning of scouring, which results in large values of  $\beta$ . As  $Q_{so}$  decreases with time, the  $\beta$  values also decrease.

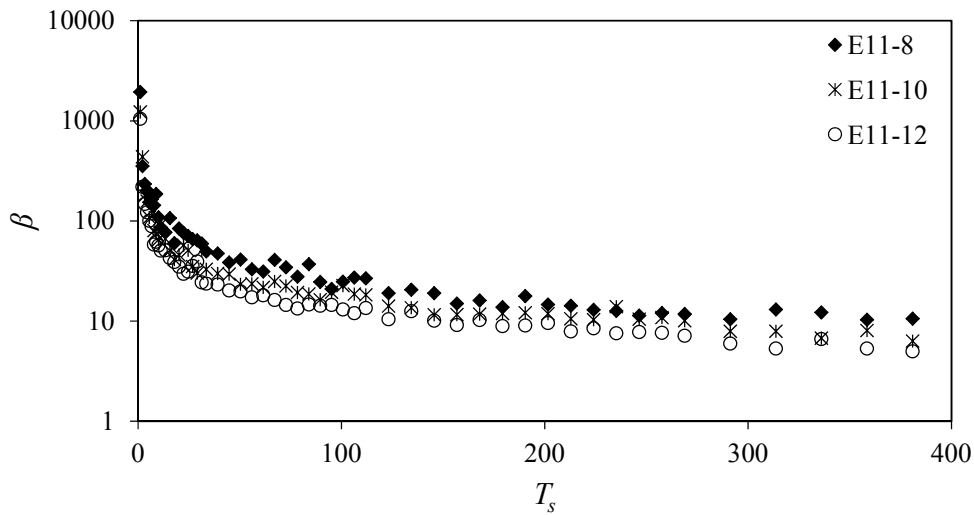


Figure 5.1 Variation of  $\beta$  with time for Runs E11

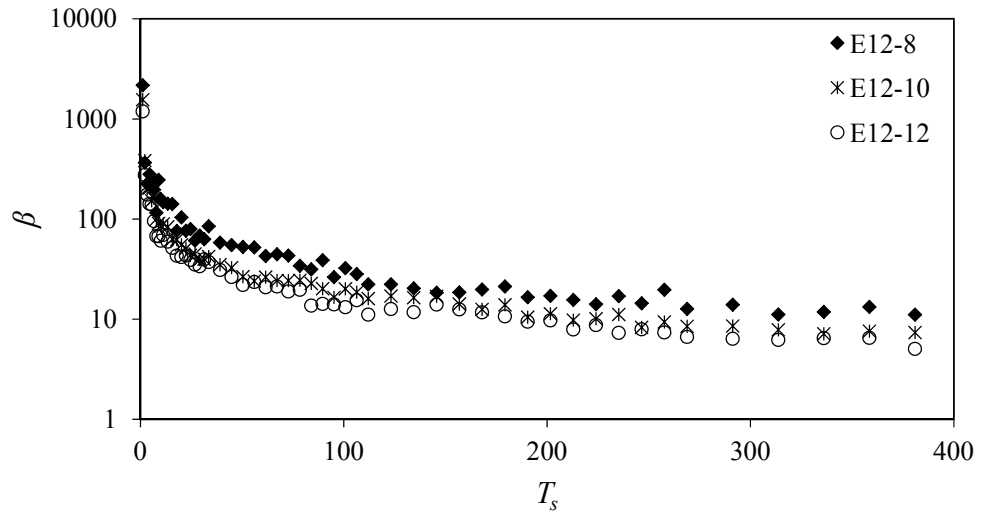


Figure 5.2 Variation of  $\beta$  with time for Runs E12

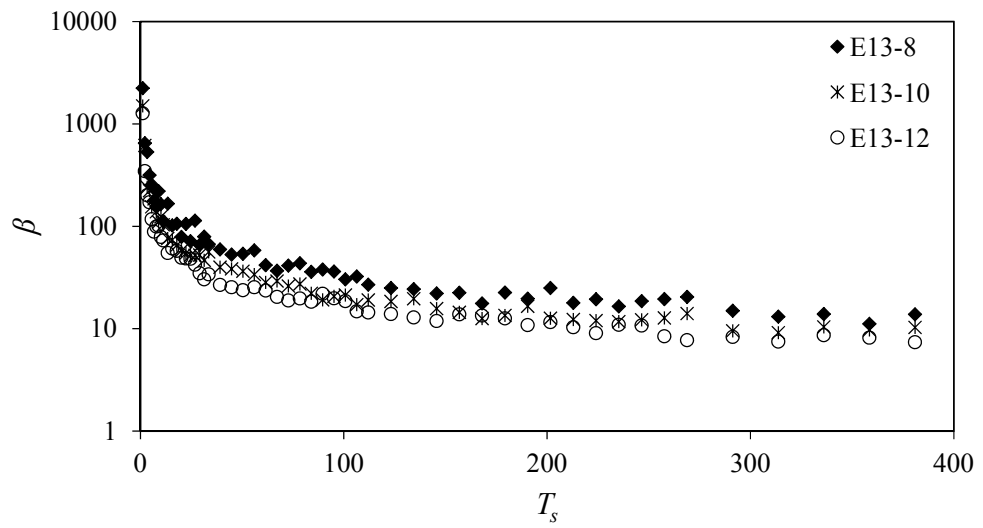


Figure 5.3 Variation of  $\beta$  with time for Runs E13

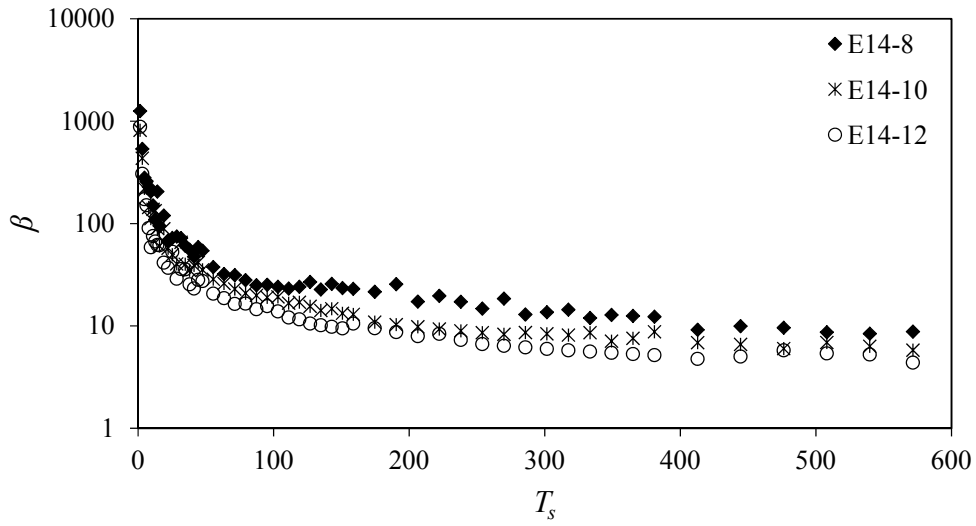


Figure 5.4 Variation of  $\beta$  with time for Runs E14

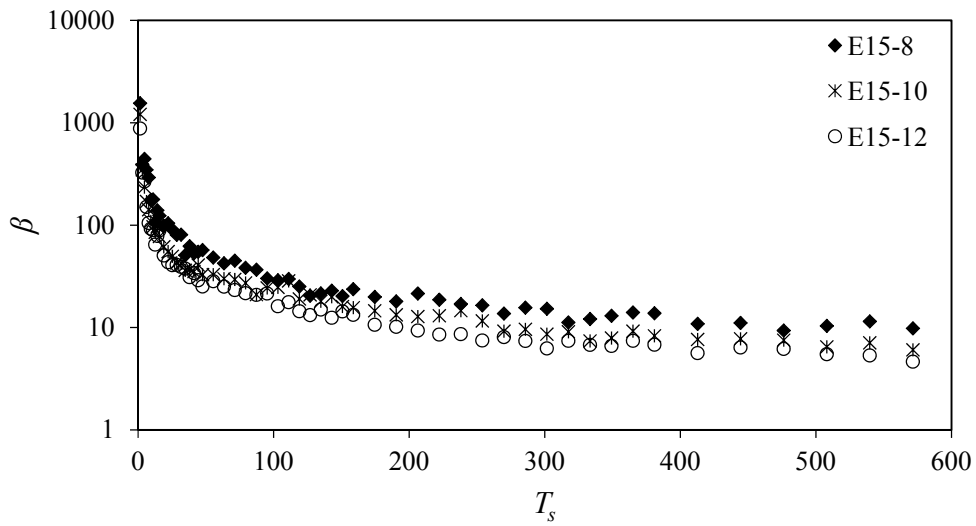


Figure 5.5 Variation of  $\beta$  with time for Runs E15

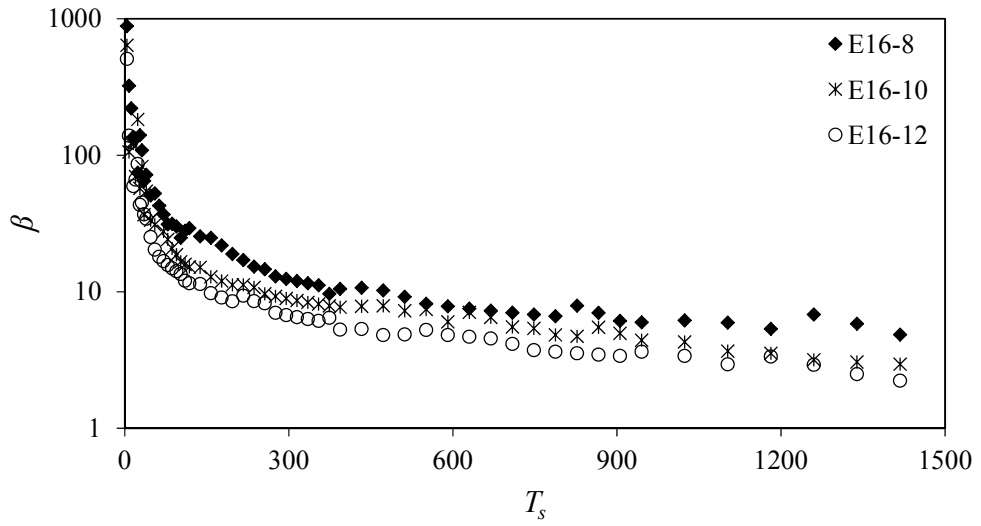


Figure 5.6 Variation of  $\beta$  with time for Runs E16

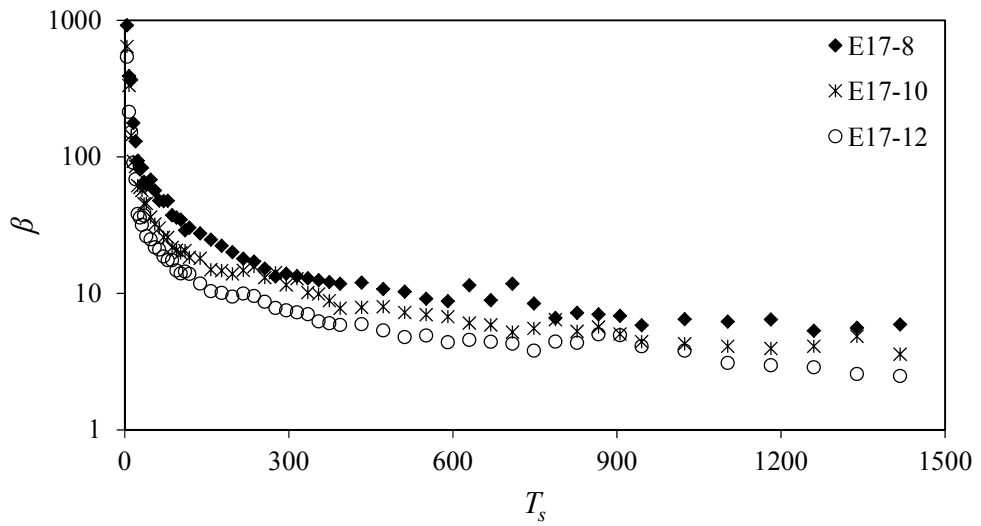


Figure 5.7 Variation of  $\beta$  with time for Runs E17

To determine the time-variation of the scour depth,  $\beta$  term is to be expressed in an explicit form. Since  $\beta$  term reflects the combined effects of scour hole geometry, pier size, time, and properties of sediment and flow, possible combinations of dimensionless parameters accounting for these characteristics are tested. To this end, functional forms of the dimensionless parameters  $u_*t/b$ ,  $u_*t/d_0$ ,  $u_*tD_{50}/b^2$ ,  $d_s \cot \phi / b$ , and  $u/u_c$  are combined as follows:

$$\beta_1 = m \left( \frac{u_*t}{b} \right)^{x_1} \left( \frac{d_s \cot \phi}{b} \right)^{x_2} \quad (5.8a)$$

$$\beta_2 = m \left( \frac{u_*t}{d_0} \right)^{x_1} \left( \frac{d_s \cot \phi}{b} \right)^{x_2} \quad (5.8b)$$

$$\beta_3 = m \left( \frac{u_*tD_{50}}{b^2} \right)^{x_1} \left( \frac{d_s \cot \phi}{b} \right)^{x_2} \quad (5.8c)$$

$$\beta_4 = m \left( \frac{u_*tD_{50}}{b^2} \right)^{x_1} \left( \frac{d_s \cot \phi}{b} \right)^{x_2} \left( \frac{u}{u_c} \right)^{x_3} \quad (5.8d)$$

where,  $m$  is the coefficient,  $x_1$ ,  $x_2$ , and  $x_3$  are exponents of the functional form of  $\beta$ . Using a multiple linear regression analysis,  $m$ ,  $x_1$ ,  $x_2$ , and  $x_3$  are calculated.

### 5.1.1 Selection of $\beta$ Combination and Solution Method

In the selection of the representative  $\beta$  combination to apply for all experiments, sensitivity analyses are carried out to select the proper solution method to solve  $d(d_s)/dt$  in Eq. (5.9), which is a first-order nonlinear differential equation. With  $\psi = 0.5$  as an initial guess,  $\beta_1$  combination is used to test numerical solution methods, such as Euler, modified Euler, and 4<sup>th</sup> order Runge-Kutta method. Using these solution methods, Eqs. (5.1), (5.2), (5.6), and (5.8a) are solved together for  $d(d_s)/dt$ . The experimental  $d_s - t$  data of all experiments are compared with computed  $d_s - t$  values using the solution methods mentioned above. Considering the correlation coefficient ( $R^2$ ) and root mean square error of the estimate (RMSE),

modified Euler method is selected as the proper solution method to solve for  $d(d_s)/dt$  (See Table 5.1). Once the solution method is selected, the optimum  $\beta$  combination is selected again with  $\psi = 0.5$  and considering the average  $R^2$  and RMSE values of the experiments. As can be seen from Table 5.1, The representative combination is selected as  $\beta_1$ , to be used in the numerical solution of  $d(d_s)/dt$ .

Table 5.1 Decision table for solution method and  $\beta$  combination

Statistics	Solution method			$\beta$ combination			
	Euler	Modified Euler	4th order Runge Kutta	$\beta_1$	$\beta_2$	$\beta_3$	$\beta_4$
$R^2$	0.963	0.977	0.981	0.977	0.974	0.978	0.971
RMSE(cm)	0.58	0.42	0.50	0.42	0.44	0.61	0.85

### 5.1.2 Selection of $\psi$ values

Together with the similar selection criteria as mentioned above,  $\psi$  values of the experiments are selected by graphical comparison between experimental and computed values of  $d_s$  versus  $t$ . A representative value of  $\psi$  is intended to be obtained for a particular value of  $\lambda$ , regarding the basic similarity of vortex fields in the scour hole. Table 5.2 shows the  $R^2$  and RMSE values of the  $\psi$  trials. As discussed above, the experiments are grouped according to their  $\lambda$  values, since the scour hole volume depends on the  $\lambda$  value. Therefore,  $\psi = 0.6$  is selected for  $\lambda = 0.5$  (Run E11) and  $\psi = 0.5$  is selected for both  $\lambda = 0.33$  and  $0.25$  (Runs E12-17).

Table 5.2 Decision table for  $\psi$  value

Run	$\psi = 0.4$		$\psi = 0.45$		$\psi = 0.48$		$\psi = 0.50$		$\psi = 0.52$		$\psi = 0.55$		$\psi = 0.6$	
	$R^2$	RMSE (cm)	$R^2$	RMSE (cm)	$R^2$	RMSE (cm)	$R^2$	RMSE (cm)	$R^2$	RMSE (cm)	$R^2$	RMSE (cm)	$R^2$	RMSE (cm)
E11-8	0.990	0.40	0.990	0.33	0.991	0.29	0.991	0.27	0.991	0.24	0.991	0.20	0.990	0.14
E11-10	0.959	0.31	0.959	0.29	0.959	0.28	0.958	0.27	0.955	0.27	0.949	0.28	0.990	0.23
E11-12	0.980	0.41	0.983	0.35	0.985	0.31	0.986	0.29	0.987	0.25	0.988	0.22	0.989	0.16
E12-8	0.974	0.53	0.977	0.57	0.979	0.59	0.980	0.62	0.981	0.65	0.983	0.69	0.983	0.79
E12-10	0.986	0.18	0.989	0.17	0.991	0.15	0.992	0.14	0.993	0.13	0.995	0.10	0.996	0.06
E12-12	0.962	0.43	0.967	0.45	0.970	0.48	0.972	0.50	0.974	0.51	0.977	0.56	0.981	0.64
E13-8	0.985	0.46	0.987	0.51	0.988	0.56	0.989	0.61	0.990	0.65	0.991	0.71	0.992	0.84
E13-10	0.979	0.23	0.981	0.20	0.981	0.19	0.981	0.19	0.981	0.18	0.981	0.17	0.979	0.19
E13-12	0.961	0.35	0.964	0.41	0.966	0.45	0.967	0.46	0.968	0.50	0.970	0.56	0.971	0.67
E14-8	0.969	0.56	0.969	0.47	0.970	0.42	0.969	0.37	0.969	0.33	0.968	0.26	0.965	0.18
E14-10	0.992	0.57	0.991	0.56	0.990	0.58	0.990	0.57	0.989	0.57	0.989	0.59	0.937	0.74
E14-12	0.995	0.49	0.994	0.53	0.994	0.57	0.993	0.59	0.993	0.60	0.992	0.65	0.990	0.72
E15-8	0.998	0.51	0.998	0.44	0.998	0.38	0.998	0.33	0.998	0.29	0.998	0.22	0.997	0.08
E15-10	0.958	0.86	0.960	0.87	0.961	0.87	0.961	0.86	0.961	0.86	0.961	0.87	0.959	0.89
E15-12	0.987	0.17	0.986	0.21	0.986	0.24	0.985	0.25	0.984	0.28	0.982	0.33	0.974	0.43
E16-8	0.991	0.10	0.991	0.22	0.990	0.29	0.989	0.35	0.989	0.41	0.987	0.50	0.984	0.67
E16-10	0.964	0.40	0.964	0.34	0.964	0.32	0.964	0.29	0.964	0.27	0.964	0.24	0.965	0.19
E16-12	0.961	0.65	0.963	0.61	0.964	0.60	0.964	0.58	0.965	0.56	0.966	0.54	0.969	0.50
E17-8	0.988	0.31	0.989	0.40	0.989	0.47	0.989	0.52	0.989	0.57	0.989	0.65	0.989	0.81
E17-10	0.962	0.29	0.962	0.27	0.962	0.26	0.961	0.24	0.960	0.24	0.959	0.24	0.951	0.28
E17-12	0.934	0.61	0.937	0.62	0.939	0.62	0.940	0.61	0.942	0.62	0.944	0.62	0.949	0.63

For the selected numerical solution method,  $\beta_I$  combination, and  $\psi$  values, Table 5.3 shows  $m$  coefficient and  $x_1$  and  $x_2$  exponents for corresponding  $\lambda$  values. Since  $\beta$  equation is calibrated using the time-variation of maximum experimental scour depths at the upstream of the front pier, the computed scour depths by Eq. (5.9) also addresses the same location.

Hence, using the corresponding  $\beta$  functions and other relevant parameters mentioned previously,  $d(d_s)/dt$  is solved and the differential equations for  $\lambda = 0.5$ , 0.33, and 0.25 are obtained in Eq. (5.9a), (5.9b), and (5.9c), respectively:

$$\frac{d(d_s)}{dt} = 1695 \left( \frac{u_* t}{b} \right)^{-0.347} \left( \frac{d_s \cot \phi}{b} \right)^{-3.367} \frac{(2d_s \cot \phi + b)}{c_1 c_2 t^{0.327}} - \frac{0.327 d_s}{t} \quad (5.9a)$$

$$\frac{d(d_s)}{dt} = 2603 \left( \frac{u_* t}{b} \right)^{-0.595} \left( \frac{d_s \cot \phi}{b} \right)^{-1.465} \frac{(2d_s \cot \phi + b)}{c_1 c_2 t^{0.327}} - \frac{0.327 d_s}{t} \quad (5.9b)$$

$$\frac{d(d_s)}{dt} = 2449 \left( \frac{u_* t}{b} \right)^{-0.563} \left( \frac{d_s \cot \phi}{b} \right)^{-1.674} \frac{(2d_s \cot \phi + b)}{c_1 c_2 t^{0.327}} - \frac{0.327 d_s}{t} \quad (5.9c)$$

Table 5.3 Coefficient and exponents of the functional form of  $\beta_I$

$\lambda$	$\psi$	$m$	$x_1$	$x_2$
0.5	0.6	1695	-0.347	-3.367
0.33	0.5	2603	-0.595	-1.465
0.25	0.5	2449	-0.563	-1.674

## 5.2 Comparison of Scour Prediction Models

The experimental scour depths are compared with the results of empirical regression equations given by Eq. (4.2) and the semi-empirical model results obtained by Eq. (5.9) are compared for all 21 runs and their graphical comparison is presented in Figures 5.8 – 5.28. The results are also compared for their RMSE and  $R^2$  values for each run as can be seen in Table 5.4. The semi-empirical model

results for  $d_s - t$  from Eq. (5.9), in which  $\Delta = 1.65$  for quartz sand and  $\phi = 33^\circ$ , are satisfactorily in good agreement with the experimental results. The empirical equation results show that the results of Eq. (4.2) also provide good prediction for the variation of scour depth with time. However, Figures 5.8 – 5.28 and Table 5.4 show that the semi-empirical model provides better estimation for the scour depths than the empirical equation. Therefore, the use of semi-empirical model results is recommended.

Another important fact is that the semi-empirical model includes the application of a conservation law, i.e. sediment continuity equation and a volumetric sediment transport rate from the scour hole with the use of a sediment pickup function. Therefore, semi-empirical model includes the physics of the scouring process and sediment transport mechanism in the scour hole in its background, compared to the empirical approach.

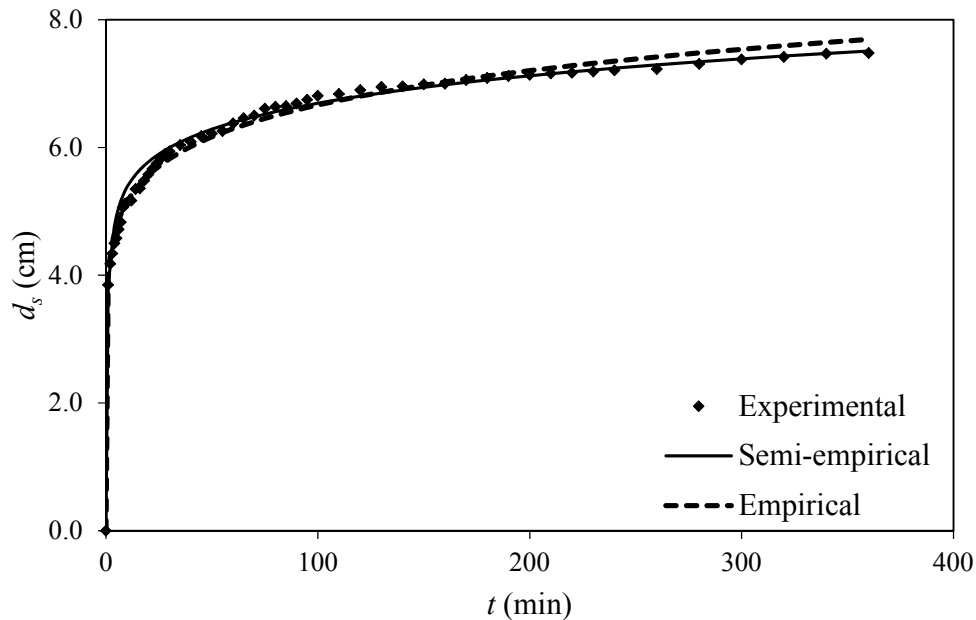


Figure 5.8 Comparison for Run E11-8

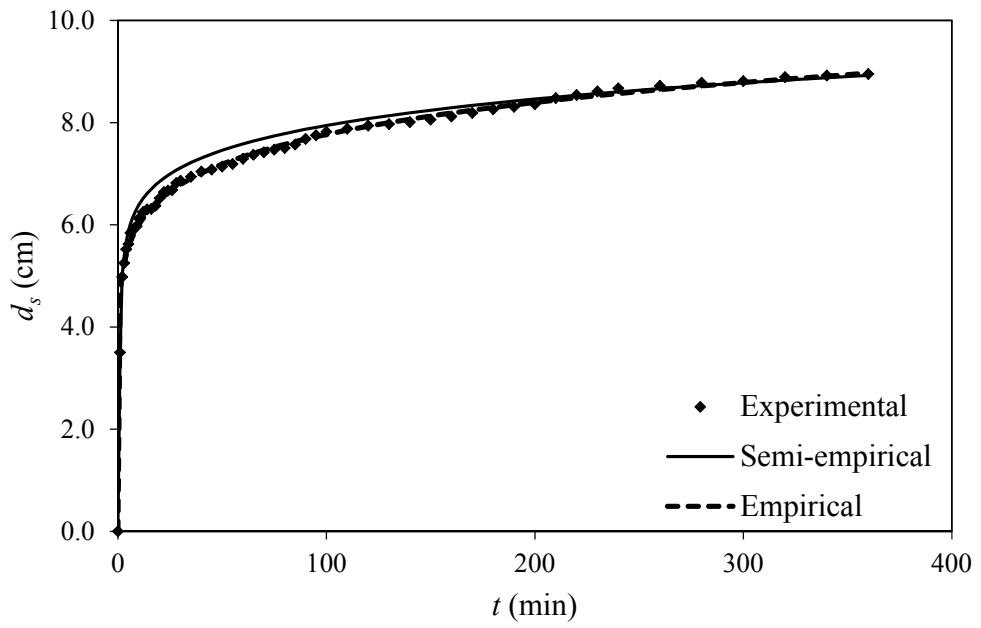


Figure 5.9 Comparison for Run E11-10

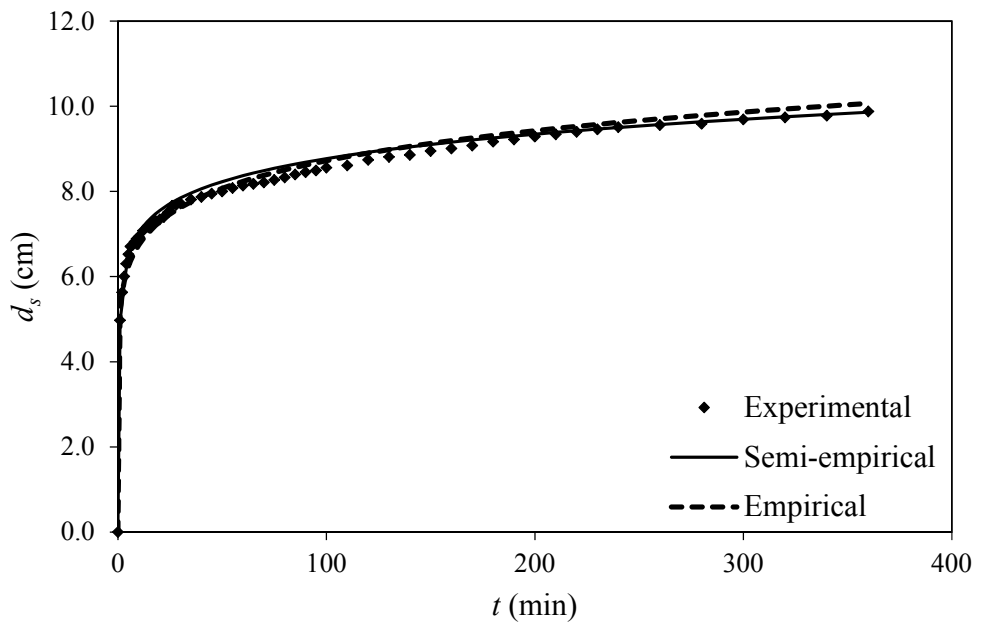


Figure 5.10 Comparison for Run E11-12

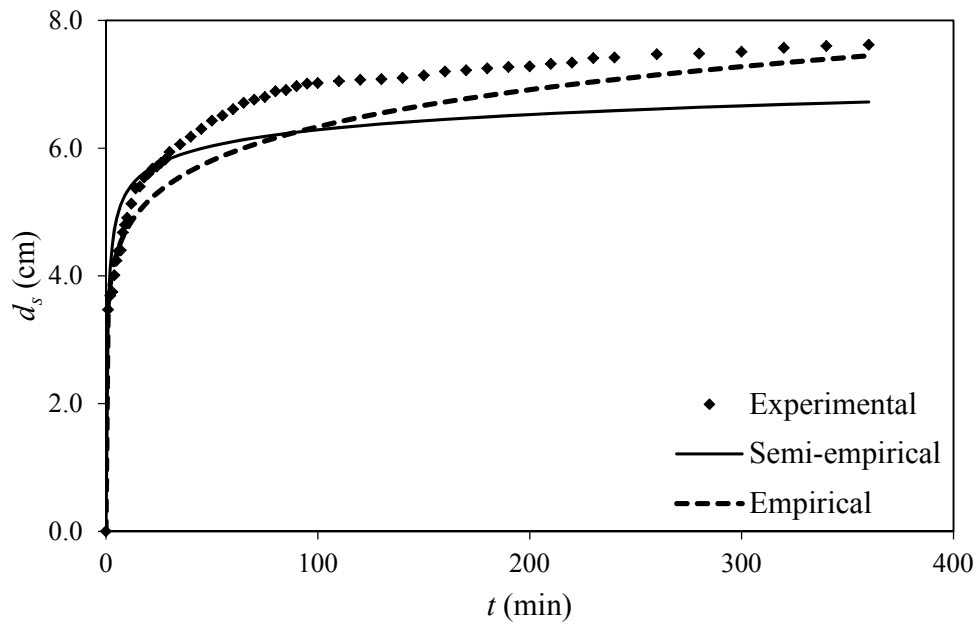


Figure 5.11 Comparison for Run E12-8

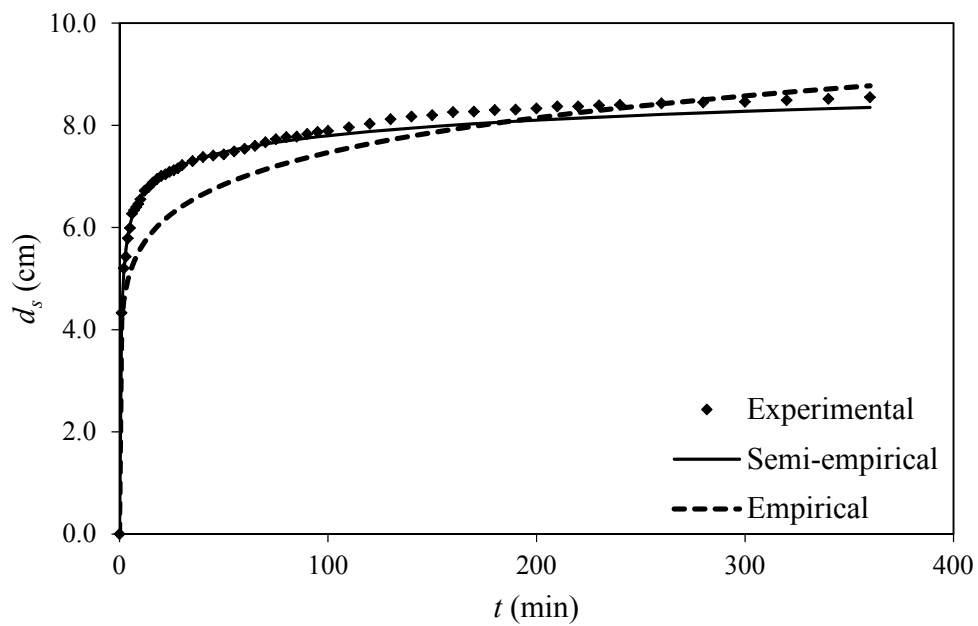


Figure 5.12 Comparison for Run E12-10

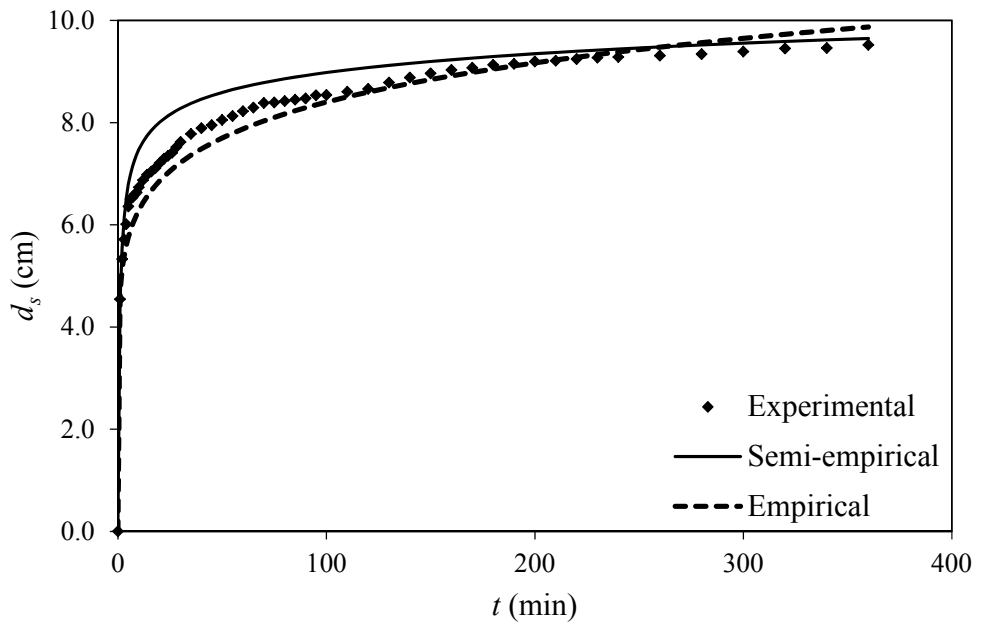


Figure 5.13 Comparison for Run E12-12

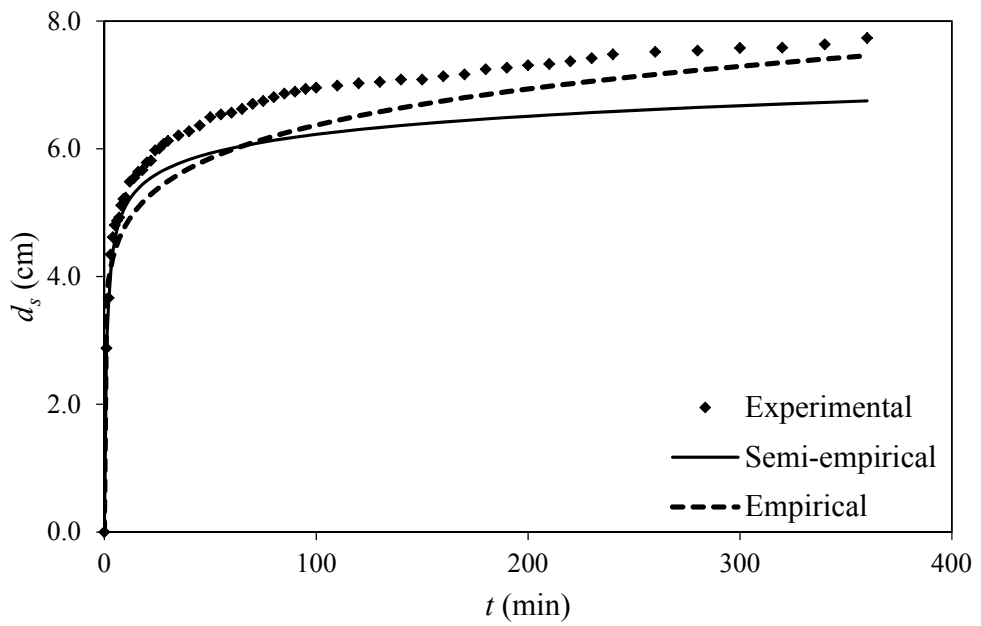


Figure 5.14 Comparison for Run E13-8

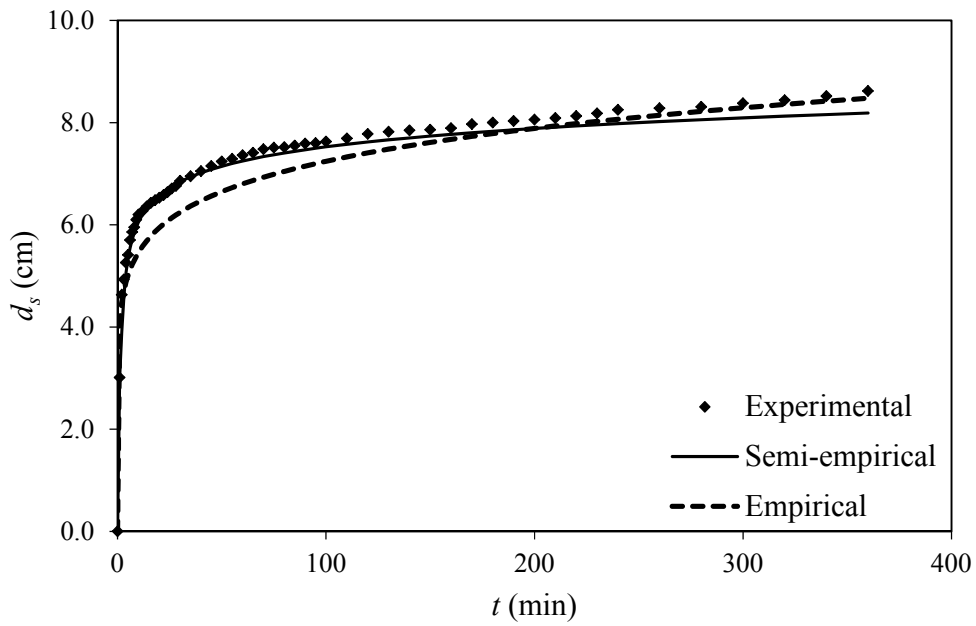


Figure 5.15 Comparison for Run E13-10

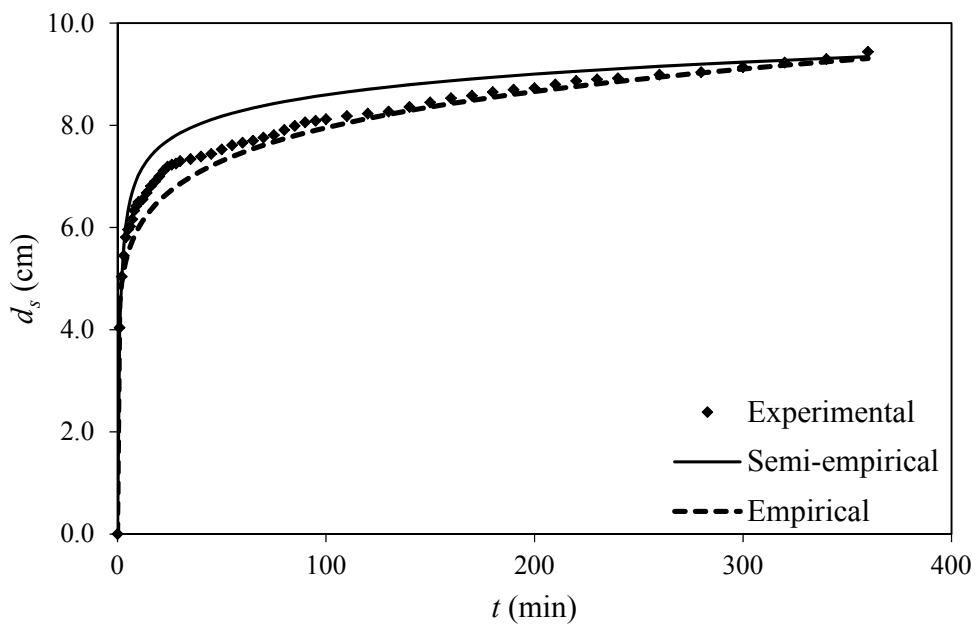


Figure 5.16 Comparison for Run E13-12

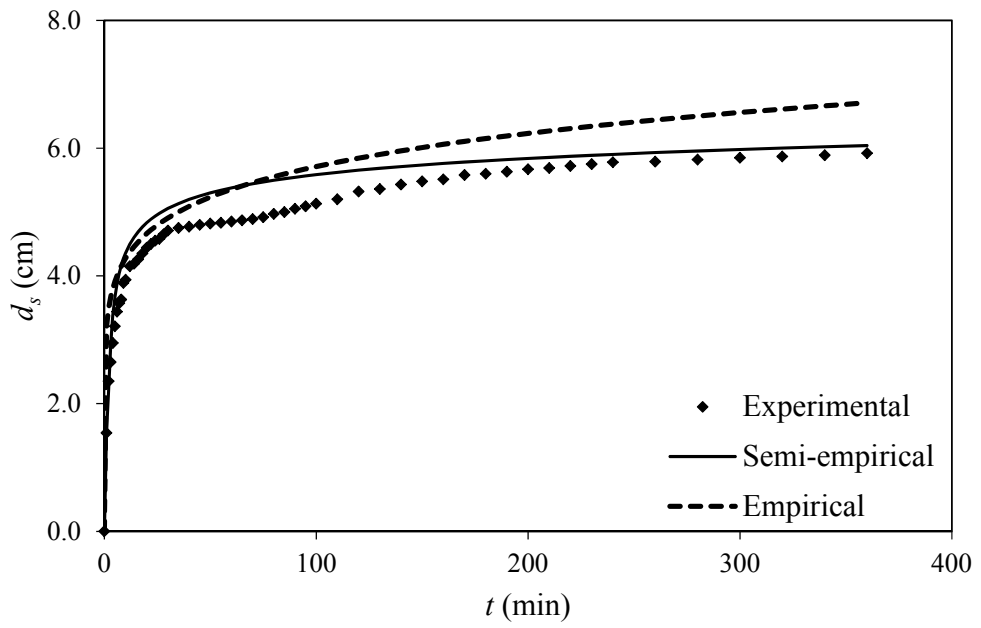


Figure 5.17 Comparison for Run E14-8

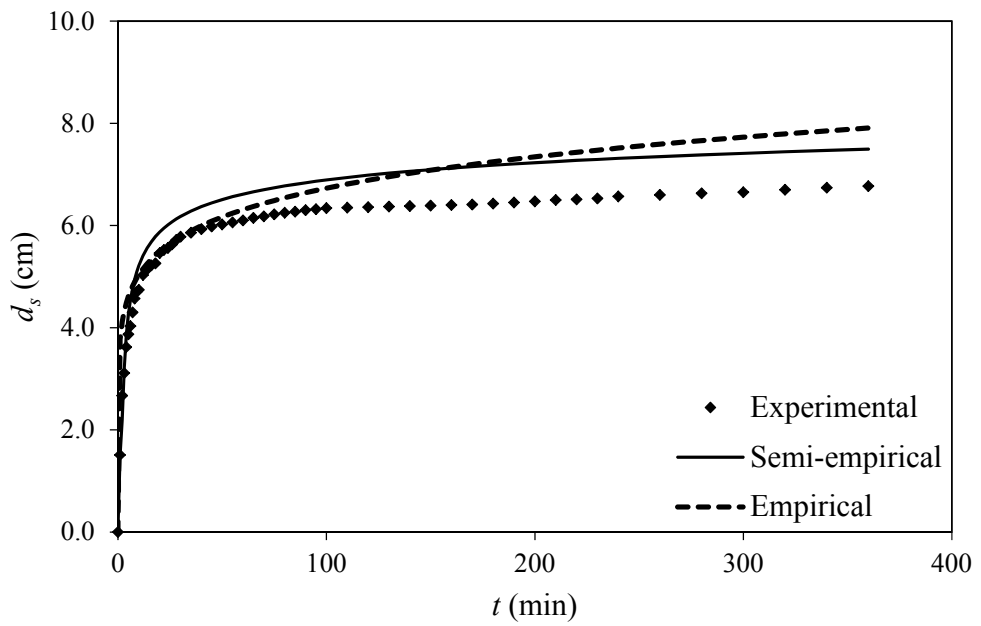


Figure 5.18 Comparison for Run E14-10

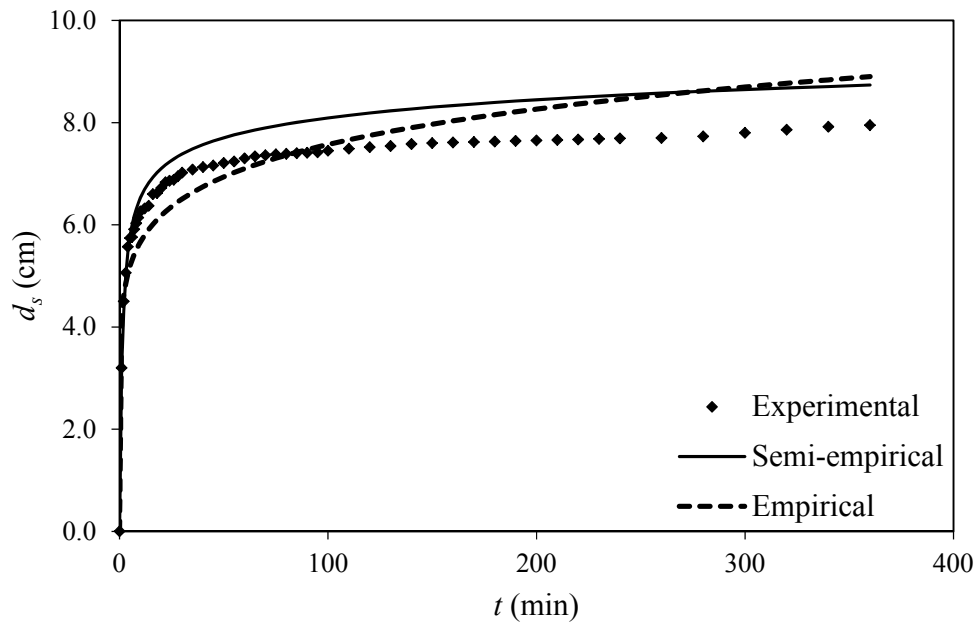


Figure 5.19 Comparison for Run E14-12

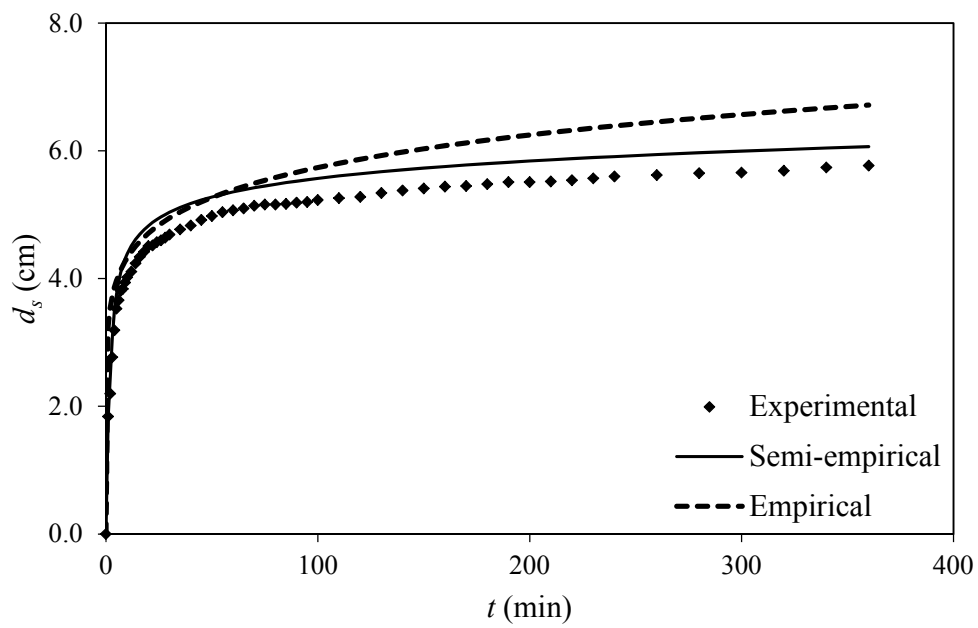


Figure 5.20 Comparison for Run E15-8

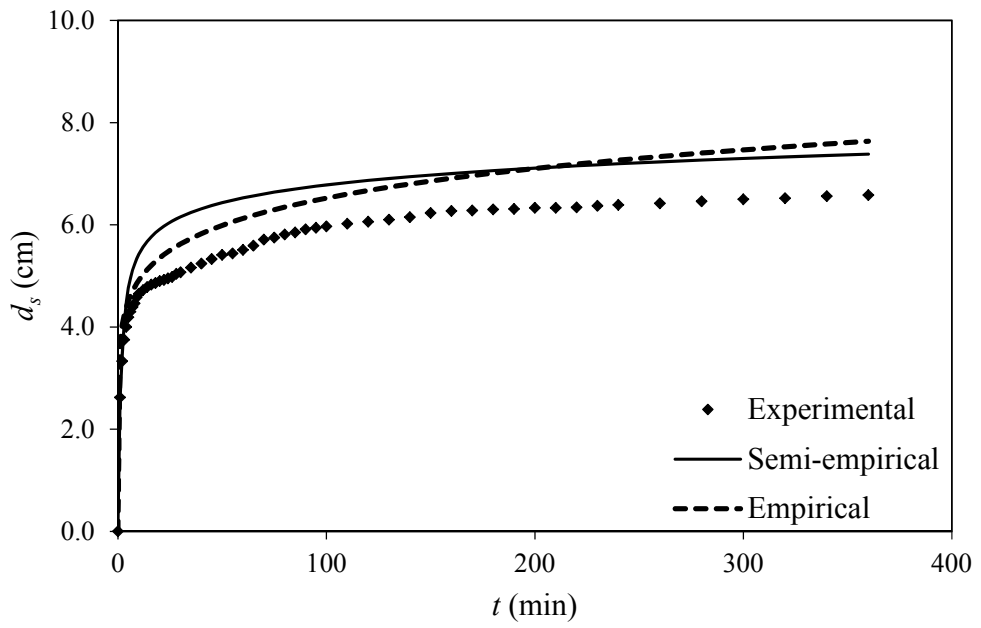


Figure 5.21 Comparison for Run E15-10

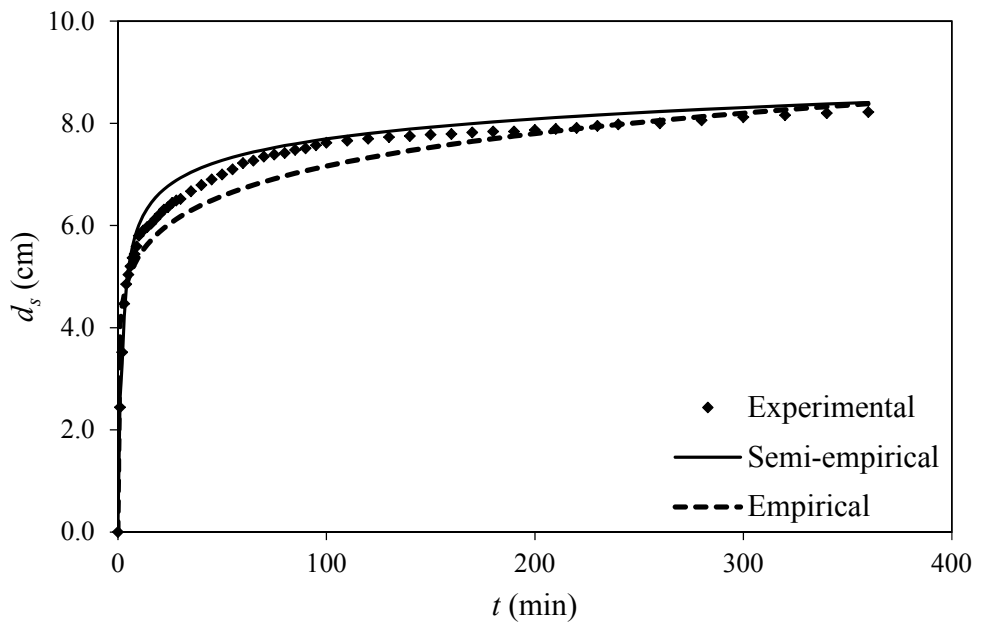


Figure 5.22 Comparison for Run E15-12

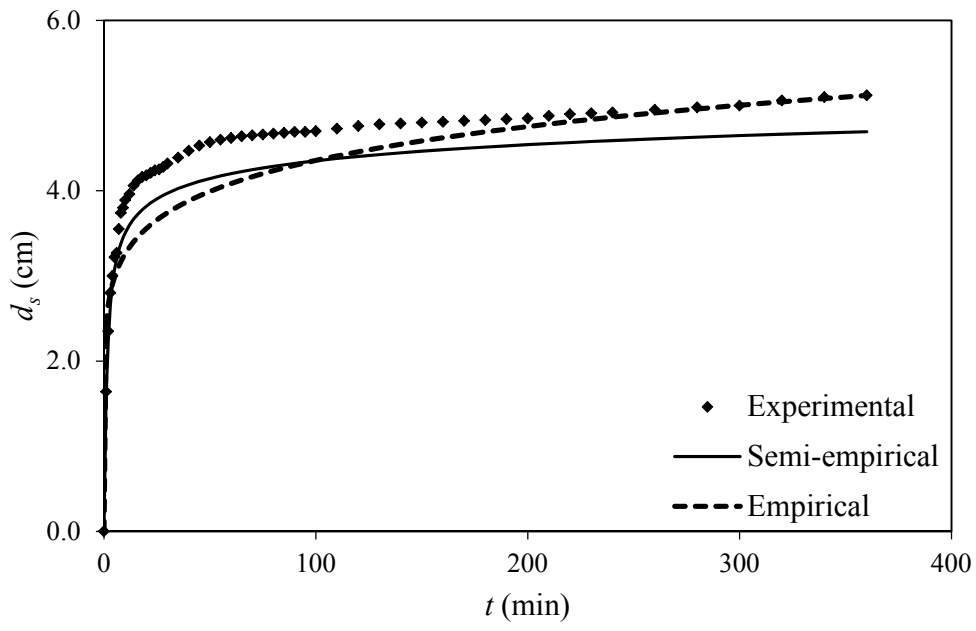


Figure 5.23 Comparison for Run E16-8

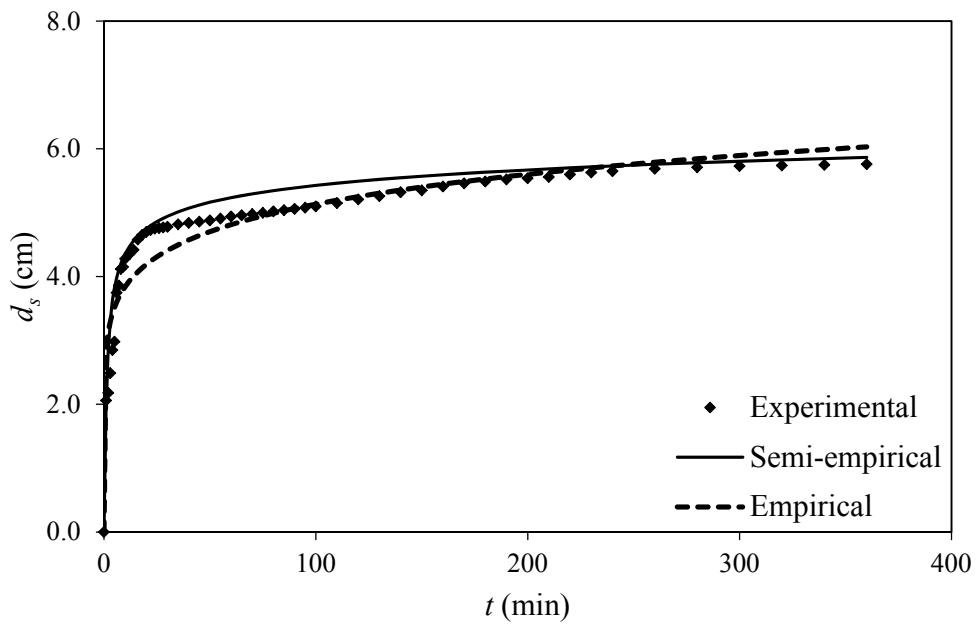


Figure 5.24 Comparison for Run E16-10

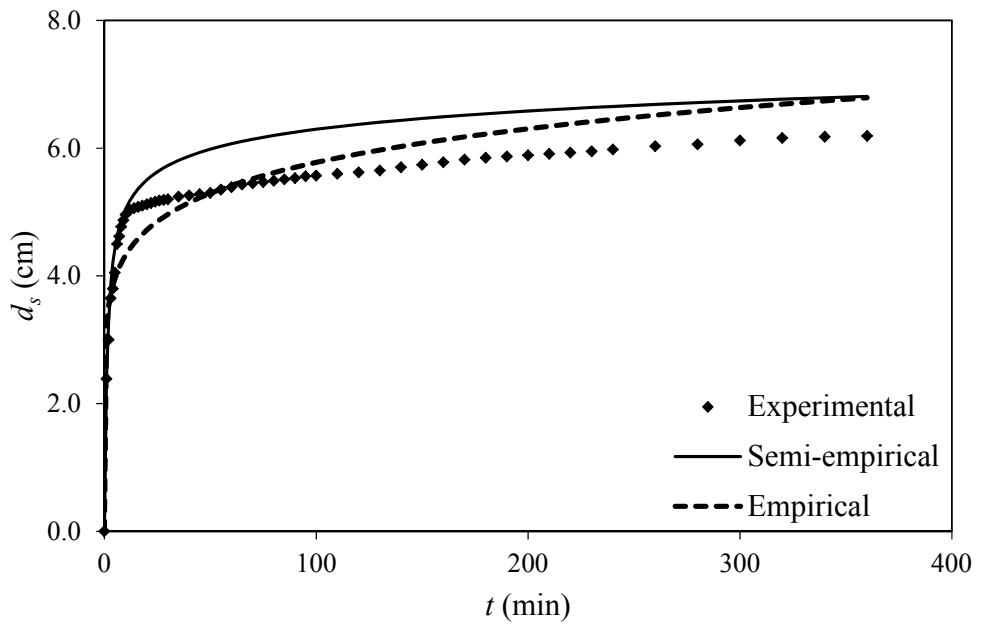


Figure 5.25 Comparison for Run E16-12

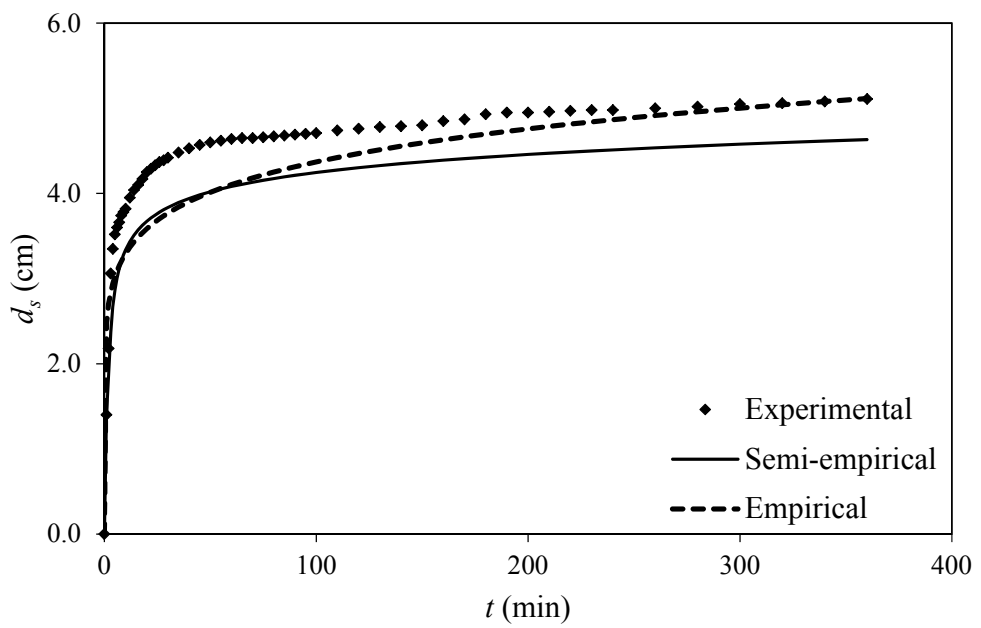


Figure 5.26 Comparison for Run E17-8

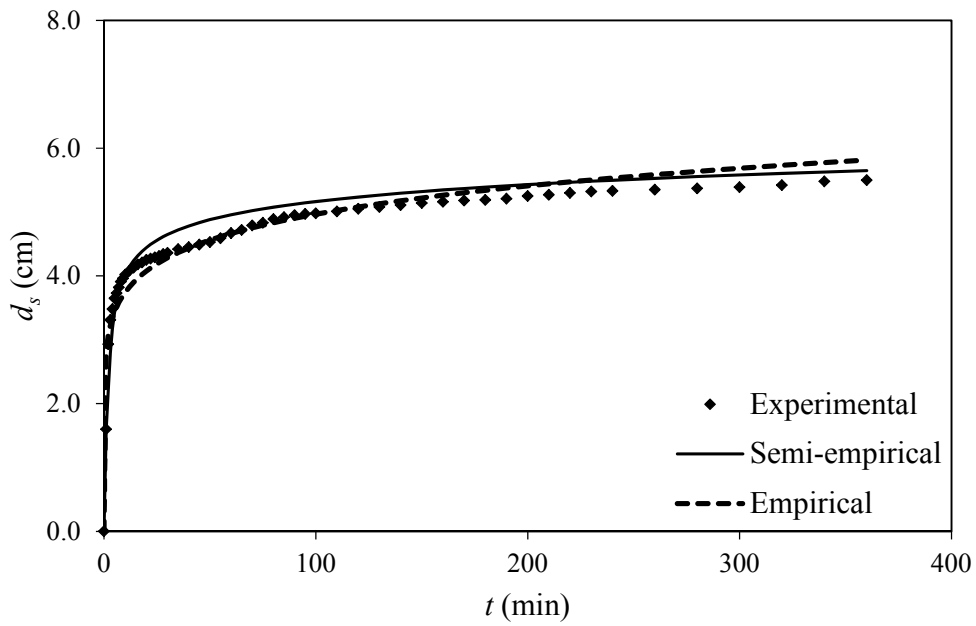


Figure 5.27 Comparison for Run E17-10

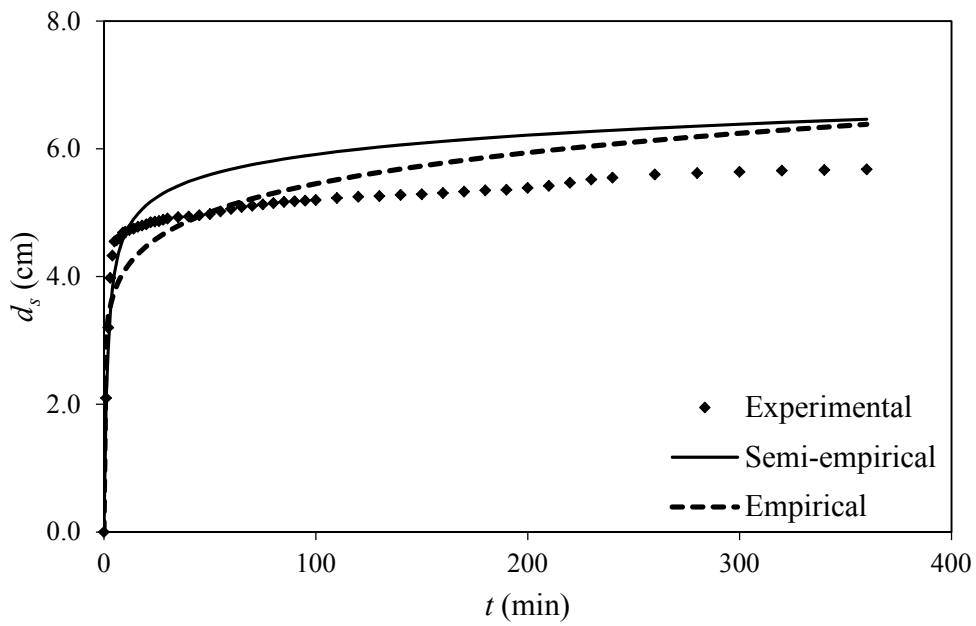


Figure 5.28 Comparison for Run E17-12

Table 5.4 Comparison of semi-empirical model with empirical equation

Run	Semi-Empirical Model		Empirical Equation	
	$R^2$	RMSE (cm)	$R^2$	RMSE (cm)
E11-8	0.990	0.14	0.986	0.11
E11-10	0.990	0.23	0.997	0.06
E11-12	0.989	0.16	0.995	0.17
E12-8	0.980	0.62	0.959	0.46
E12-10	0.992	0.14	0.970	0.63
E12-12	0.972	0.50	0.988	0.31
E13-8	0.989	0.61	0.972	0.49
E13-10	0.981	0.19	0.977	0.46
E13-12	0.967	0.46	0.992	0.29
E14-8	0.969	0.37	0.948	0.56
E14-10	0.990	0.57	0.859	0.65
E14-12	0.993	0.59	0.893	0.52
E15-8	0.998	0.33	0.914	0.58
E15-10	0.961	0.86	0.983	0.63
E15-12	0.985	0.25	0.948	0.34
E16-8	0.989	0.35	0.870	0.42
E16-10	0.964	0.29	0.853	0.32
E16-12	0.964	0.58	0.871	0.38
E17-8	0.989	0.52	0.869	0.44
E17-10	0.961	0.24	0.979	0.17
E17-12	0.940	0.61	0.874	0.44

Since the use of semi-empirical model is recommended, dimensionless form of Eq. (5.9) may be of practical interest. The following dimensionless equations are obtained by substituting the dimensionless time,  $T_s$  and dimensionless scour depth,  $S = d_s/b$  into Eq. (5.9):

$$\frac{dS}{dT_s} = \frac{p(2S \cot \phi + 1)}{T_s^{0.674} (S \cot \phi)^{3.367}} - \frac{0.327S}{T_s} \quad (\lambda = 0.5) \quad (5.10a)$$

$$\frac{dS}{dT_s} = \frac{p(2S \cot \phi + 1)}{T_s^{0.922} (S \cot \phi)^{1.465}} - \frac{0.327S}{T_s} \quad (\lambda = 0.33) \quad (5.10b)$$

$$\frac{dS}{dT_s} = \frac{p(2S \cot \phi + 1)}{T_s^{0.890} (S \cot \phi)^{1.674}} - \frac{0.327S}{T_s} \quad (\lambda = 0.25) \quad (5.10c)$$

Here,  $p$  is calculated by:

$$p = 0.267k^{-0.347} \frac{TD_*^{0.24} \sigma_g^{1.9}}{F^{0.347}} \quad (\lambda = 0.5) \quad (5.11a)$$

$$p = 0.41k^{-0.595} \frac{TD_*^{0.24} \sigma_g^{1.9}}{F^{0.595}} \quad (\lambda = 0.33) \quad (5.11b)$$

$$p = 0.386k^{-0.563} \frac{TD_*^{0.24} \sigma_g^{1.9}}{F^{0.563}} \quad (\lambda = 0.25) \quad (5.11c)$$

where,  $k = b/D_{50}$  and  $F = u_* / (\Delta g D_{50})^{0.5}$  is the square root of Shields' parameter. The value of  $p$  is constant, for a particular combination of flow, sediment properties, and pier size and spacing. In fact  $p$  is composed of design input parameters. Therefore, the variation of  $S$  with respect to  $T_s$  is obtained by the numerical solution of the nonlinear differential equation given in Eq. (5.10).

### 5.3 Design Charts

For the practical use of Eq. (5.10), the solution is presented as design charts in Figures 5.29 – 5.35, to reduce computational efforts. To use the design charts for a particular  $\lambda$  value,  $p$  is computed for given pier size and spacing, sediment properties, and design flow data. Then,  $T_s$  is computed for the time-to-peak value of the design flood and corresponding  $S$  is determined from the respective curve for  $p$ . Linear interpolation may be applied for  $p$  values outside the range of those considered in this study. The design chart implies that for a particular  $\lambda$  value, as the  $p$  value increases, the dimensionless scour depth,  $S$  increases.

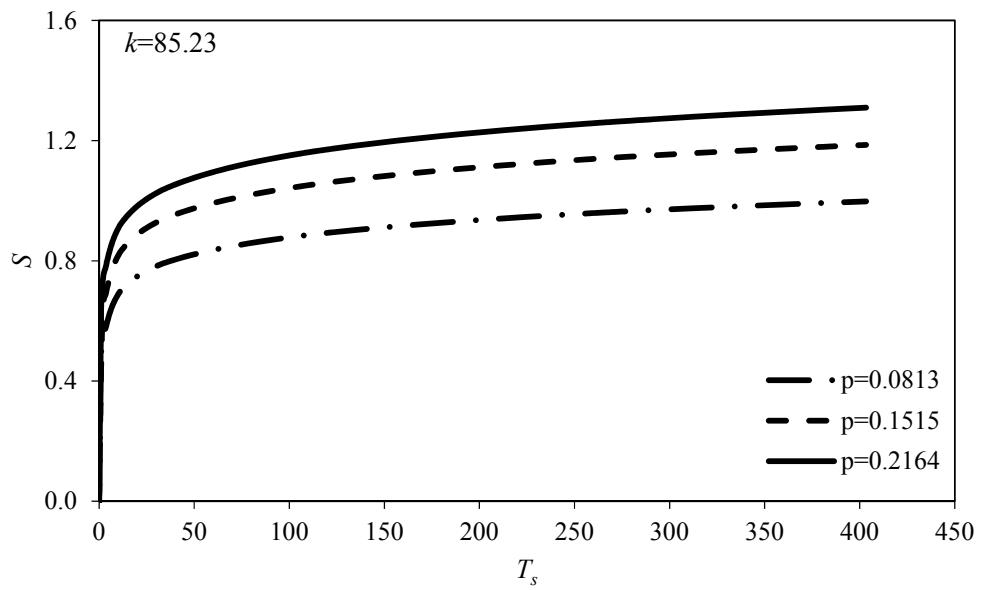


Figure 5.29 Design chart for  $\lambda = 0.5$  and  $k = 85.23$

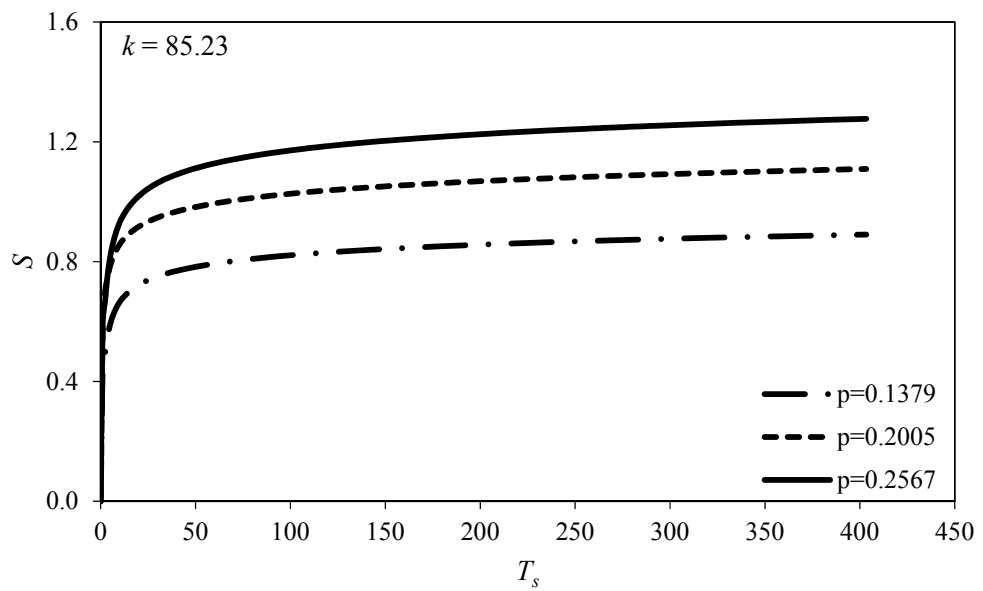


Figure 5.30 Design chart for  $\lambda = 0.33$  and  $k = 85.23$

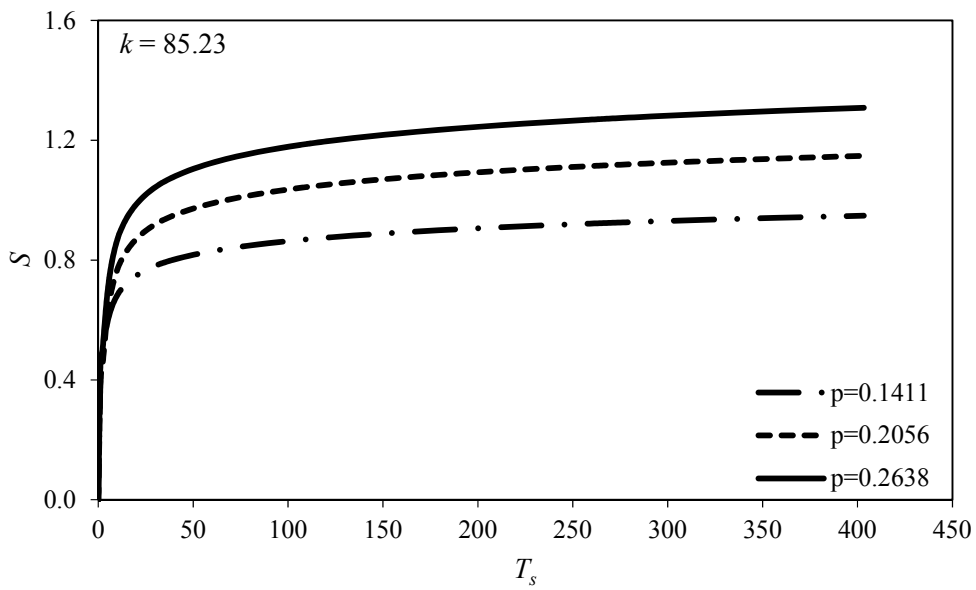


Figure 5.31 Design chart for  $\lambda = 0.25$  and  $k = 85.23$

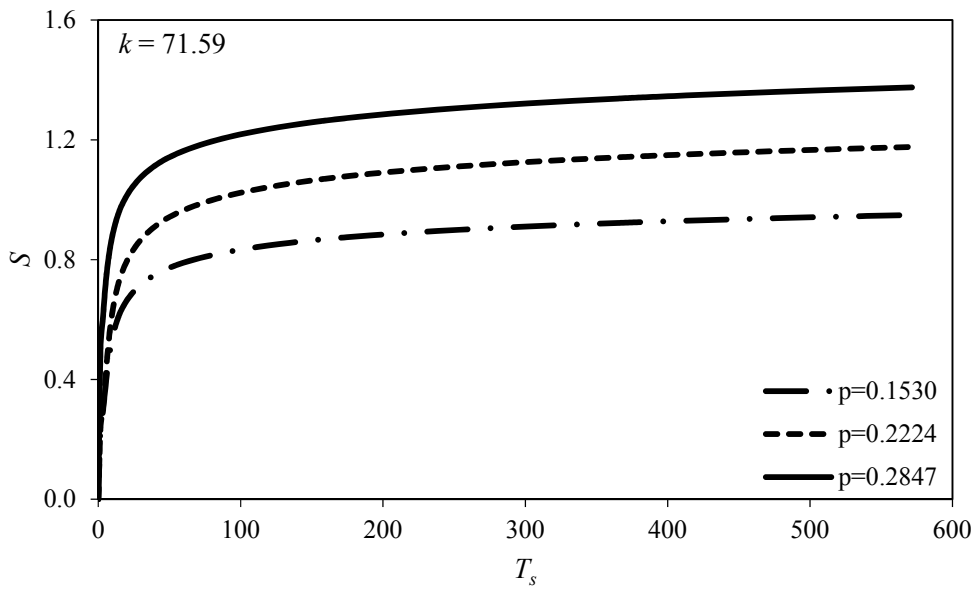


Figure 5.32 Design chart for  $\lambda = 0.33$  and  $k = 71.59$

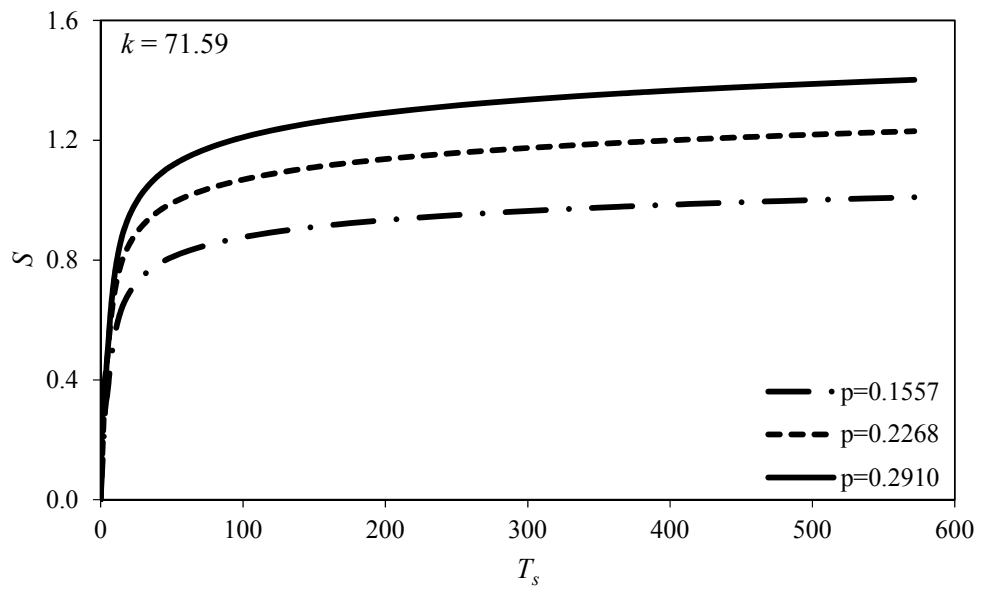


Figure 5.33 Design chart for  $\lambda = 0.25$  and  $k = 71.59$

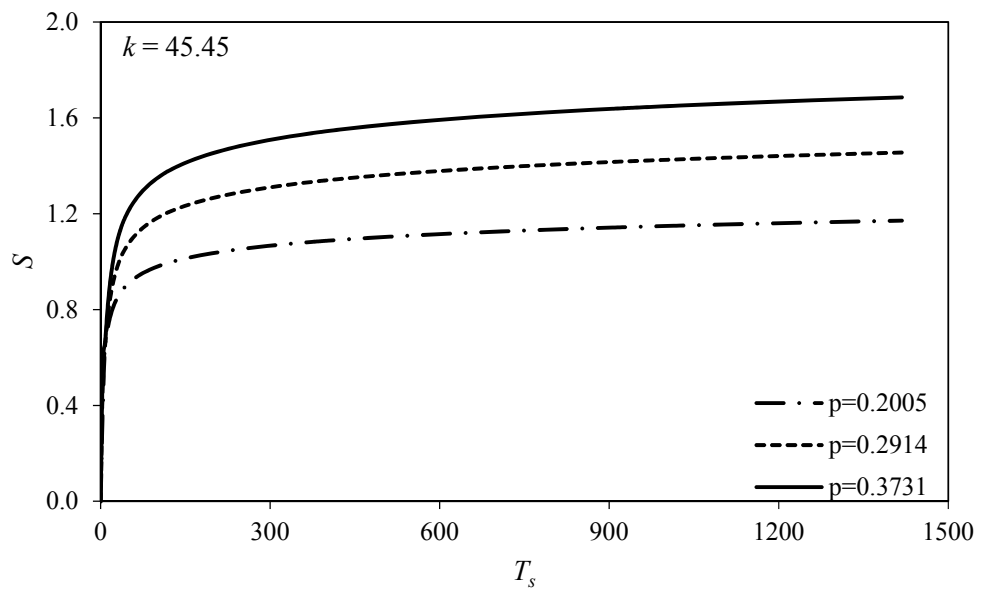


Figure 5.34 Design chart for  $\lambda = 0.33$  and  $k = 45.45$

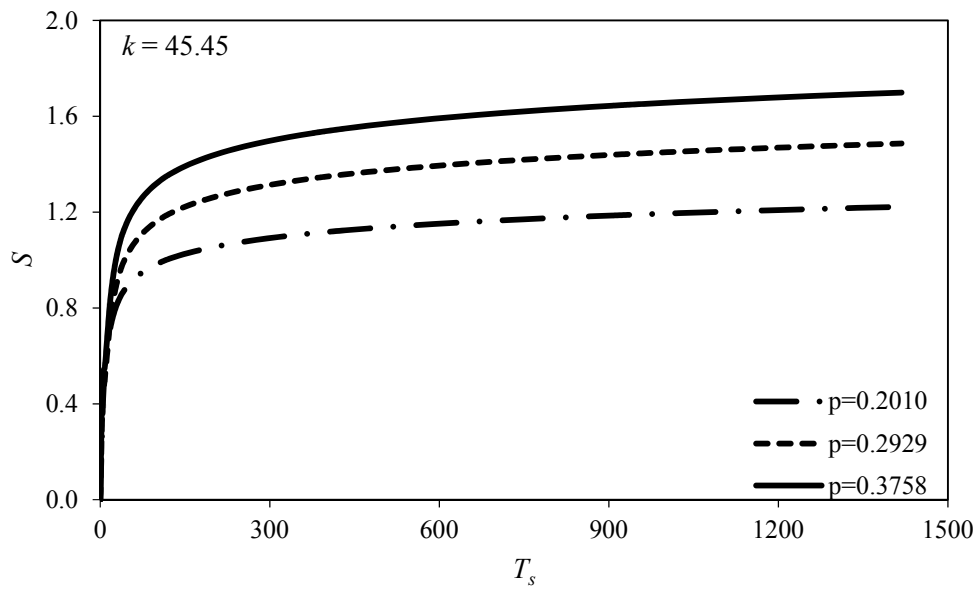


Figure 5.35 Design chart for  $\lambda = 0.25$  and  $k = 45.45$

## CHAPTER 6

### CONCLUSIONS

#### 6.1 Summary and Conclusions

Studies on the prediction of clear-water scour depth at bridge piers are mostly based on experimental investigation of the scour depth at a laboratory medium. Empirical equations for the prediction of equilibrium scour depth at bridge piers are valid and provide relatively good estimation of scour depth for the range of experimental conditions. However, an empirical equation applicable to universal conditions of clear-water scour depth at bridge piers is not available as a consequence of inability of perfect similitude in laboratory medium and model calibration absence due to lack of field data. Therefore, the studies on scour depth prediction are based on narrow range of experimental conditions. In addition to the narrow range of experimental conditions, the group effect of piers on scour depth is another restriction to the use of a common equation to both single pier case and pier group case. The additional scouring mechanisms in case of pier groups complicate the prediction of maximum clear-water scour depth inside the combined scour hole of piers. Another important fact is, previous studies on clear-water scour depth at bridge piers are mostly devoted to the prediction of the maximum equilibrium scour depth, which requires very long duration of experiments. However, in field, a design flood peak may not last long as the time to attain equilibrium conditions in the laboratory medium. Therefore, investigation

of temporal variation of scour depth at bridge piers will provide more realistic estimates for the scour depth.

Considering all these facts, a semi-empirical model is developed in this study to predict the temporal variation of maximum clear-water scour depth at dual cylindrical uniform piers in tandem arrangement. The experiments are carried out with uniformly graded bed material, using three different pier diameters with three different pier diameter to spacing ratio. The semi-empirical model is developed on the basis of sediment continuity approach and volumetric sediment transport rate from the scour hole using a proper sediment pickup function proposed by Dey and Debnath. Bed topography maps of the scour hole and accretion zones are obtained and time-evolution of the scour hole volume around the piers is derived from those maps to be used in the model development. Finally, the semi-empirical model is developed giving the temporal variation of maximum scour depth at tandem piers. Design charts are presented to obtain the dimensionless scour depth versus dimensionless time for practical use. In addition to the semi-empirical model, an empirical equation is also proposed for the prediction of maximum scour depth for different pier spacing conditions.

The findings of the study are as follows:

- The maximum scour depth around dual piers in tandem arrangement always occurs at the upstream face of the front pier.
- For a particular flow intensity and  $\lambda$ , the maximum scour depth increases with the increasing pier size. Also, for a particular pier size and  $\lambda$ , the maximum scour depth increases with the increasing flow intensity. In addition, for a given pier size and flow intensity, the maximum scour depth increases with increasing  $\lambda$ . This is a consequence of reinforcing effect of pier groups. It is observed that the strength of reinforcing effect decreases with decreasing  $\lambda$  value.

- The scour depth at the upstream of the rear pier is always less than the scour depth at the downstream of the front pier. This is a consequence of sheltering effect of pier groups.
- To form an opinion for the bed shear stress variation in the scour hole, a model proposed by Kothyari et al. for the variation of shear stress at single piers is used. Accordingly, the bed shear stress at the front pier nose decreases as the scour depth and projected area of the scour hole develops in time. Eventually, it tends to a range of  $0.51\tau_{cr} - 0.71\tau_{cr}$ .
- The scour holes are widening and deepening in time. Location of the maximum scour depth at the sides of the front piers remains constant in time. However, the maximum scour depth at the dune cross-section between piers and rear pier cross-section moves towards the centerline of flow direction in time.
- Side slopes and the longitudinal slopes of the front pier do not change in time. Therefore, shape of the scour hole at front pier remained almost constant throughout the experiments. However, side slopes of the rear pier and so the scour hole shape changes in time, due to simultaneous erosion at the pier and accretion of materials transported from the front pier.
- Longitudinal slopes at the rear pier remain constant in time. Slopes at the upstream of the front pier and rear pier are identical and approximately equal to the angle of repose of the sediment. Furthermore, slopes at the downstream of both piers are equal too.
- The maximum scour depth between the piers is obtained for different experimental conditions. The location of maximum scour depth between piers has an eccentricity in both positive and negative y-direction. It is observed that the location shows little variation in time. For a particular pier size and flow intensity, the maximum scour depth is compared for different  $\lambda$  values. The maximum scour depth increases when  $\lambda$  increases, as a consequence of reinforcing effect of pier groups.

- Dune location along the flow direction remains constant in time. For the maximum pier size, the distance of the dune from the center of rear pier is obtained as approximately 38% of  $d$ . Pier size to spacing ratio does not have considerable effect on the location of the dune.
- The accretion zone at the downstream of the rear pier is relatively steep in the beginning of the experiments. However, the accretion propagates downstream in time and its profile becomes flatter.
- The variation of scour depth at the sides of the front pier and rear pier are obtained. It is observed that the scour depths at the side of the front pier are always less than that at its upstream face. Also, the scour depths at the side of the rear pier are always smaller than that at the side of the front pier.
- The results of the semi-empirical model are compared with the experimental results. It is observed that the predicted scour depths are relatively in good agreement with the experimental results, in the test range.
- The results of the empirical equation are compared with the experimental results and the semi-empirical model. Although the empirical equation provides quite good prediction for the time-dependent maximum scour depth, semi-empirical model results are in better agreement with the experimental results. Furthermore, it is based on conservation of mass principle which is coupled with sediment transport mechanism in the scour hole.

## 6.2 Novelty of the Study

The worth of this study is in relation to following considerations:

- Rate of sediment transport from the combined scour hole around dual piers is formulated using conservation of mass principle and a sediment pickup function. Since the bed load transport formulas reported in the literature normally refer to horizontal and sloping beds, formulation of bed load rate

from a hole may be a contribution to the classical sediment transport theories.

- The volume of the scour hole around dual piers is calculated by frequent bed topography measurements. Expressions for the variation of dimensionless scour hole volume and surface area are obtained with respect to  $\lambda$  and dimensionless  $T_s$ . This information may provide useful tool for designing armoring countermeasures around dual piers, concerning areal extension of scour protection and number of protective layers.
- A semi-empirical model is proposed for the prediction of the time-variation of the maximum scour depth at dual piers. Sediment continuity approach is utilized and it is coupled with the volumetric sediment transport rate and sediment pickup function.
- In development of the model, sensitivity analysis is made for the  $\psi$  term to select a proper value to apply to the experimental data. Therefore, the effect of vortices on shear stress development in the scour hole is searched with reference to the comparison of the measured scour depths with those obtained from the semi-empirical model.
- The mathematical expressions and design charts presented for the temporal variation of maximum scour depth at dual piers allow researchers to calculate the scour depth corresponding to a design flood duration.

### **6.3 Recommendations for Future Research**

During this study, the investigation of temporal variation of the maximum scour depth at dual piers is carried out by detailed experimental work and semi-empirical model development. However, due to the complexity of scour phenomenon, which further increases in case of dual piers, and physical conditions of the current laboratory and the equipment, several research limitations came into the picture. These limitations may be overcome in the future studies and wider range of parameters may be considered as follows:

- Longer flow durations may be considered to observe subsequent phases of scouring before the equilibrium clear-water scour condition.
- To obtain a mathematical expression for the effect of  $\lambda$  on the reinforcing effect of dual piers, different pier spacings may be tested.
- Lower flow intensities may also be considered to further investigate the effect of flow intensity on the scour depth evolution using more sophisticated measuring equipment.
- Detailed investigation for the dimensionless surface area of the scour hole may be beneficial to obtain design guidelines for proper placement of armoring scour countermeasures.
- Different arrangement of piers such as side-by-side placement, etc. may be tested.
- Numerical simulation of the scouring characteristics at pier groups may also be carried out using a proper Computational Fluid Dynamics software.

## REFERENCES

- Ataie-Ashtiani, B., and Beheshti, A. A. (2006). "Experimental investigation of clear-water local scour at pile groups." *Journal of Hydraulic Engineering*, 132(10), 1100–1104.
- Barbhuiya, A. K. (2003). "Clear water scour at abutments." PhD thesis, Indian Institute of Technology, Kharagpur, India.
- Başak, V., Başlamışlı, Y., and Ergun, O. (1978). "Local scour depths around circular crosssectioned pier group." *State Hydraulic Works Technical Bulletin*, 28, 20–52 (in Turkish).
- Beg, M. (2004). "Mutual interference of bridge piers on local scour." *Proceedings of the Second International Conference on Scour and Erosion*, Singapore, 111–118.
- Beg, M. (2014). "Mutual interference of bridge piers placed in staggered arrangement on local scour." *Proceedings of the Seventh International Conference on Scour and Erosion*, Perth, Western Australia, 483–488.
- Beg, M., and Beg, S. (2015). "Scour hole characteristics of two unequal size bridge piers in tandem arrangement." *ISH Journal of Hydraulic Engineering*, 21(1), 85–96.
- Bozkuş, Z., and Çeşme, M. (2010). "Reduction of scouring depth by using inclined piers." *Canadian Journal of Civil Engineering*, 37(12), 1621–1630.
- Breusers, H. N. C., Nicollet, G., and Shen, H. W. (1977). "Local scour around cylindrical piers." *Journal of Hydraulic Research*, 15(3), 211–252.
- Breusers, H. N. C., and Raudkivi, A. J. (1991). *Scouring*. Balkema, Rotterdam, Netherlands.
- Cardoso, A., and Bettess, R. (1999). "Effects of time and channel geometry on scour at bridge abutments." *Journal of Hydraulic Engineering*, 125(4), 388–399.

- Chabert, J., and Engeldinger, P. (1956). *Etude des affouillements autour des piles de ponts*. Laboratoire National d'Hydraulique, Chatou, France (in French).
- Chang, W.-Y., Lai, J.-S., and Yen, C.-L. (2004). "Evolution of scour depth at circular bridge piers." *Journal of Hydraulic Engineering*, 130(9), 905–913.
- Çeşme, M. (2005). "Experimental investigation of local scour around inclined dual bridge piers." MSc thesis, Middle East Technical University, Ankara, Turkey.
- Dey, S. (1996). "Sediment pick-up for evolving scour near circular cylinders." *Applied Mathematical Modelling*, 20(7), 534–539.
- Dey, S., and Barbhuiya, A. K. (2005). "Time variation of scour at abutments." *Journal of Hydraulic Engineering*, 131(1), 11–23.
- Dey, S., Bose, S., and Sastry, G. (1995). "Clear water scour at circular piers: A model." *Journal of Hydraulic Engineering*, 121(12), 869–876.
- Dey, S., and Debnath, K. (2001). "Sediment pickup on streamwise sloping beds." *Journal of Irrigation and Drainage Engineering*, 127(1), 39–43.
- Diwedat, A. S. I. (2013). "Investigating the impact of pile group arrangement on local scour around bridge pier using physical model." *Nile Water Science & Engineering Journal*, 6(2), 12–25.
- Elliott, K. R., and Baker, C. J. (1985). "Effect of pier spacing on scour around bridge piers." *Journal of Hydraulic Engineering*, 111(7), 1105–1109.
- Ettema, R. (1980). "Scour at bridge piers." *Rep. No.216*, Dept. of Civil Engineering, Univ. of Auckland, Auckland, New Zealand.
- Ettema, R., Melville, B., and Barkdoll, B. (1998). "Scale effect in pier-scour experiments." *Journal of Hydraulic Engineering*, 124(6), 639–642.
- Fael, C. M. S., Simarro-Grande, G., Martín-Vide, J. P., and Cardoso, A. H. (2006). "Local scour at vertical-wall abutments under clear-water flow conditions." *Water Resources Research*, 42(10), 388–399.
- Gao, D. G., Posada, L. G., and Nordin, C. F. (1993). *Pier scour equations used in People's Republic of China: Review and summary*. Tech. Rep., Dept. of Civil Engineering, Colorado State University, Fort Collins, Colorado.

- Gao, P., Duan, M., Zhong, C., Yuan, Z., and Wang, J. (2013). "Current induced scour around single piles and pile groups." *Proceedings of the Twenty-third International Offshore and Polar Engineering*, Alaska, USA, 472–477.
- Garde, R. J., and Ranga Raju, K. G. (2006). *Mechanics of sediment transport and alluvial stream problems*. New Age Int. Publ., New Delhi, India.
- Grimaldi, C., Gaudio, R., Cardoso, A. H., and Calomino, F. (2006). "Local scouring at bridge piers and abutments: Time evolution and equilibrium." *3rd International Conference on Fluvial Hydraulics*, Lisbon, Portugal, 1657–1664.
- Guo, J. (2014). "Semi-analytical model for temporal clear-water scour at prototype piers." *Journal of Hydraulic Research*, 52(3), 366–374.
- Hager, W. H., and Unger, J. (2010). "Bridge pier scour under flood waves." *Journal of Hydraulic Engineering*, 136(10), 842–847.
- Hannah, C. R. (1978). "Scour at pile groups." *Research Rep. No. 28-3*, Civil Engineering Dept., Univ. of Canterbury, Christchurch, New Zealand.
- Heidarpour, M., Afzalimehr, H., and Izadinia, E. (2010). "Reduction of local scour around bridge pier groups using collars." *International Journal of Sediment Research*, 25(4), 411–422.
- Hoffmans, G., and Verheij, H. J. (1997). *Scour manual*. Balkema, Rotterdam, Netherlands.
- Hong, J. H., Goyal, M. K., Chiew, Y. M., and Chua, L. H. C. (2012). "Predicting time-dependent pier scour depth with support vector regression." *Journal of Hydrology*, 468-469, 241–248.
- Hosseini, R., and Amini, A. (2015). "Scour depth estimation methods around pile groups." *KSCE Journal of Civil Engineering*, 00(0000), 1–13.
- Kalantari, O. (2014). "Time-dependent local scour of circular bridge pier." PhD thesis, The Graduate College at the University of Nebraska-Lincoln, NE.
- Kim, H. S., Nabi, M., Kimura, I., and Shimizu, Y. (2014). "Numerical investigation of local scour at two adjacent cylinders." *Advances in Water Resources*, 70, 131–147.
- Köse, O., and Yanmaz, A. M. (2010). "Scouring reliability of bridge abutments." *Turkish Chamber of Civil Engineers Digest 2010*, 21, 1387–1402.

- Kothyari, U. C., and Kumar, A. (2012). "Temporal variation of scour around circular compound piers." *Journal of Hydraulic Engineering*, 138(11), 945–957.
- Kothyari, U. C., and Ranga Raju, K. G. (2001). "Scour around spur dikes and bridge abutments." *Journal of Hydraulic Research*, 39(4), 367–374.
- Kothyari, U., Garde, R., and Ranga Raju, K. (1992). "Temporal variation of scour around circular bridge piers." *Journal of Hydraulic Engineering*, 118(8), 1091–1106.
- Link, O. (2006). "Time scale of scour around a cylindrical pier in sand and gravel." *Proceedings of Third Chinese-German Joint Symposium on Coastal and Ocean Engineering*, Tainan, Taiwan.
- Lu, J.-Y., Shi, Z.-Z., Hong, J.-H., Lee, J.-J., and Raikar, R. V. (2011). "Temporal variation of scour depth at nonuniform cylindrical piers." *Journal of Hydraulic Engineering*, 137(1), 45–56.
- Melville, B., and Chiew, Y. (1999). "Time scale for local scour at bridge piers." *Journal of Hydraulic Engineering*, 125(1), 59–65.
- Melville, B. W., and Coleman, S. E. (2000). *Bridge scour*. Water Resources Publications, Highlands Ranch, Colorado, USA.
- Melville, B. W., and Raudkivi, A. J. (1977). "Flow characteristics in local scour at bridge piers." *Journal of Hydraulic Research*, 15(4), 373–380.
- Mia, F., and Nago, H. (2003). "Design method of time-dependent local scour at circular bridge pier." *Journal of Hydraulic Engineering*, 129(6), 420–427.
- Nazariha, M. (1996). "Design relationships for maximum local scour depth for bridge pier groups." PhD thesis, University of Ottawa, Ottawa, Canada.
- Oliveto, G., and Hager, W. H. (2002). "Temporal evolution of clear-water pier and abutment scour." *Journal of Hydraulic Engineering*, 128(9), 811–820.
- Oliveto, G., and Hager, W. H. (2005). "Further results to time-dependent local scour at bridge elements." *Journal of Hydraulic Engineering*, 131(2), 97–105.
- Özalp, M. C. (2013). "Experimental investigation of local scour around bridge pier groups." MSc thesis, Middle East Technical University, Ankara, Turkey.
- Raudkivi, A. J. (1986). "Functional trends of scour at bridge piers." 112(1), 1–13.

- Raudkivi, A. J., and Ettema, R. (1983). "Clear-water scour at cylindrical piers." *109*(3), 338–350.
- Richardson, E. V., and Davis, S. R. (2001). *Evaluating scour at bridges*. Hydraulic Engineering Circular No:18, Report No: FHWA NHI 01-001, FHWA, US Dept. of Transportation, Washington, D.C.
- Salim, M., and Jones, J. S. (1998). "Scour around exposed pile foundations." *Compilation of Conf. Scour Papers (1991-1998)*, ASCE, Reston, VA.
- Schillinger, M. (2011). "Temporal pier scour evolution under stepped hydrographs." MSc thesis, University of Clemson, SC.
- SeaTek. (2015). "SeaTek instrumentation and engineering." <<http://seatek.members.atlantic.net/>> (May 4, 2015).
- Setia, B. (2008). "Equilibrium scour depth time." *3rd IASME/WSEAS International Conference on Water Resources, Hydraulics and Hydrology (WHH '08)*, University of Cambridge, UK, 114–117.
- Shames, I. H. (1992). *Mechanics of fluids*. McGraw-Hill, New York.
- Sheppard, D., Odeh, M., and Glasser, T. (2004). "Large scale clear-water local pier scour experiments." *Journal of Hydraulic Engineering*, 130(10), 957–963.
- Simarro-Grande, G., and Martin-Vide, J. P. (2004). "Exponential expression for time evolution in local scour." *Journal of Hydraulic Research*, 42(6), 663–665.
- Yanmaz, A. M. (1989). "Time-dependent analysis of clear-water scour around bridge piers." PhD thesis, Middle East Technical University, Ankara, Turkey.
- Yanmaz, A. M. (1994). "Modelling of sediment saltation." *Symposium for the 15th Anniversary of Engineering and Architectural Faculty*, Adana, Turkey, 125–136 (in Turkish).
- Yanmaz, A. M. (2002). *Bridge hydraulics*. METU Press, Ankara, Turkey (in Turkish).
- Yanmaz, A. M. (2006). "Temporal variation of clear water scour at cylindrical bridge piers." *Canadian Journal of Civil Engineering*, 33(8), 1098–1102.

- Yanmaz, A. M., and Altınbilek, H. D. (1991). “Study of time dependent local scour around bridge piers.” *Journal of Hydraulic Engineering*, 117(10), 1247–1268.
- Yanmaz, A. M., and Apaydın, M. (2012). “Bridge scour risk assessment and countermeasure design.” *Journal of Performance of Constructed Facilities*, 26(4), 499–506.
- Yanmaz, A. M., and Köse, O. (2009). “A semi-empirical model for clear-water scour evolution at bridge abutments.” *Journal of Hydraulic Research*, 47(1), 110–118.
- Zanke, U. (1978). *Zusammenhänge zwischen stromung und sedimenttransport*. Mitteilungen des Franzius, Hannover, Germany (in German).

## **APPENDIX A**

### **BED TOPOGRAPHY MAPS OF THE SCOUR HOLE**

The bed topography maps of the scour hole obtained from the measurements taken in the Experiments Part I are presented in Figures A.1 – A.46. The flow direction in the maps is from left to right.

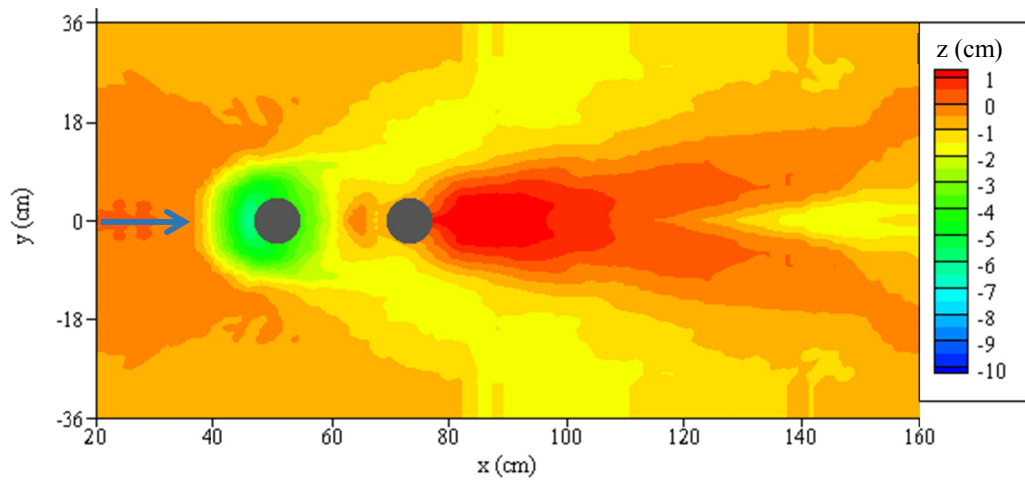


Figure A.1 Bed topography map of run E2 at t = 5 min

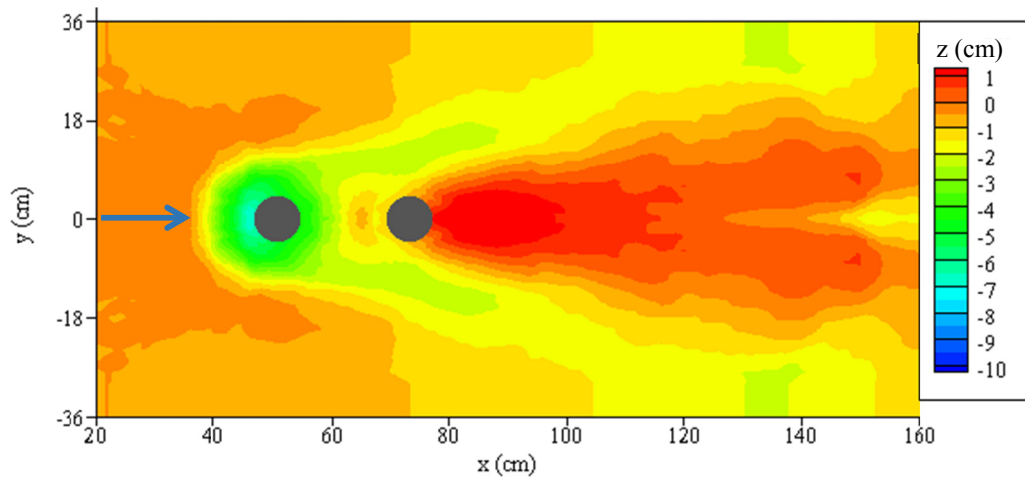


Figure A.2 Bed topography map of run E2 at t = 10 min

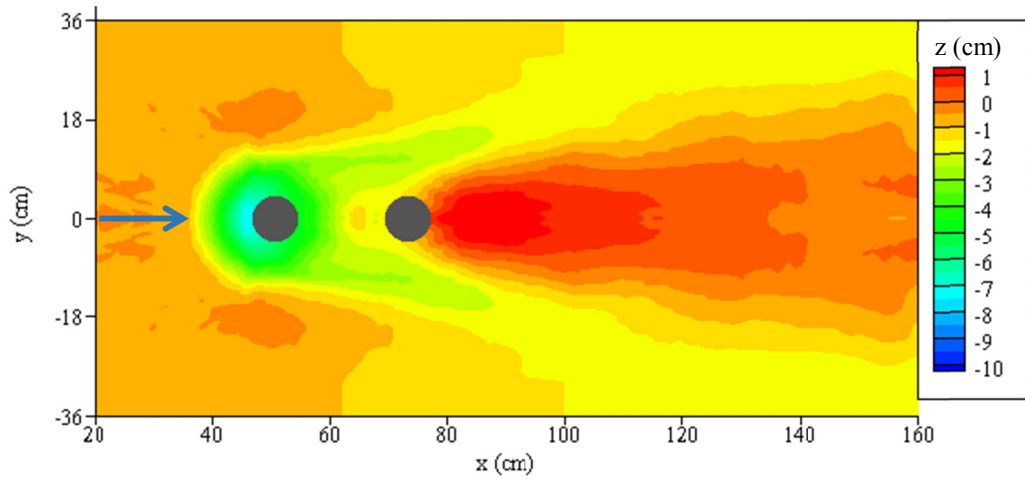


Figure A.3 Bed topography map of run E2 at  $t = 15$  min

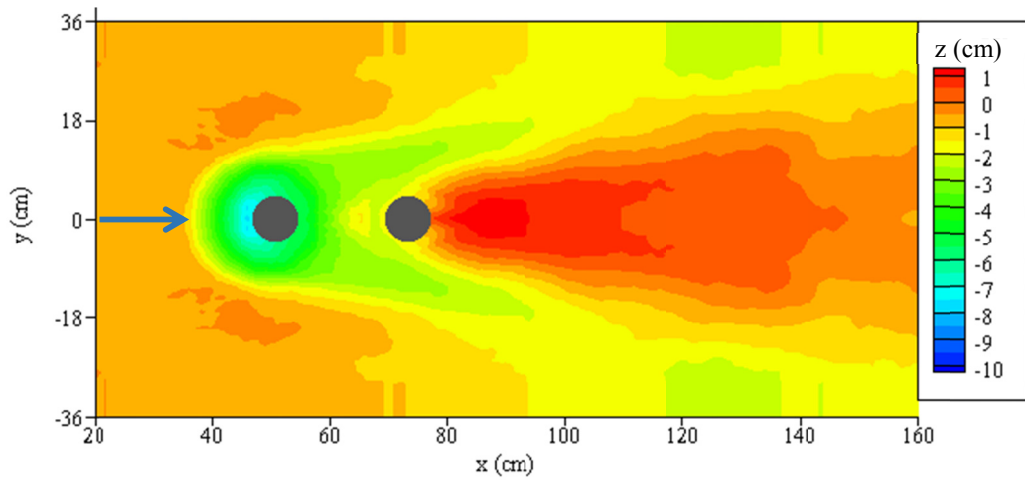


Figure A.4 Bed topography map of run E2 at  $t = 20$  min

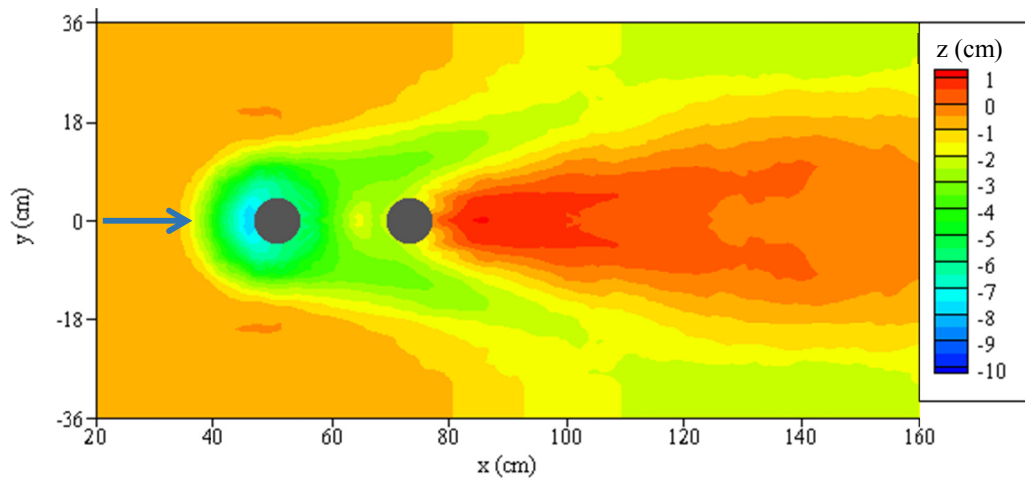


Figure A.5 Bed topography map of run E2 at t = 30 min

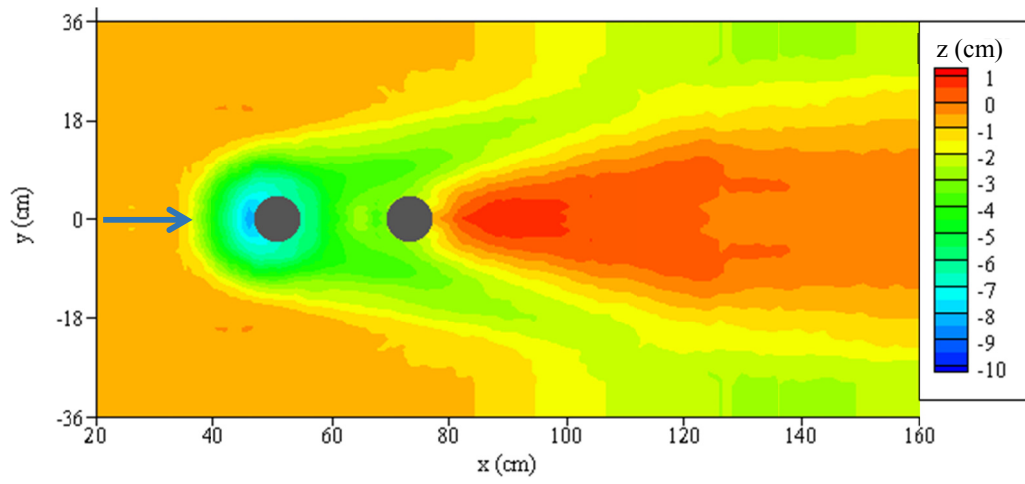


Figure A.6 Bed topography map of run E2 at t = 45 min

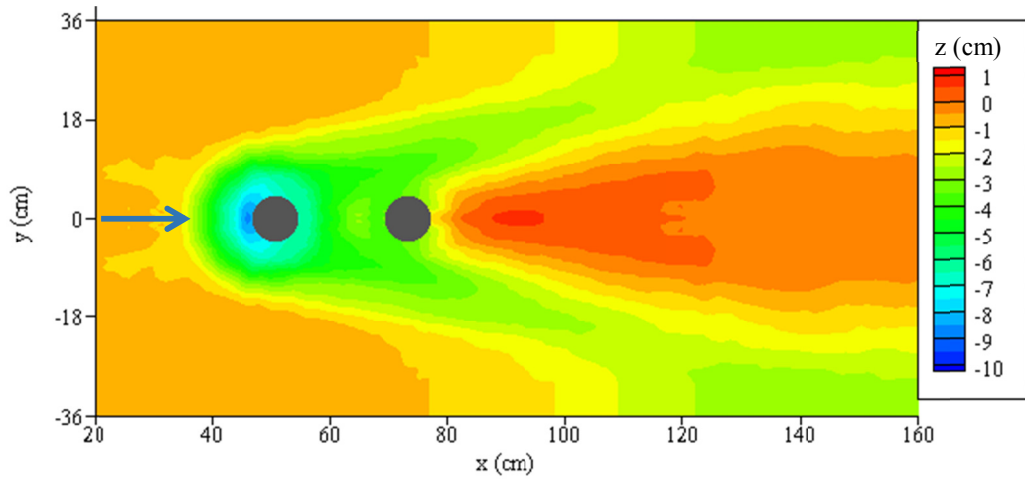


Figure A.7 Bed topography map of run E2 at t = 60 min

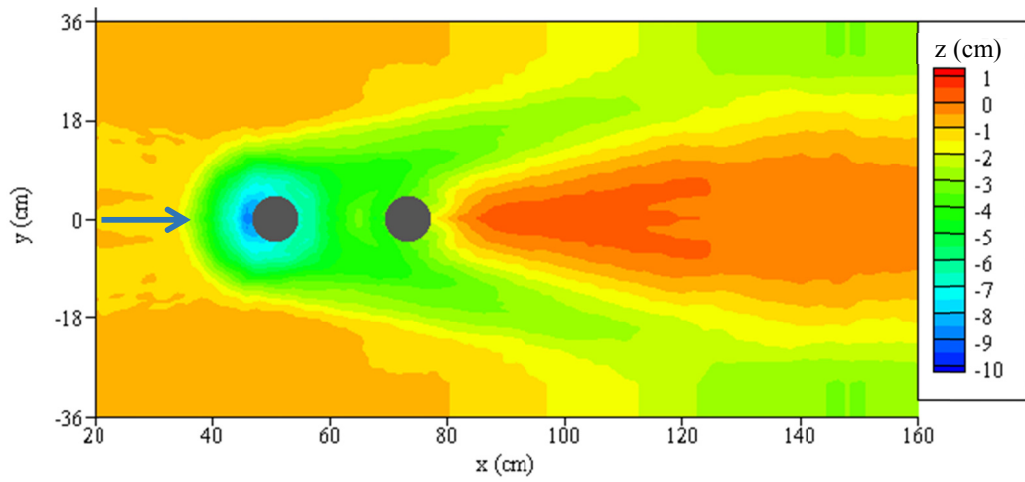


Figure A.8 Bed topography map of run E2 at t = 80 min

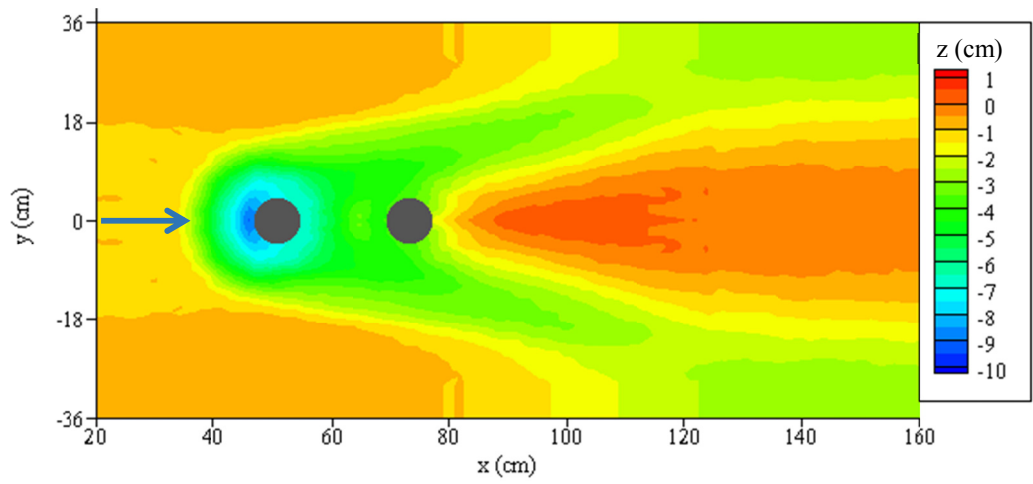


Figure A.9 Bed topography map of run E2 at t = 100 min

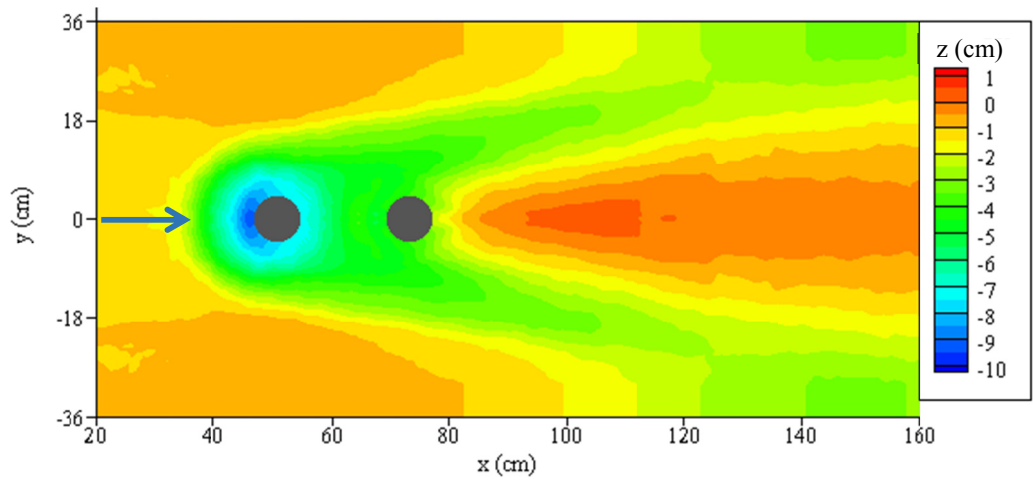


Figure A.10 Bed topography map of run E2 at t = 150 min

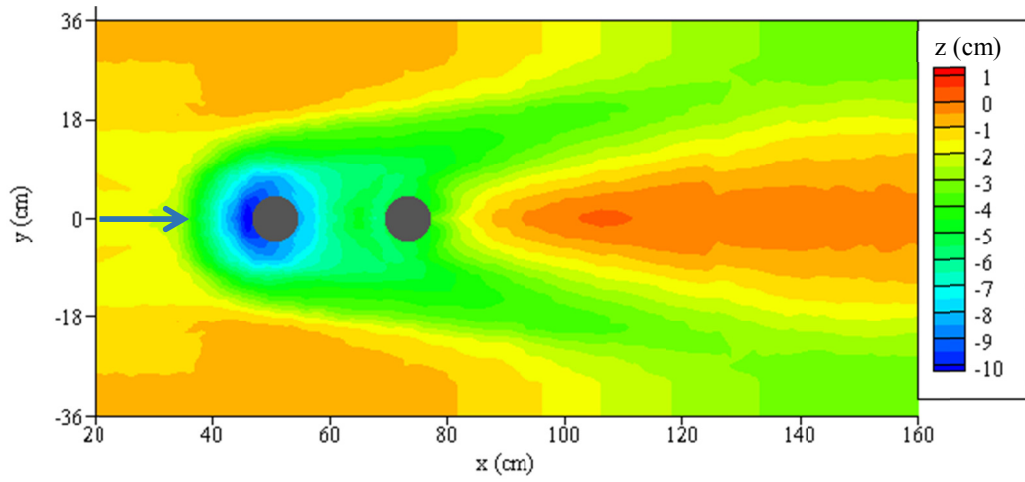


Figure A.11 Bed topography map of run E2 at  $t = 360$  min

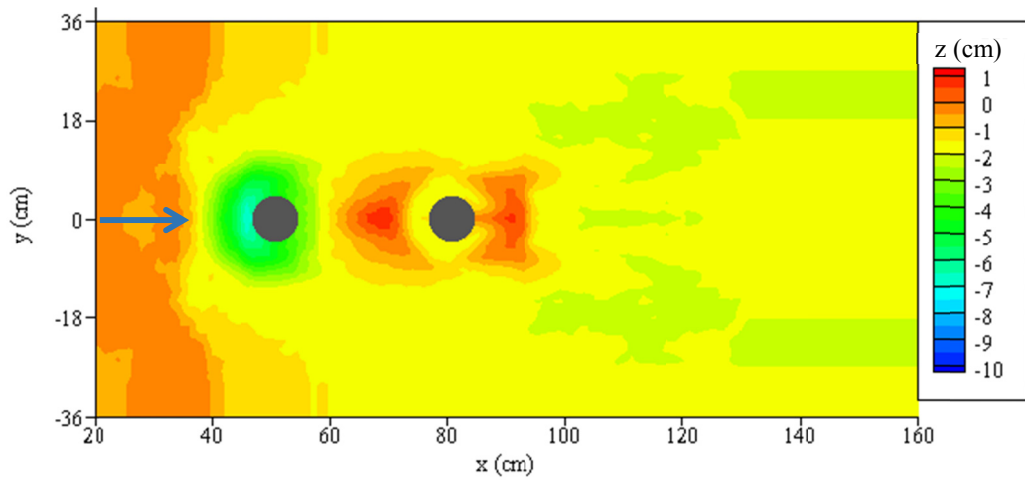


Figure A.12 Bed topography map of run E3 at  $t = 5$  min

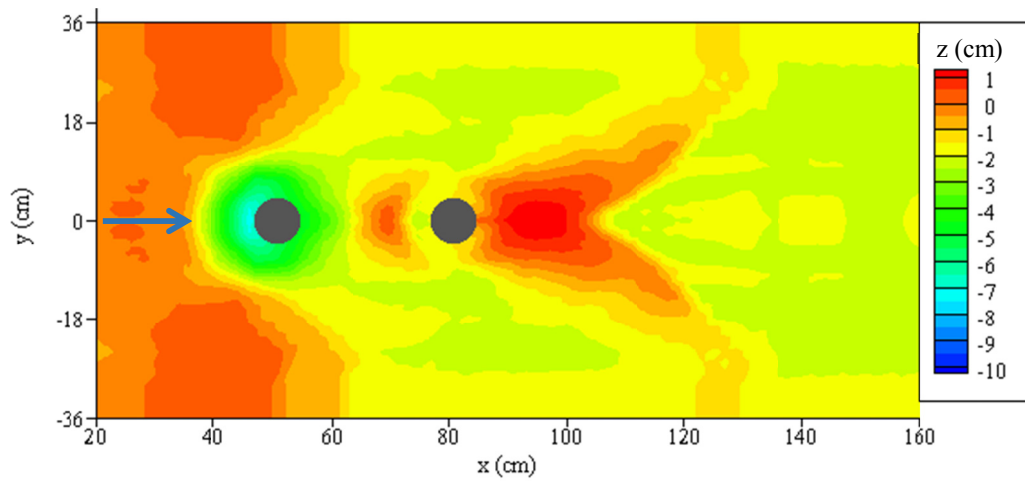


Figure A.13 Bed topography map of run E3 at t = 10 min

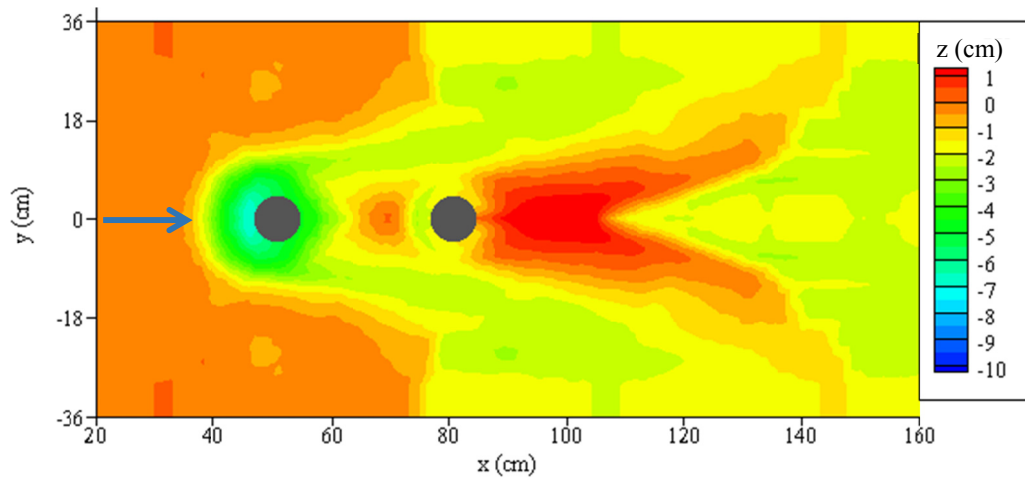


Figure A.14 Bed topography map of run E3 at t = 15 min

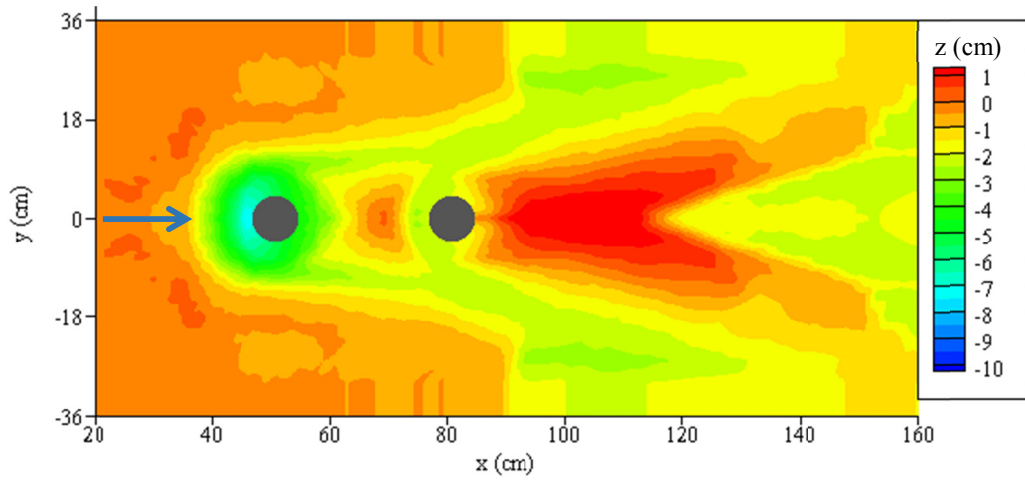


Figure A.15 Bed topography map of run E3 at  $t = 20$  min

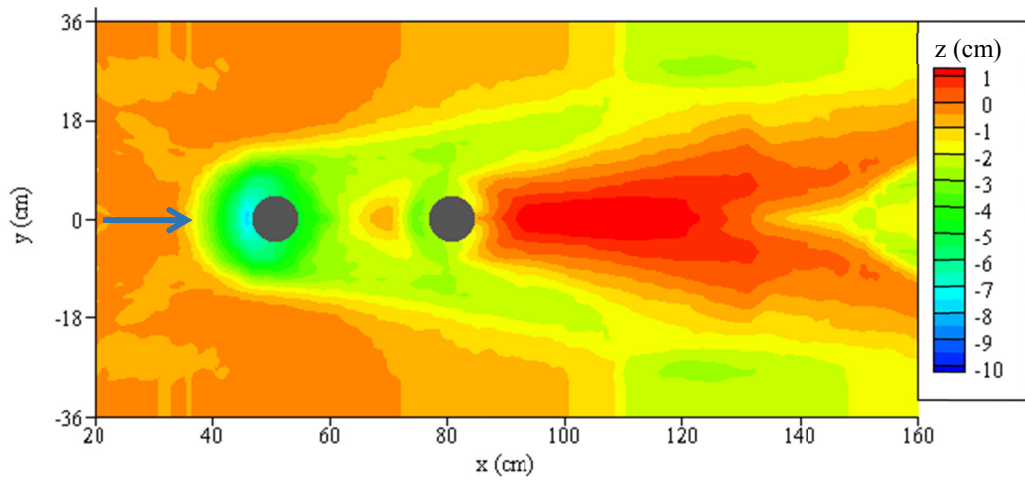


Figure A.16 Bed topography map of run E3 at  $t = 30$  min

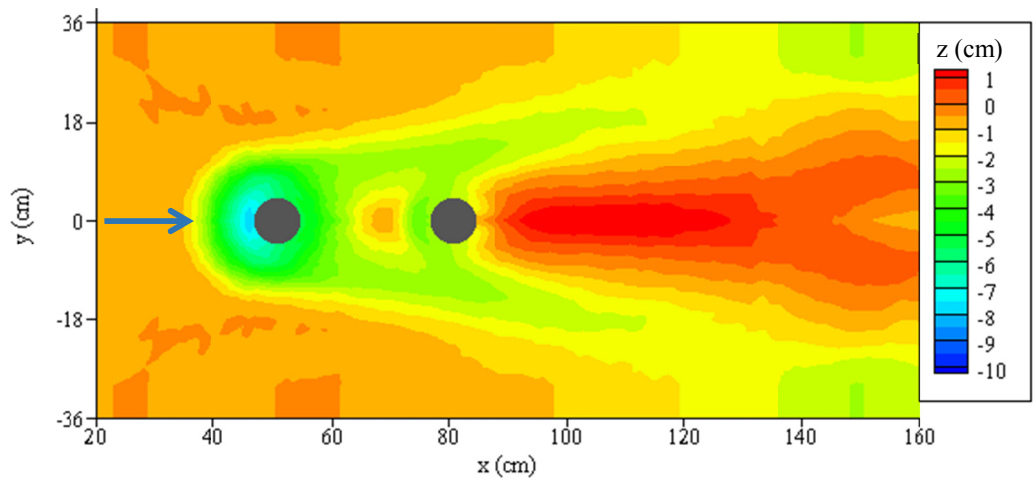


Figure A.17 Bed topography map of run E3 at t = 45 min

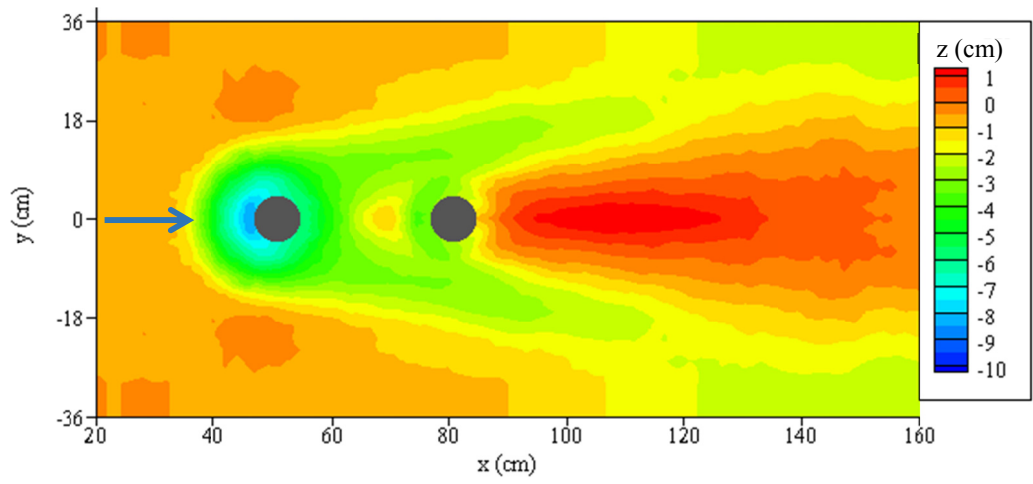


Figure A.18 Bed topography map of run E3 at t = 60 min

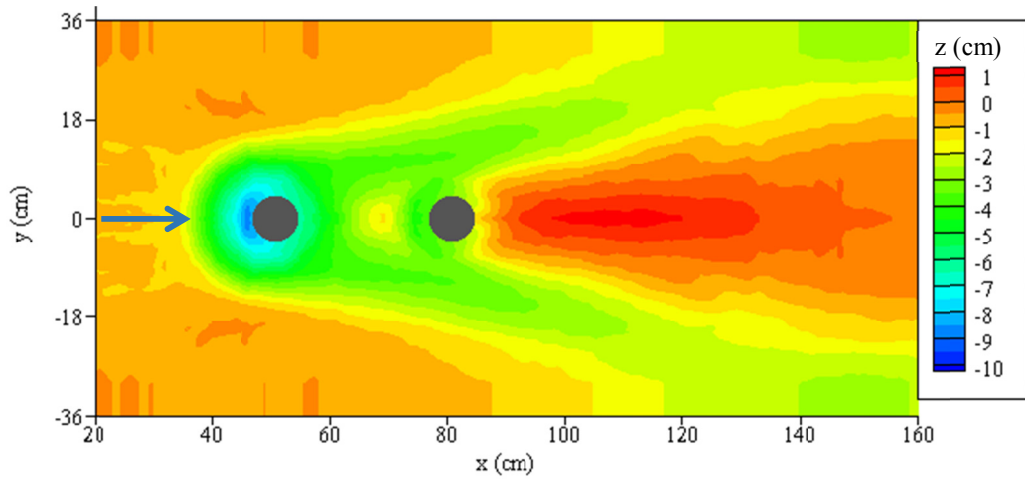


Figure A.19 Bed topography map of run E3 at  $t = 80$  min

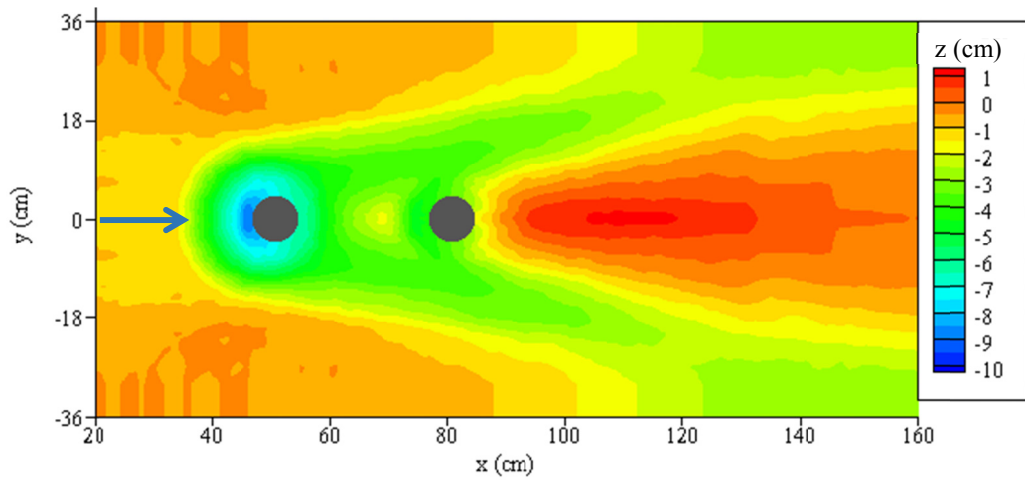


Figure A.20 Bed topography map of run E3 at  $t = 100$  min

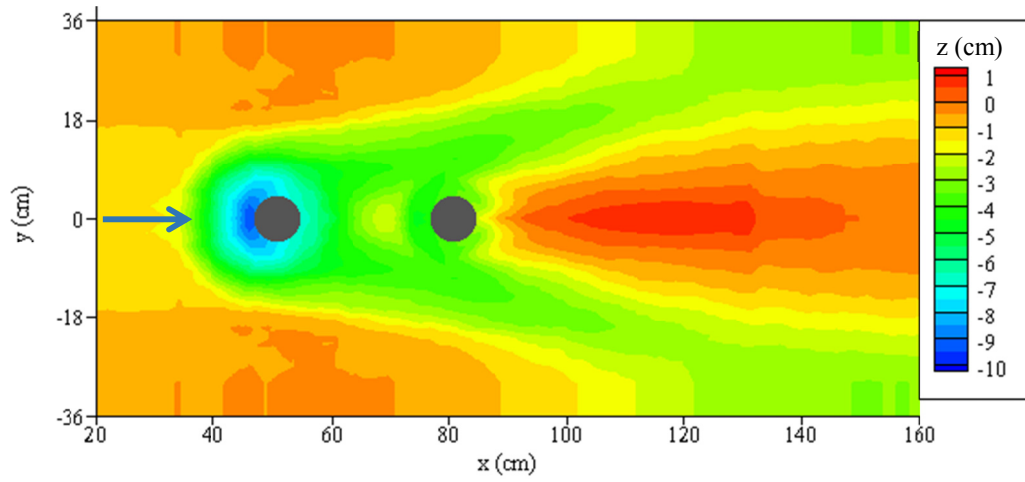


Figure A.21 Bed topography map of run E3 at t = 150 min

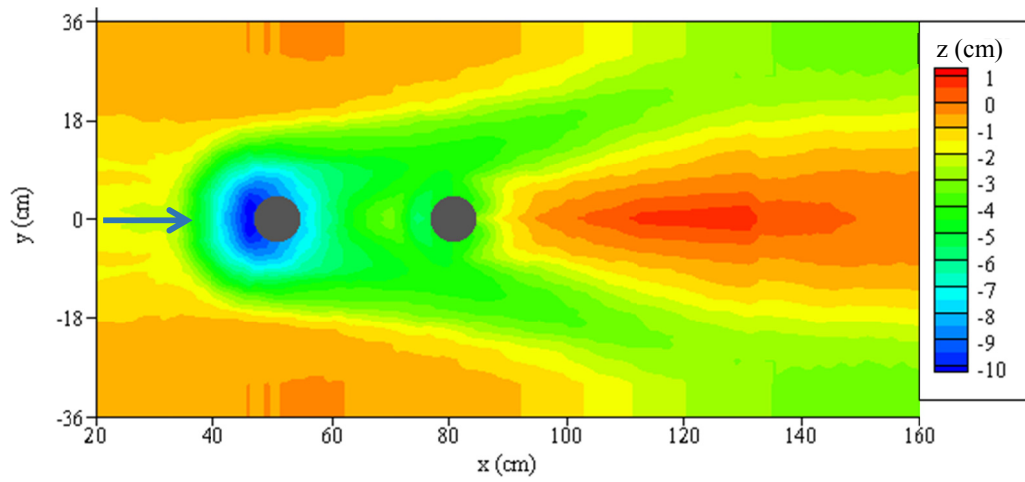


Figure A.22 Bed topography map of run E3 at t = 360 min

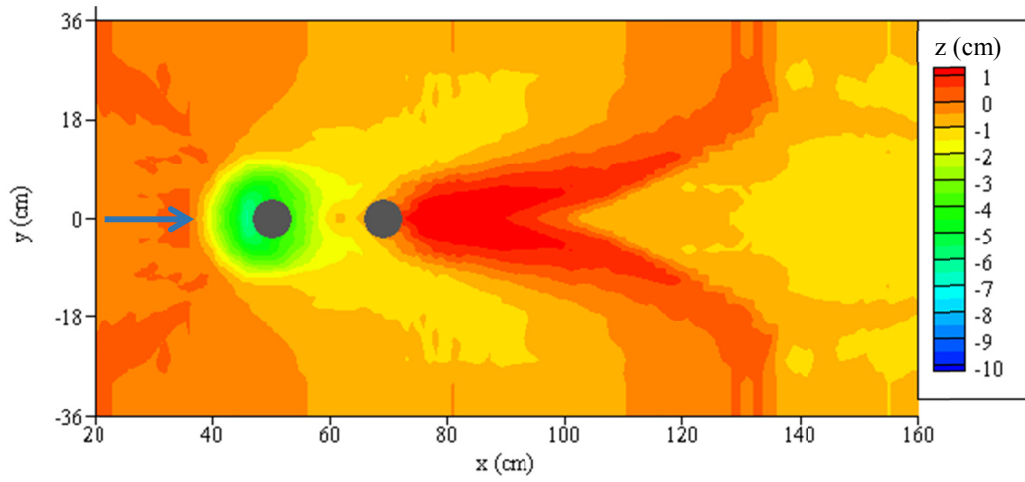


Figure A.23 Bed topography map of run E4 at t = 5 min

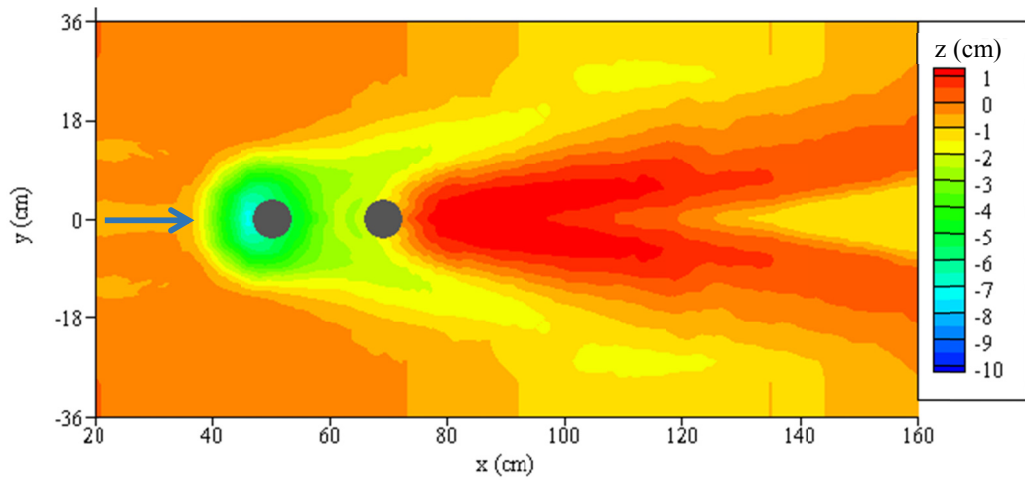


Figure A.24 Bed topography map of run E4 at t = 20 min

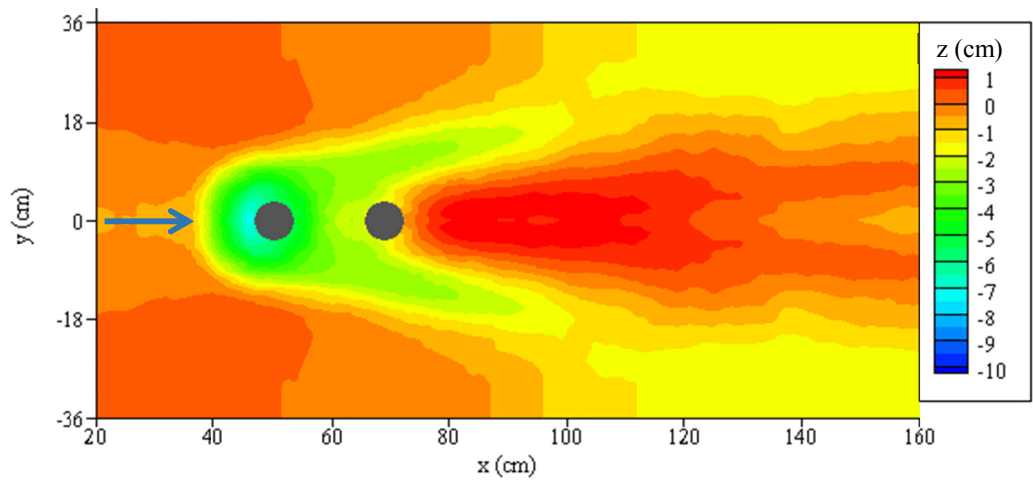


Figure A.25 Bed topography map of run E4 at  $t = 60$  min

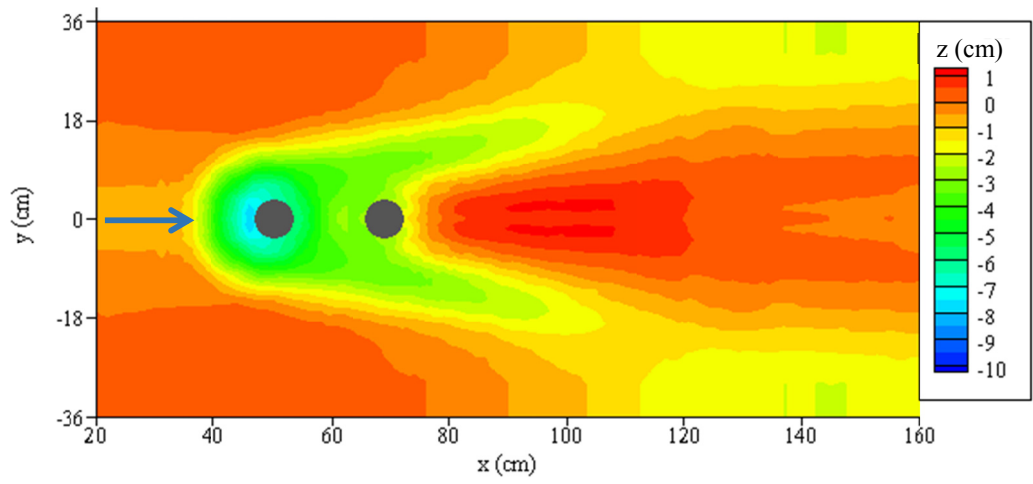


Figure A.26 Bed topography map of run E4 at  $t = 100$  min

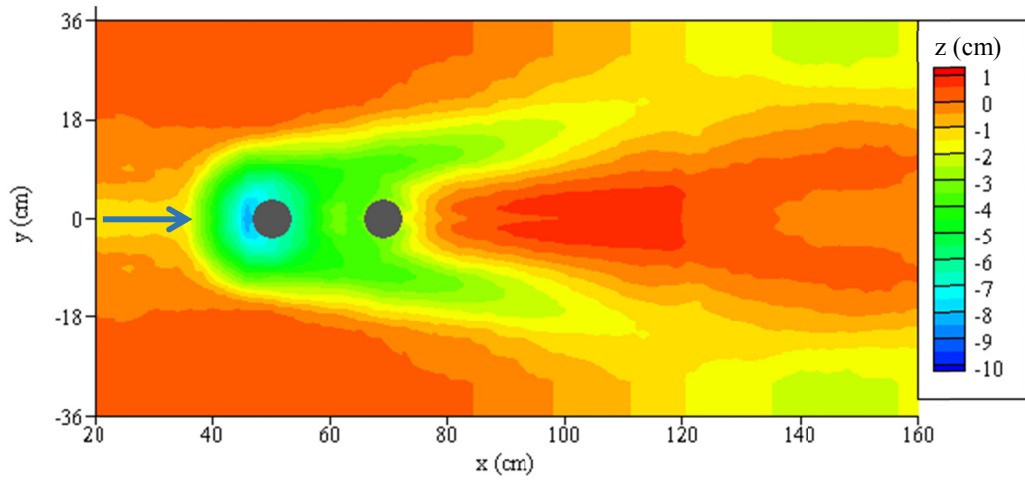


Figure A.27 Bed topography map of run E4 at  $t = 150$  min

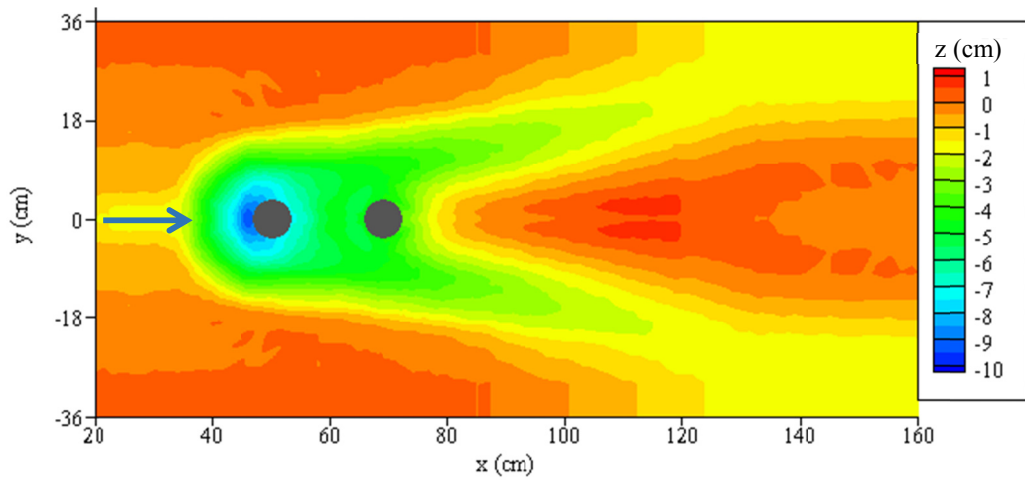


Figure A.28 Bed topography map of run E4 at  $t = 360$  min

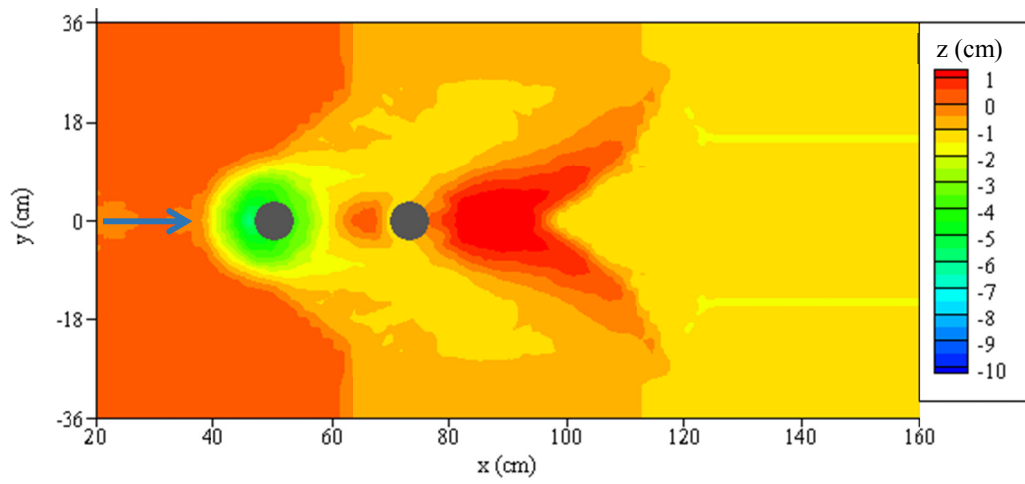


Figure A.29 Bed topography map of run E5 at t = 5 min

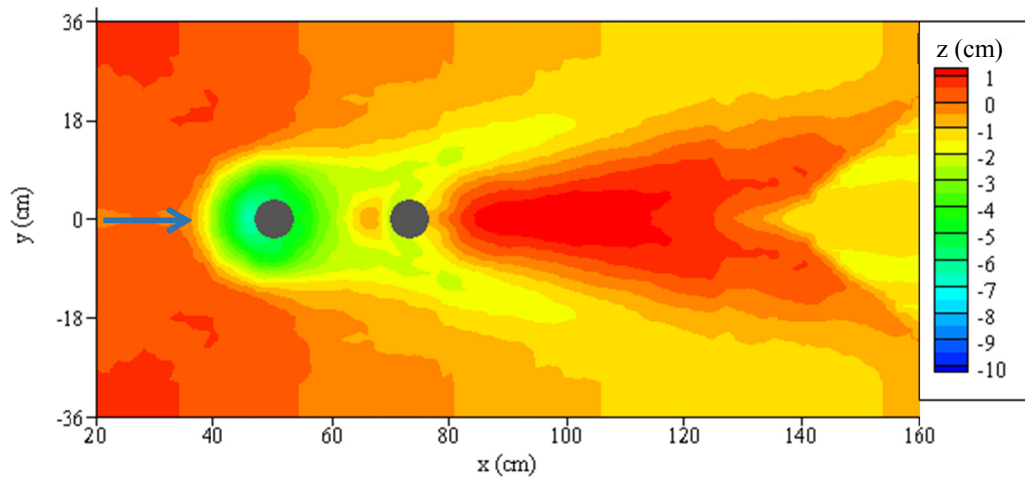


Figure A.30 Bed topography map of run E5 at t = 20 min

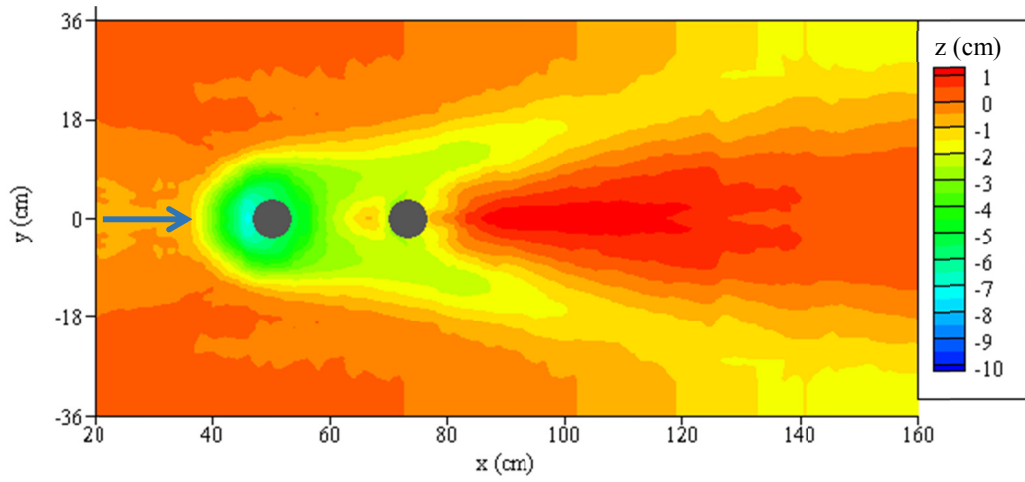


Figure A.31 Bed topography map of run E5 at  $t = 60$  min

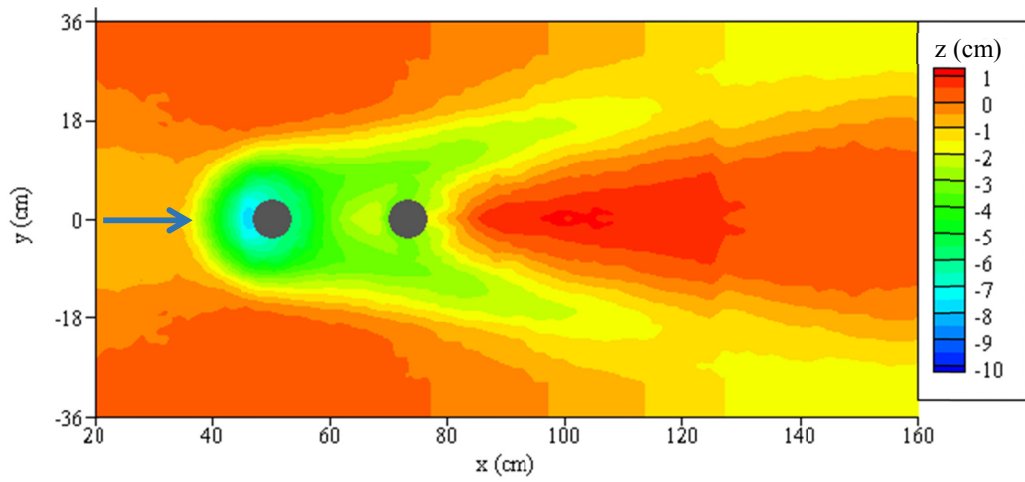


Figure A.32 Bed topography map of run E5 at  $t = 100$  min

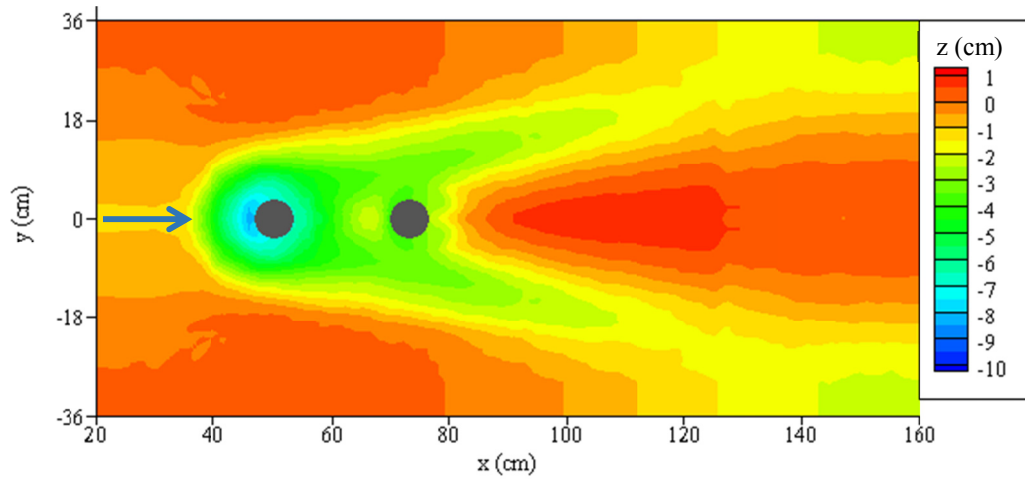


Figure A.33 Bed topography map of run E5 at  $t = 150$  min

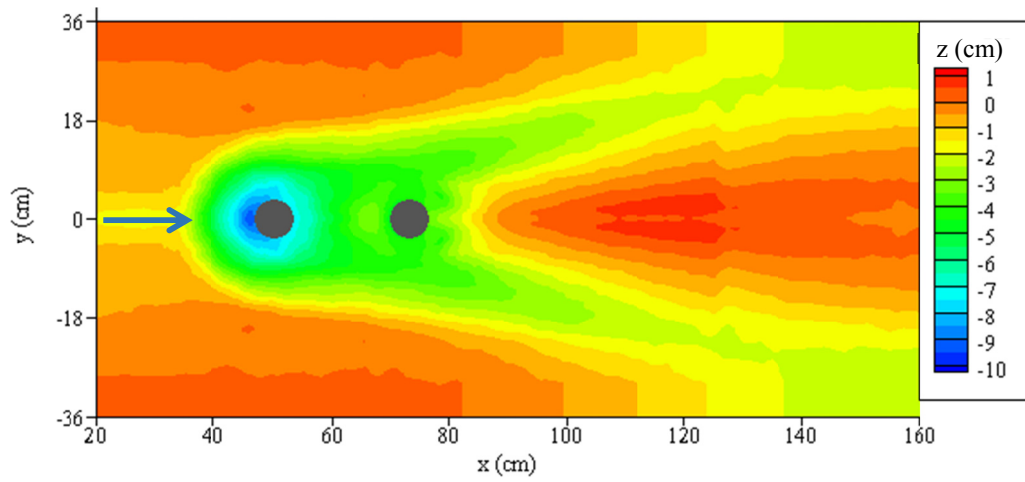


Figure A.34 Bed topography map of run E5 at  $t = 360$  min

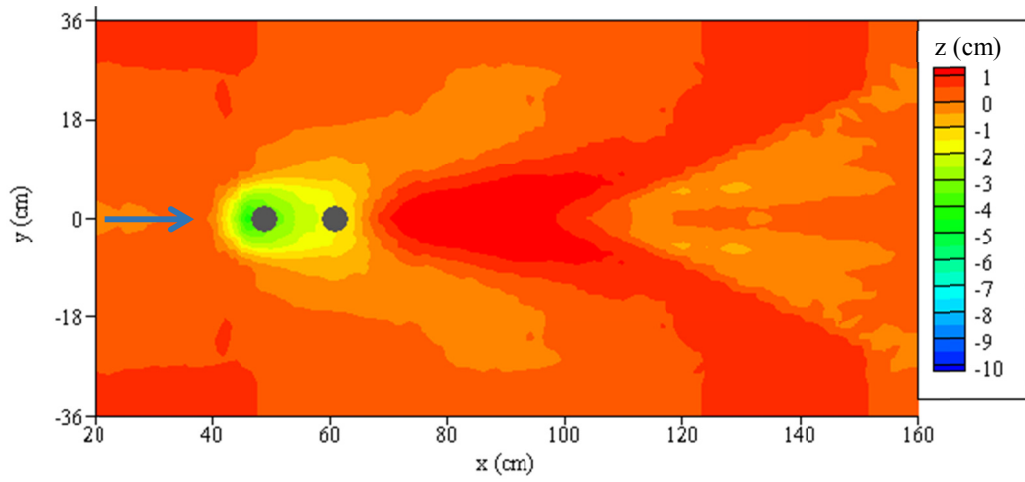


Figure A.35 Bed topography map of run E6 at  $t = 5$  min

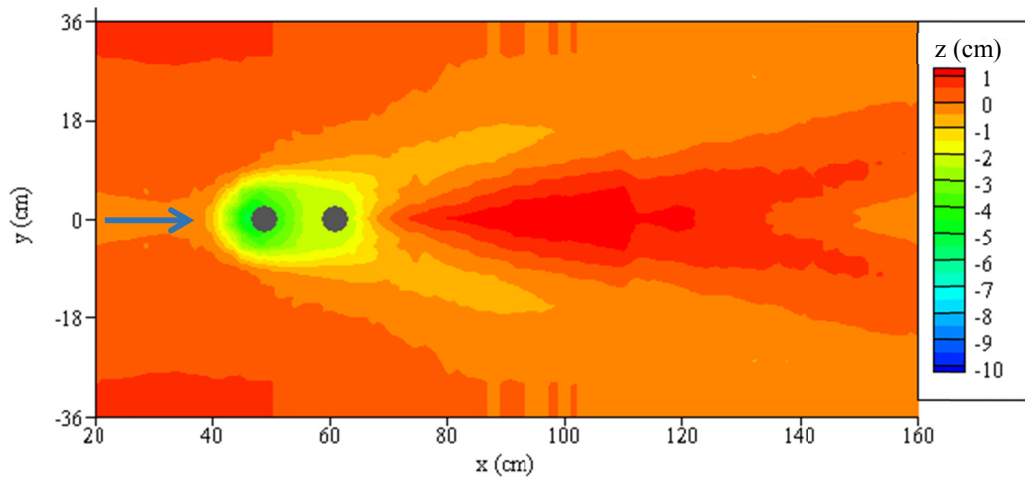


Figure A.36 Bed topography map of run E6 at  $t = 20$  min

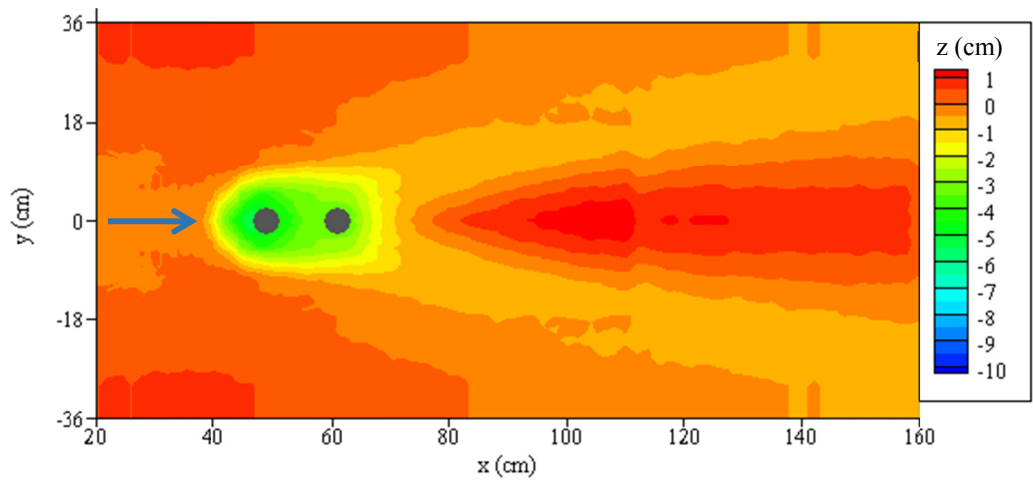


Figure A.37 Bed topography map of run E6 at t = 60 min

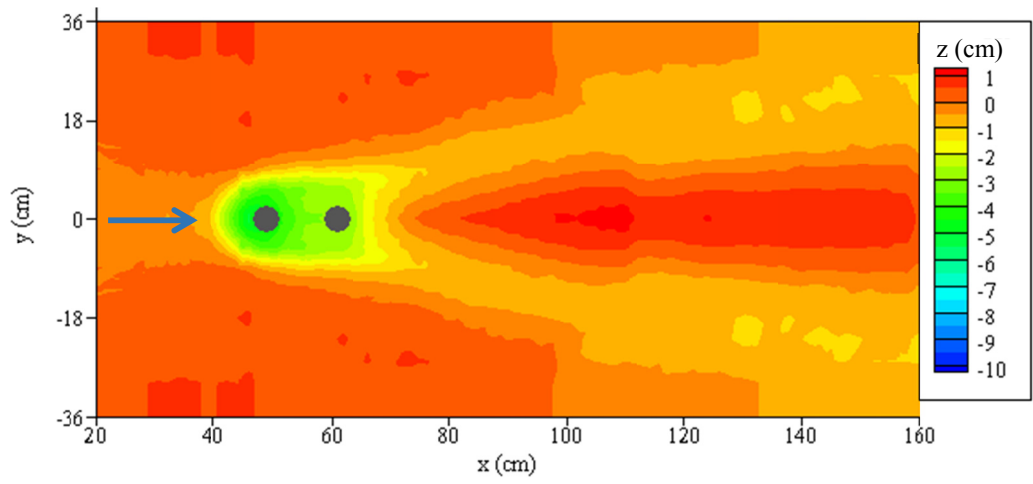


Figure A.38 Bed topography map of run E6 at t = 100 min

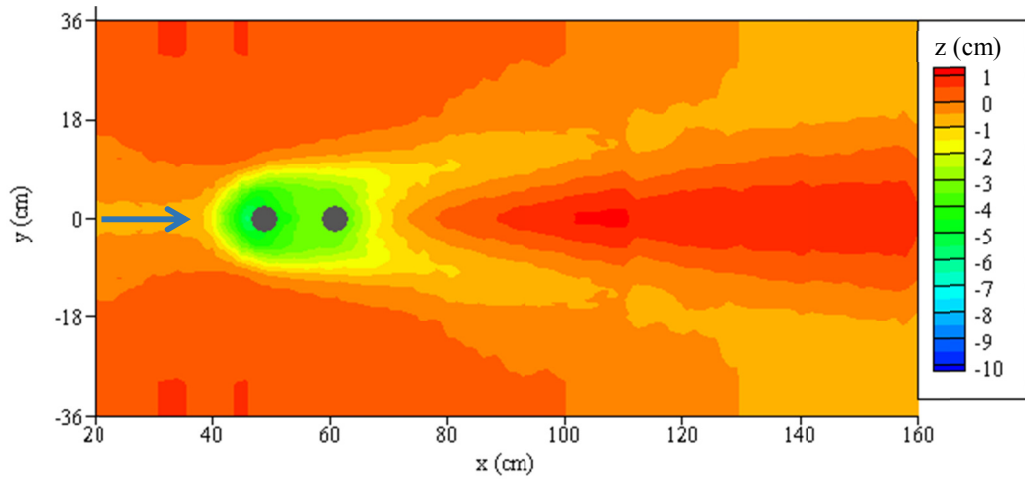


Figure A.39 Bed topography map of run E6 at t = 150 min

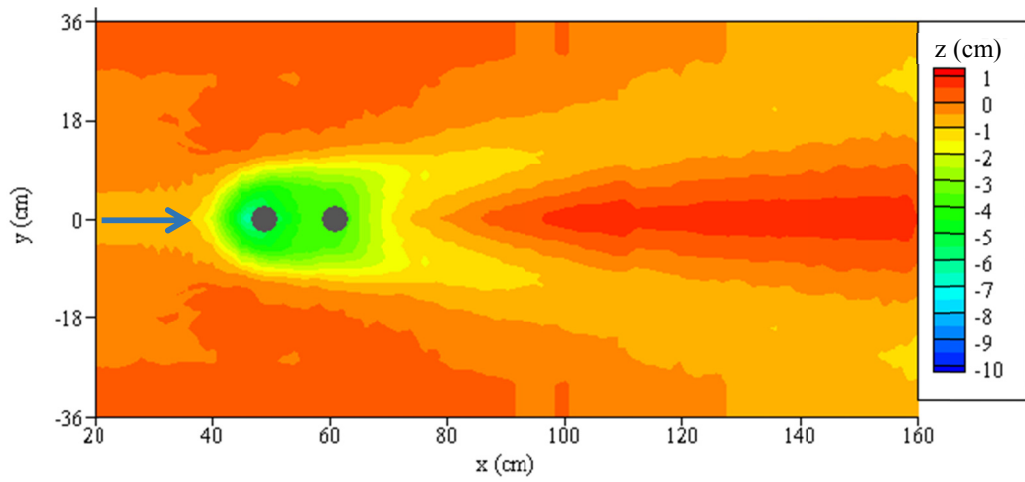


Figure A.40 Bed topography map of run E6 at t = 360 min

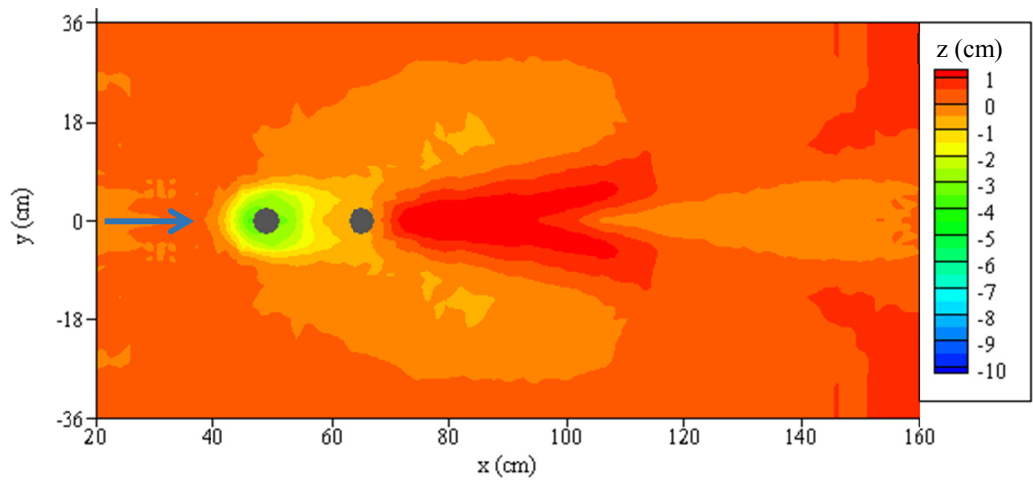


Figure A.41 Bed topography map of run E7 at t = 5 min

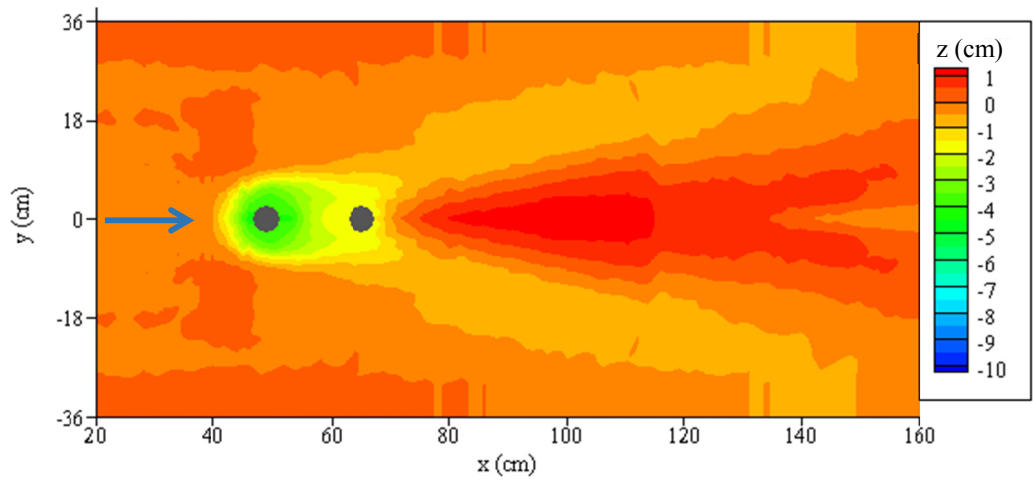


Figure A.42 Bed topography map of run E7 at t = 20 min

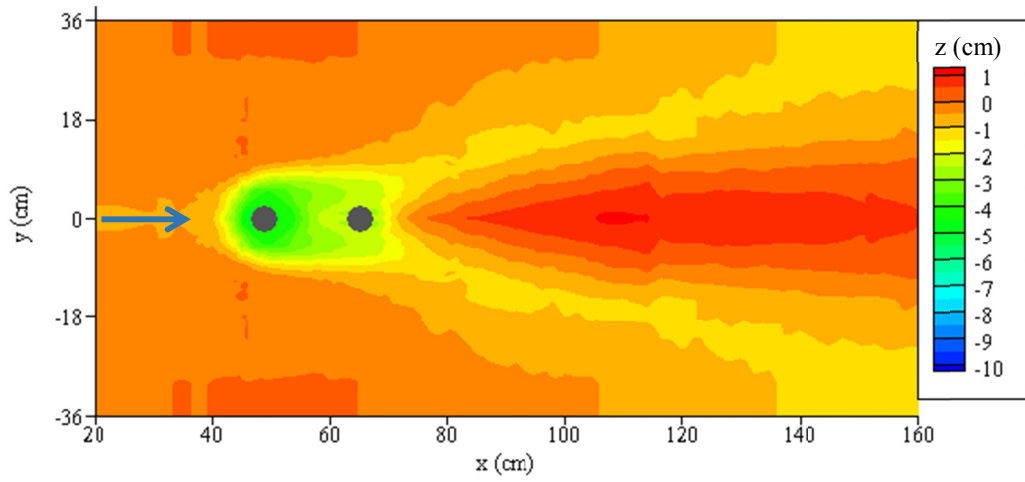


Figure A.43 Bed topography map of run E7 at  $t = 60$  min

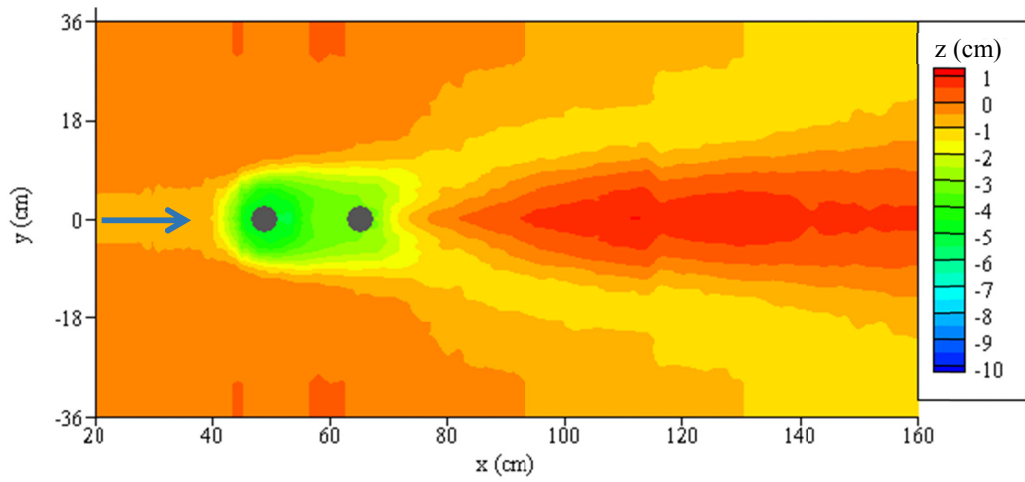


Figure A.44 Bed topography map of run E7 at  $t = 100$  min

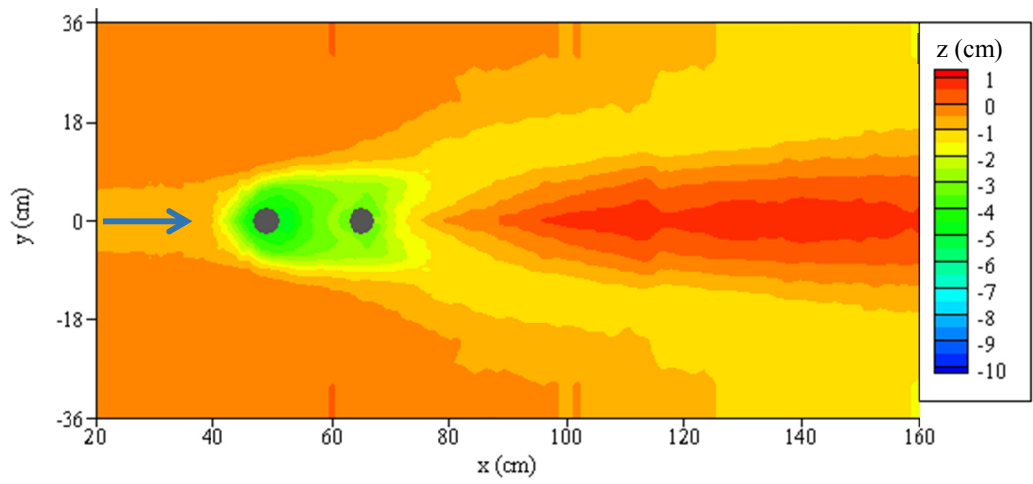


Figure A.45 Bed topography map of run E7 at t = 150 min

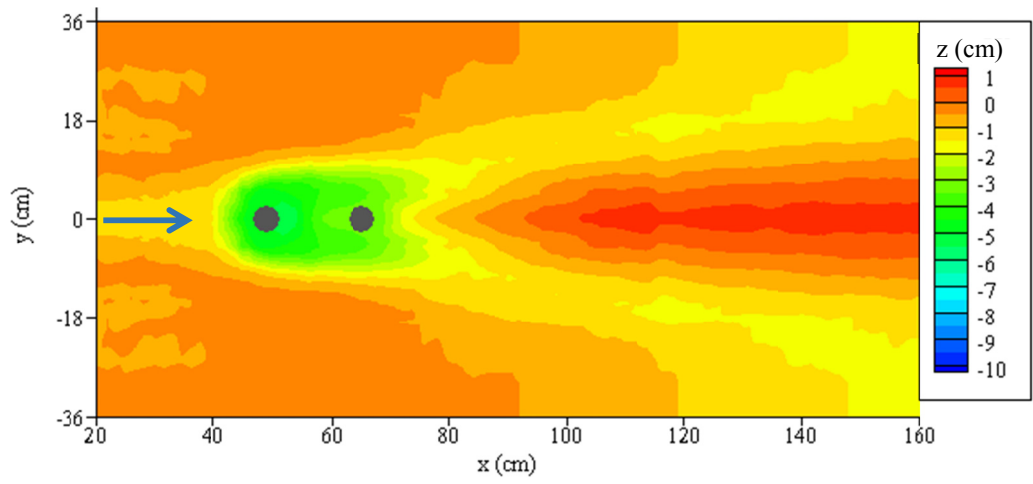


Figure A.46 Bed topography map of run E7 at t = 360 min

## **APPENDIX B**

### **EXPERIMENTAL SCOUR DEPTH**

Variation of maximum scour depth versus time values obtained from the Experiments Part II are presented here in Table B.1.

Table B.1 Experimental  $d_s - t$  values

$t$ (min)	$d_s$ (cm)						
	E11-8	E11-10	E11-12	E12-8	E12-10	E12-12	E13-8
0	0.00	0.00	0.00	0.00	0.00	0.00	0.00
1	3.85	3.50	4.97	3.47	4.33	4.54	2.88
2	4.18	4.98	5.63	3.69	5.20	5.33	3.67
4	4.50	5.52	6.30	4.01	5.79	6.01	4.62
6	4.72	5.84	6.71	4.39	6.27	6.50	4.88
8	5.06	5.94	6.82	4.68	6.40	6.59	5.12
10	5.14	6.12	6.94	4.91	6.55	6.73	5.24
14	5.35	6.30	7.17	5.37	6.79	6.98	5.55
18	5.48	6.37	7.31	5.54	6.95	7.11	5.67
22	5.67	6.64	7.40	5.68	7.04	7.29	5.82
26	5.83	6.68	7.66	5.77	7.12	7.41	6.01
30	5.94	6.86	7.72	5.94	7.22	7.62	6.13
40	6.09	7.04	7.87	6.18	7.38	7.89	6.28
50	6.22	7.14	8.00	6.43	7.43	8.05	6.50
60	6.38	7.29	8.14	6.61	7.54	8.22	6.57
70	6.50	7.42	8.21	6.76	7.67	8.38	6.71
80	6.64	7.50	8.33	6.89	7.77	8.42	6.81
90	6.69	7.68	8.45	6.97	7.83	8.47	6.90
100	6.81	7.82	8.56	7.02	7.89	8.54	6.96
120	6.90	7.94	8.74	7.07	8.03	8.66	7.03
140	6.96	8.01	8.86	7.10	8.17	8.88	7.09
160	7.00	8.12	9.01	7.20	8.26	9.03	7.14
180	7.09	8.26	9.17	7.25	8.30	9.13	7.25
200	7.14	8.36	9.29	7.28	8.33	9.19	7.31
240	7.21	8.67	9.51	7.42	8.40	9.28	7.48
280	7.31	8.78	9.59	7.48	8.45	9.34	7.54
320	7.42	8.89	9.74	7.57	8.49	9.45	7.59
360	7.48	8.95	9.88	7.62	8.55	9.52	7.74

Table B.1 (continued)

$t$ (min)	$d_s$ (cm)						
	E13-10	E13-12	E14-8	E14-10	E14-12	E15-8	E15-10
0	0.00	0.00	0.00	0.00	0.00	0.00	0.00
1	3.01	4.04	1.54	1.51	3.20	1.84	2.62
2	4.63	5.04	2.35	2.67	4.50	2.20	3.33
4	5.26	5.81	2.95	3.62	5.57	3.19	4.00
6	5.70	6.02	3.44	4.03	5.76	3.66	4.30
8	5.95	6.33	3.63	4.57	6.03	3.84	4.46
10	6.20	6.50	3.94	4.74	6.26	4.02	4.65
14	6.36	6.68	4.19	5.14	6.37	4.24	4.78
18	6.48	6.90	4.35	5.26	6.62	4.42	4.86
22	6.58	7.11	4.50	5.52	6.83	4.52	4.92
26	6.71	7.23	4.58	5.63	6.88	4.60	4.98
30	6.86	7.30	4.71	5.78	7.02	4.69	5.07
40	7.05	7.39	4.77	5.93	7.13	4.83	5.24
50	7.24	7.53	4.82	6.02	7.21	4.98	5.41
60	7.36	7.66	4.85	6.10	7.30	5.07	5.51
70	7.48	7.76	4.89	6.18	7.36	5.14	5.71
80	7.52	7.91	4.97	6.25	7.39	5.16	5.81
90	7.59	8.06	5.05	6.30	7.41	5.19	5.91
100	7.63	8.12	5.13	6.34	7.45	5.23	5.97
120	7.78	8.23	5.32	6.36	7.52	5.28	6.06
140	7.85	8.36	5.43	6.38	7.58	5.38	6.15
160	7.89	8.53	5.51	6.40	7.61	5.44	6.27
180	8.00	8.65	5.60	6.43	7.63	5.48	6.30
200	8.06	8.73	5.67	6.47	7.65	5.51	6.33
240	8.25	8.92	5.78	6.57	7.69	5.60	6.39
280	8.31	9.04	5.82	6.63	7.73	5.65	6.46
320	8.44	9.23	5.87	6.70	7.86	5.69	6.52
360	8.62	9.44	5.92	6.77	7.95	5.77	6.58

Table B.1 (continued)

<i>t</i> (min)	<i>d<sub>s</sub></i> (cm)						
	E15-12	E16-8	E16-10	E16-12	E17-8	E17-10	E17-12
0	0.00	0.00	0.00	0.00	0.00	0.00	0.00
1	2.44	1.64	2.06	2.39	1.40	1.60	2.10
2	3.52	2.35	2.18	3.00	2.18	2.93	3.20
4	4.85	3.00	2.85	3.80	3.35	3.48	4.33
6	5.20	3.27	3.75	4.50	3.60	3.73	4.57
8	5.44	3.74	4.12	4.77	3.74	3.91	4.62
10	5.80	3.89	4.28	4.96	3.82	4.02	4.70
14	5.97	4.06	4.42	5.06	4.04	4.13	4.75
18	6.13	4.16	4.65	5.10	4.17	4.21	4.80
22	6.31	4.21	4.73	5.14	4.29	4.27	4.85
26	6.44	4.25	4.76	5.18	4.37	4.31	4.87
30	6.52	4.32	4.78	5.20	4.42	4.36	4.91
40	6.79	4.47	4.84	5.26	4.53	4.45	4.94
50	7.00	4.57	4.88	5.30	4.60	4.53	4.98
60	7.22	4.62	4.94	5.39	4.64	4.67	5.06
70	7.35	4.65	4.98	5.45	4.65	4.79	5.11
80	7.42	4.67	5.02	5.49	4.67	4.89	5.15
90	7.51	4.69	5.06	5.53	4.69	4.95	5.18
100	7.62	4.70	5.10	5.57	4.71	4.98	5.20
120	7.70	4.76	5.21	5.62	4.76	5.05	5.25
140	7.75	4.79	5.32	5.70	4.79	5.11	5.28
160	7.79	4.81	5.41	5.78	4.85	5.16	5.31
180	7.84	4.83	5.49	5.85	4.93	5.19	5.35
200	7.87	4.85	5.54	5.89	4.95	5.25	5.39
240	7.98	4.92	5.65	5.98	4.98	5.33	5.55
280	8.06	4.98	5.71	6.06	5.02	5.37	5.62
320	8.16	5.06	5.74	6.16	5.06	5.42	5.66
360	8.22	5.12	5.76	6.19	5.11	5.50	5.68

## CURRICULUM VITAE

### PERSONAL INFORMATION

Surname, Name: Selamoğlu, Meriç

Nationality: Turkish (TC)

Date and Place of Birth: 25 June 1986, Ankara, Turkey

Marital Status: Single

### EDUCATION

Degree	Institution	Year of Graduation
M.S.	METU Civil Engineering	2010
B.S.	METU Civil Engineering	2007
High School	TED Ankara College High School	2003

### PROFESSIONAL EXPERIENCE

Year	Place	Enrollment
2007-present	METU Civil Engineering Dept.	Research Assistant

### FOREIGN LANGUAGES

English (Full professional proficiency)

German (Elementary proficiency)

## PUBLICATIONS

### Journal Papers

- 1) **Selamoğlu, M.**, Yanmaz, A.M., and Köken, M. (2015). Time-evolution of clear-water scouring at dual bridge piers. *Journal of Water Resources Management*, submitted.
- 2) **Selamoğlu, M.**, Yanmaz, A.M., and Köken, M. (2015). Modeling clear-water scouring at bridge piers in tandem arrangement. *ASCE Journal of Hydraulic Engineering*, submitted.
- 3) Yanmaz, A.M. and **Apaydın\***, M. (2012). Bridge scour risk assessment and countermeasure design. *ASCE Journal of Performance of Constructed Facilities*, 26(4), 499-506.

### Conference Papers

- 1) **Selamoğlu, M.**, Yanmaz, A.M., and Köken, M. (2014). Temporal variation of scouring topography around dual bridge piers. *Proceedings of the 7th International Conference on Scour and Erosion*, Perth, Western Australia, 495-500.
- 2) **Selamoğlu M.**, Sürer S., Akyürek Z., Yanmaz A.M. (2013). A case study on river navigation system design with upstream control. *Proceedings of the 6th International PIANC-SMART Rivers Conference (CD-ROM)*, Liège, Belgium.
- 3) Yanmaz, A.M. and **Apaydın\***, M. (2011). Assessment of riprap protection of existing bridges against scouring. *Proceedings of the 2nd Symposium on Bridges and Viaducts (CD-ROM)*, Eskisehir, Turkey (in Turkish).
- 4) **Apaydın\***, M. and Yanmaz, A.M. (2011). Investigation of failure risk of river bridges. *Proceedings of the 6th Urban Infrastructure Symposium*, Antalya, Turkey, 551-558 (in Turkish).
- 5) Yanmaz, A.M. and **Selamoğlu, M.** (2010). A case study on bridge-scour risk assessment. *Proceedings of the 9th International Congress on Advances in Civil Engineering (CD-ROM)*, Trabzon, Turkey.

\*Former last name

## HOBBIES

Cooking, Reading, Traveling